CHALMERS
UNIVERSITY OF TECHNOLOGY

Experimental Magnetic and Iron Loss Degradation in Electrical Machines

Measurements and Analysis of Laser Cut Degradation with Sinusoidal and Non-Sinusoidal Flux Distribution

Master's Thesis in Sustainable Electric Power Engineering and Electromobility

VICTOR LIDSKOG

DEPARTMENT OF ELECTRICAL ENGINEERING

CHALMERS UNIVERSITY OF TECHNOLOGY
Gothenburg, Sweden 2023
www.chalmers.se

Master's thesis 2023

Experimental Magnetic and Iron Loss Degradation in Electrical Machines

Measurements and Analysis of Laser Cut Degradation with Sinusoidal and Non-Sinusoidal Flux Distribution

VICTOR LIDSKOG

CHALMERS
UNIVERSITY OF TECHNOLOGY

Department of Electrical Engineering
Division of Electrical Power Engineering
Chalmers University of Technology
Gothenburg, Sweden 2023

Experimental Magnetic and Iron Loss Degradation in Electrical Machines
Measurements and Analysis of Laser Cut Degradation with Sinusoidal and Non-Sinusoidal Flux Distribution
VICTOR LIDSKOG

Supervisor: Sima Soltanipour, Volvo Cars Corporation
Examiner: Torbjörn Thiringer, Electrical Power Engineering

Master's Thesis 2023
Department of Electrical Engineering
Division of Electrical Power Engineering
Chalmers University of Technology
SE-412 96 Gothenburg
Telephone +46 31 772 1000

Typeset in LaTeX
Printed by Chalmers Reproservice
Gothenburg, Sweden 2023

Experimental Magnetic and Iron Loss Degradation in Electrical Machines
Measurements and Analysis of Laser Cut Degradation with Sinusoidal and Non-Sinusoidal Flux Distribution
VICTOR LIDSKOG
Department of Electrical Engineering
Chalmers University of Technology

Abstract

With the automotive industry increasingly transitioning towards a fully electric fleet of vehicles, the development of highly efficient electrical machines has become a crucial undertaking. In order to achieve precise simulation outcomes during the design phase of these electrical machines, it is imperative to consider the impact of cutting the lamination steel utilized in the stator and rotor. This research work focuses on the utilization of an Epstein frame and a Single Strip Tester to evaluate the effects of cutting on the electrical steel, specifically using a laser cut technique. The study encompasses both sinusoidal and non-sinusoidal flux distributions. Magnetic property degradation and iron losses were measured and subjected to comprehensive analysis. A test sequence encompassed multiple fundamental frequencies and varied flux density levels, resulting in over 1500 individual test measurements. The outcomes of these measurements were extensively analyzed and discussed. To generate the non-sinusoidal flux, Pulse Width Modulation (PWM) was used, and the effects of altering the amplitude modulation index and frequency modulation index were measured and analyzed. The degradation of magnetic properties exhibited an exponential pattern, with the greatest degradation occurring closest to the cut edge, reaching an increase of 3.3 times as much magnetic field strength . Conversely, the degradation of iron losses exhibited a more linear increase, with the highest degradation reaching 1.5 times increase, near the cut edge. The magnitude of degradation depended on both the flux density level and the fundamental frequency, with greater degradation observed at lower frequencies and reduced degradation at saturation levels in the electrical steel. Based on the measured results, a model was developed to incorporate the degradation into a Finite Element Method (FEM) simulation model of a Permanent Magnet Synchronous Machine (PMSM). The FEM simulation was conducted at various frequencies, focusing on a single load point at half the rated current. It is important to note that the degradation resulting from non-sinusoidal flux is a highly intricate topic that necessitates further investigation. Multiple factors, including fundamental frequency, frequency modulation index, amplitude modulation index, flux density level, distance from the cut edge, and more, contribute to the degradation, resulting in a multitude of degrees of freedom and increased complexity. The simulation outcomes indicated a decrease in torque and an increase in iron losses when compared to a non-degraded model. Consequently, the machine's efficiency was reduced by approximately 0.5% to 2%, depending on the fundamental frequency.

Keywords: PWM excitation, sinusoidal excitation, laser cut degradation, iron loss degradation, Epstein Frame, FEM, IPMSM, Manufacturing process.

Acknowledgements

I have had a great experience at Chalmers University of Technology and I will never forget the memories and friends that I have made here.

I would like the thank my manager at Volvo Cars, Anders Thulin, for the opportunity to complete a Master Thesis together with an industry, such as Volvo Cars. I would also like to thank my examiner Torbjörn Thiringer from Chalmers for the feedback and guidance throughout this thesis work. I would also like to thank my fellow class mates, Gustav, Malte, Tim, Zijie, Oskar, Binaya, Valdrin, Abshir, just to name a few. Completing a thesis alone can be a hard task, but thanks to you all I have been able to bounce ideas when I have been stuck, and this I am grateful for. I wish you all guys the best for the future and continue your amazing work as engineers.

I would like to give a huge thank you to Sima Soltanipour, my supervisor throughout this thesis. It has been great to have a supervisor to bounce ideas, and laugh in the lab with. I am grateful to all the help and guidance, you have made this thesis fun and learning. I wish you the best of luck and best wishes finishing your PhD, Thank you.

Since this is the end of my journey at Chalmers, I put in the extra hours to finish on top, basically I have been dreaming about degradation and Epstein frames for months. There has been early mornings and late nights, so drinking good quality coffee has been very important, and also going out and enjoying a few beers with friends to try keep sane.

Last but not least, I want to give my biggest gratitude to my wife, Rachael Lidskog, who has been through this whole journey with me. You have been so supportive through my whole time at Chalmers and always encouraging and understand of late night hours programming. Thank you for making this possible, and moving countries with me. I could not have done it without your love, support, and you are the world to me, I love you Rachael.

Victor Lidskog, Gothenburg, June 2023

Contents

1 Introduction **1**
1.1 Background . . . 1
1.2 Previous Work . . . 2
1.3 Aim . . . 2

2 Stator and Rotor Manufacturing Processes, Losses and Testing **3**
2.1 Manufacturing Process . . . 3
2.1.1 Cutting Process . . . 4
2.1.1.1 Punching . . . 4
2.1.1.2 Laser Cutting . . . 5
2.1.1.3 Water Jet Cutting . . . 6
2.1.1.4 Electric Discharge Machining . . . 6
2.1.2 Interconnection . . . 6
2.1.2.1 Welding . . . 6
2.1.2.2 Gluing . . . 7
2.1.3 Other Manufacturing Processes . . . 7
2.1.4 Cutting Process Effects Summary . . . 7
2.2 Measurement Methods . . . 8
2.2.1 Epstein Frame . . . 10
2.2.2 Single Strip Tester . . . 10
2.2.3 Other Measurement Methods . . . 11
2.3 Iron Losses in Electrical Machines . . . 11
2.3.1 Hysteresis Losses . . . 12
2.3.2 Eddy Current Losses . . . 13
2.3.3 Excess Losses . . . 13
2.4 Iron Loss Models . . . 14
2.4.1 Steinmetz Loss Model . . . 14
2.4.2 Jordan's Loss Model . . . 15
2.4.3 Bertotti's Loss Model . . . 15
2.5 Pulse Width Modulation . . . 16

3 Experimental Testing and Measurement Setup **19**
3.1 Electrical Steel Samples . . . 19
3.1.1 Epstein Frame Test Samples . . . 20
3.1.2 SST Test Samples . . . 22
3.2 Epstein Test Setup . . . 24

3.3 SST Test Setup . . . 24
3.4 MPG Expert PWM . . . 24

4 Equipment Testing, Repeatability and Sensitivity to Parameters 27
4.1 Determine Repeatability of Measurements . . . 27
4.1.1 Repeatability of SST Measurements . . . 27
4.1.2 Repeatability of Epstein Measurements . . . 29
4.1.2.1 Sensitivity to Settings . . . 29
4.2 Recreation of Data Sheet . . . 31
4.3 Epstein and SST Comparison . . . 33
4.4 Loss Separation for Sinusoidal Feeding . . . 35
4.4.1 Jordan's Loss Model . . . 35
4.4.2 Bertotti's Loss Model . . . 36
4.5 Specifying PWM Signal in MPG Expert . . . 39
4.5.1 Unipolar Switching . . . 41
4.5.2 Bipolar Switching . . . 44

5 Cut Effects with Sinusoidal Flux Density 47
5.1 Epstein Frame Testing . . . 47
5.1.1 Magnetic Field Strength Degradation . . . 48
5.1.2 Specific Power Loss Degradation . . . 57
5.2 SST Cut Effect Testing, Comparison and Verification . . . 60
5.2.1 H Degradation with SST . . . 64
5.2.2 Ps Degradation with SST . . . 66

6 Cut Effects with PWM Excitation 69
6.1 Effect of Cutting with Non-Sinusoidal Flux Distribution . . . 69
6.1.1 Magnetic Field Strength Degradation . . . 70
6.1.1.1 With PWM Sample A as Reference . . . 70
6.1.1.2 With Sinusoidal Sample A as Reference . . . 80
6.1.1.3 Comparing PWM Sample's with Sinusoidal Sample's 85
6.1.2 Specific Power Loss Degradation . . . 87
6.1.2.1 With PWM Sample A as Reference . . . 87
6.1.2.2 With Sinusoidal Sample A as Reference . . . 91
6.1.2.3 Comparing PWM Sample with Sinusoidal Sample . . 94
6.2 Effects of Changing Fha . . . 96
6.2.1 Effects of Fha at 400 Hz . . . 96
6.2.2 Effects of Fha at 50 Hz . . . 102
6.3 Effects of Changing Vr . . . 105

7 Comparing losses in FEM based simulations 109
7.1 Model of PMSM . . . 109
7.2 Implementation of Degradation Models . . . 110
7.2.1 Implementation of Sinusoidal Degradation . . . 111
7.2.2 Implementation of PWM Degradation . . . 115
7.3 FEM Simulations of PMSM . . . 117
7.3.1 Non-Degraded Material Simulation with Sinusoidal Flux . . . 117

7.3.2 Degraded Material Simulation With Sinusoidal Flux 119
7.3.3 Non-Degraded PWM Model Simulation 121
7.3.4 Degraded PWM Model Simulation 123

8 Discussion **125**
8.1 Measurement Uncertainty and Complexity 125
8.2 Degradation Models 126
8.3 FEM Simulations 127
8.4 Ethics and Sustainability 128

9 Conclusion **129**

References **133**

A Repeatability Test SST and Epstein **I**

B Cut Effects with Sinusoidal Flux Density **IX**

C Cut Effects with Non-Sinusoidal Flux Density **XI**

D FEM Simulation with Sinusoidal Excitation **XIII**

E FEM Simulation with PWM Excitation **XVII**

1

Introduction

1.1 Background

As sales of electric vehicles is increasing [1] and around 50% of the global electricity demand [2] is used by electric machines (EM), the design of highly efficient EMs is a very important task.

This thesis work will compare the iron losses when feeding a sinusoidal flux density and non sinusoidal flux density. The work will also analyze the degradation of the magnetic properties in the electrical steel material due to manufacturing effects when shaping the rotor and stator of an EM, and more specifically the cutting effect when using a laser.

One aspect of designing an efficient EM is considering the losses in the stator and rotor due to the magnetic field which drives the EM, the so called iron/core losses. Traditionally when designing an EM the estimations and simulations of iron losses is based on the data sheet provided by the manufacturer of the electrical steel. These data sheets however are based on sinusoidal shaped flux [3], they are also often limited in frequency and amplitudes of magnetic flux density and magnetic field strength [4]. Therefore its very difficult to accurately estimate iron losses.

Another difference from the data sheet is due to the manufacturing effects. This could be from, cutting the stator and rotor into its final shapes from the mother coil (MC), combining the multiple electrical steels to a core with different joining processes, or other effects, such as shrink fitting and mechanical fixtures. These manufacturing effects on the electrical steel will create a difference from the data sheet due to the degradation in the materials magnetic properties. This will lead to that the final iron losses will be higher compared to the simulated ones, and the flux density in the machine will change due to its decrease in magnetic properties.

The industry standard for measuring the performance of electrical steels is using a Single Sheet Tester (SST) [5] or Epstein frame [3]. By using these measurements methods one could also perform measurements to evaluate the effects of the cutting process on the electrical steel.

1.2 Previous Work

Many research papers have investigated the effects of the cutting process on the iron losses in EM [6–10], and proposed models to replicate these losses in FEM simulations. Most research that has been done is regarding the mechanical cutting process, and fed with a sinusoidal flux density. In [11], an extensive comparison between multiple articles has been performed and the results vary drastically from article to article. This is due to the fact that there are different measurement methods and different materials. But the conclusion is that the cutting process does significantly affect the losses and magnetic properties in the EM.

In [9,11–14] the effect of laser cutting is analyzed. Although all these articles analyze different parameters, degradation depth, laser, punching and so on, they all have in common that they are fed with sinusoidal flux density.

Most data sheets regarding the electrical steel, has also been derived with a sinusoidal flux. There will therefore be a difference from the final product losses and the simulated losses. By taking the non-sinusoidal flux into consideration when looking at the cut effect degradation, a more realistic loss simulation could be found.

1.3 Aim

The main aim in this thesis project is to compare the losses and magnetic properties degradation in electrical steel sheets, feeding with a sinusoidal and a non sinusoidal flux density wave. This is to be done with the help of measurements, using Epstein frame and SST and then modelling an EM in a Finite Elements Method(FEM)-based software.

2

Stator and Rotor Manufacturing Processes, Losses and Testing

2.1 Manufacturing Process

The stator and rotor of an EM is built up from several laminates of electrical steel sheets. These electric steel sheets are made up of an iron alloy, consisting of up to 6% silicon. This is done in order to improve the magnetic properties of the electrical steel, such as decreasing eddy currents and limiting the width of the hysteresis loop [15].

When manufacturing the electrical steel, the steel is rolled to a specific thickness on the in a rolling machine. The direction that the steel is rolled in, is often referred as rolling direction, and the perpendicular direction is often referred as transverse or cross direction.

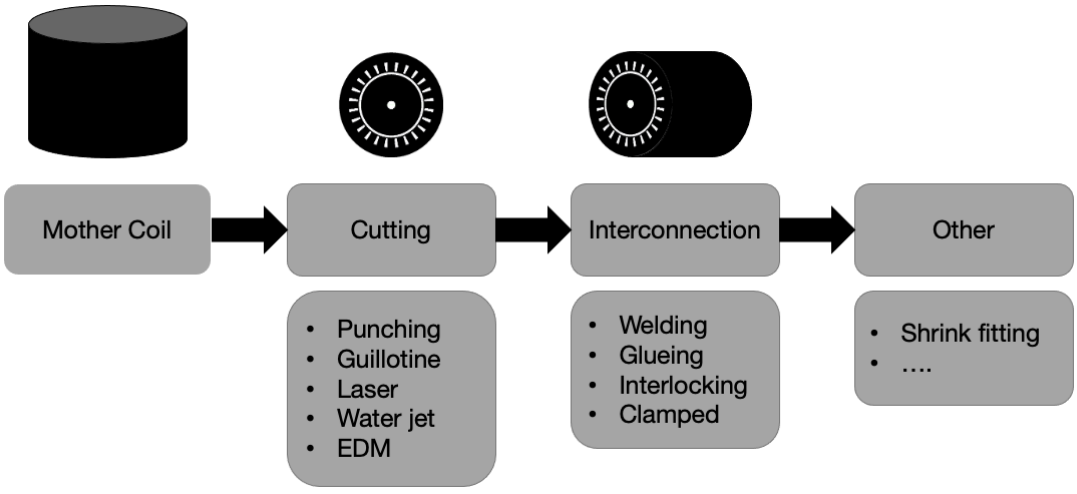

Figure 2.1: Manufacturing process of rotor and stator.

Electrical steels can be divided into grain-oriented and non-oriented steel. The difference between the two is that the grain-oriented is manufactured to have better performance in rolling direction, while non/oriented is known as isotropic, with similar performance in all direction of the steel. In EM design, non-oriented steel is

preferred [10], since the rotor and stator has a flux density that is rotating.

Figure 2.1, shows an example of the different manufacturing processes the electrical steel goes through. Some the processes could be, the electrical steel sheet is rolled onto a larger coil, then cut to its desired shape, interconnected and fitted in a stator housing. The different manufacturing processes and how it affects the electrical steel magnetic properties will be described briefly next.

2.1.1 Cutting Process

The cutting of electrical steel can be done in multiple different ways. According to [6, 7, 9], cutting process has the largest effect on the magnetic properties of the electrical steel out of all the manufacturing processes. Some of the cutting techniques will be introduced next, starting with punching.

2.1.1.1 Punching

Punching is the most common method of cutting in mass production of EM, due to its low cost [13, 14]. There is a high initial investment and every rotor/stator shape needs its custom cutting tool, but the production cost to mass produce is low compared to other cutting methods.

With punching, the electrical steel is under mechanical stress around the cut edge which deteriorates the magnetic properties of the steel [6]. The effects of the punching is from the plastic deformation around the cut edge which leads to lower magnetic permeability and therby higher iron losses [16].

The amount of effect on the electrical steel depends on multiple parameters, such as but not limited to:

1. Sharpness of cutting tool.
2. Properties of the electrical steel.
3. Complexity of the cut.

Punching could lead to burr edges on the electrical steel [17] which could lead to global eddy currents and thereby an increase of iron losses [10].

A way of measuring the degradation from punching is analyzing the micro hardness at the cut edge. Using measurement tools to analyze the microhardness, it could be seen that the micro hardness is increased drastically around the cut edge and decreases exponentially moving away from the cut edge [16].

The depth of the deterioration in the micro structure is a very complex value to achieve and it could vary from 100μm to a few of millimeters [18]. In [14], an extensive comparison between multiple articles has been performed. Here the degradation depth varies between 500μm up to 10mm. The large difference in these results could

be depending on how the results where achieved and different materials.

There is typically two different methods of achieving the degradation depth in the electrical steel, direct and indirect measurements [6]. The direct measurements measure the flux density directly through sensors in the material, by drilling small holes in the samples and inserting the sensor. Indirect measurements measures parameters such that the flux densities can be derived from. The indirect measurements could be microhardness, dark field image (DFI) or other measurement techniques [6].

2.1.1.2 Laser Cutting

Laser cutting method use a laser to cut the material into desired shape. The laser can cut the material in different ways, by heating to vaporize the material or melting and then remove material by blowing gas on the cut. Laser cutting is more common to use in small batches of EM and in prototypes. Since the cut can be customized every time, it is cheaper for these applications compared to the punching method.

The laser induce thermal stress to the material, which change its magnetic properties [12]. Laser cutting compared to punching does not affect the grain size of the material as mentioned in [9]. Laser cutting also has a low affect on the microhardness of the material, however the magnetic properties of the material is affected. Laser cutting introduces plastic, thermal and residual stresses in the material [19].

Since the laser cutting does not cut all of the material simultaneously, there is a difference from the first cut side to the second cut side [9], leading to a decrease in magnetic flux density. The degradation depth model for distance from cut edge is known to have a exponential degradation. [20]

Since the laser induces thermal stress in a large area of the material, the first cut could potentially affect the second cut side depending on how distant the cuts are [21]. At lower flux density levels mechanical cutting and laser cutting have very similar degradation [19].

Laser cutting is not as well investigated as the punching method. The research regarding affect of laser cutting conclude that the degradation depth in the material depends on a few different parameters [14]:

1. Electric steel material.
2. Geometry of cut.
3. Laser method.
4. Laser settings, such as speed and power.

In [14] it shows that the laser setting, such as the speed can increase the iron losses. The thermal stress induced in the material will depend on the power of the laser as well. The degradation depth could vary from 100μm up to 2mm. As mentioned in [14], using a neutron grating interferometer combined with neutron dark field image (NGI with nDFI) it can be noticed that the flux density of the whole electrical

steel is affected and reduced.

2.1.1.3 Water Jet Cutting

Water jet cutting uses high pressure to force water mixed with an abrasive powder through a nozzle. The pressure can vary between 300-700 Bar. The advantage of water jet cutting is that there is no thermal stress induced in the material being cut. According to [22], the water jet cutting has little affect on deterioration of the magnetic properties, and has a better performance for the permeability from 0.5 to 1.6T. However, as for the laser cutting, degradation is tied to cutting settings, material, geometry cut, and water jet method, so this degradation is tied to the specific settings in [22], and may vary compared to other water jet cuttings. The water jet technique however is more expensive compared to the other techniques and is therefore mainly used in prototypes and lower productions of electrical machines.

2.1.1.4 Electric Discharge Machining

Electric Discharge Machining (EDM), is a method of cutting where material is removed by discharging between two electrodes, creating sparks [23]. This method is considered having very low effect on the magnetic properties of the electrical steel due to that there is no mechanical stress during the process as well as limiting the thermal stress on the steel. The process is slower and more expensive compared to the punching so it is not used in mass producing of EM.

2.1.2 Interconnection

The rotor/stator laminates are interconnected to create a rotor/stator core, this interconnection creates degradation in its magnetic properties as well as iron losses. This interconnection can be done in different ways, such as welding, gluing, interlocking or clamping. The interconnection can also lead to short circuits between the different steel sheets leading to global eddy currents [13].

2.1.2.1 Welding

One way of interconnecting the electrical steel laminates and creating a rotor or stator core, is to weld them together. Welding is the most common interconnection method for mass producing stators and rotors [13]. The welds joins the laminates creating short circuit paths, which results in an increase of global eddy currents [24].

The welding process not only increases the eddy current losses but also the hysteresis losses due to the thermal and mechanical deterioration from the weld. The effect from welding on the electrical steel magnetic properties depend on the material of the steel and welds are used to interconnect the laminates [13]. A total increase of iron losses from welding could be from 32% to 44% depending on the lamination steel

material according to [24] and 5% to 20% according to [25]. In [26], its mentioned that core losses could increase up to 1% per weld spot.

2.1.2.2 Gluing

This joining process, uses glue or other adhesive material to join the lamination steel together. Gluing can also be known as sticking the electrical sheets together. According to [13] gluing has the lowest impact on the degradation out of the interconnection methods. This is also confirmed in [27], where the comparison between welding and gluing is done, where its shown that the effect of gluing is a smaller compared to the welding.

2.1.3 Other Manufacturing Processes

Some other manufacturing processes that affect the magnetic properties of the electrical steel could be,

1. Interlocking
2. Annealing
3. Shrink fitting
4. Compressing
5. Mechanical fixtures

These different processes wont be discussed in this thesis but is good to keep in mind when designing an efficient electrical machine.

2.1.4 Cutting Process Effects Summary

A short summary of the effects from cutting, and conclusions from the literature survey,

- The cutting effect depend on the method used during cutting, for example, laser, punching, water jet all have different degradation.
- Laser cutting depending on the material used, geometry of cut, laser method, and settings, such as speed and power.
- Some literature claims that laser cutting does not affect the grain size of the material.
- Deterioration depths from cutting can vary from 0.1 to 15 mm.
- The degradation is more dominant at lower flux densities.
- A common model for degradation versus distance from cut edge is an exponential degradation.
- Laser has more severe permeability degradation compared to punching.

2.2 Measurement Methods

Data sheets provided by manufacturer of electrical steels, usually specific core loss (Ps) in W/kg and a virgin magnetic flux density (B) vs magnetic field strength (H). These are derived from standardized measurements using equipment such as Epstein frame and Single Sheet Testers (SST). The International Electrotechnical Commission (IEC), has derived two standards for these two measurement equipment's. IEC60404-2 [3] for the Epstein frame, and IEC60404-3 [5] for the SST.

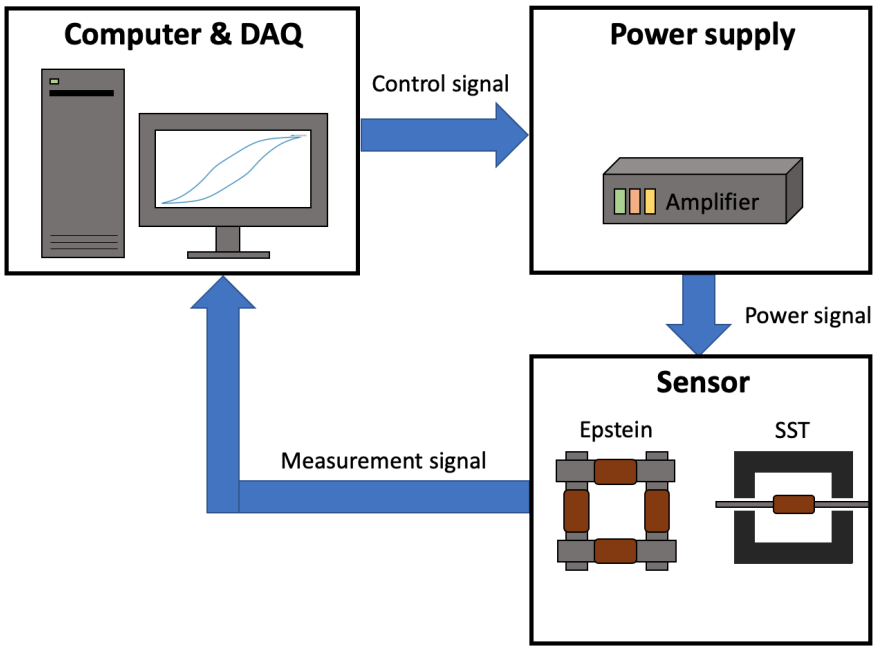

Figure 2.2: Control loop for measuring magnetic properties with Epstein or SST.

Figure 2.2 shows an example of how a measurement for the electrical steel properties is done. The control computer sets up the desired frequency (f), H, or B to measure the magnetic properties of the electrical steel. The computer can provide a specific excitation desired from the user, sinusoidal, specific harmonics, Pulse Width Modulation (PWM), and free form. The current from the desired shape is provided from the amplifier [28].

The measurement method is based on Amperes law,

$$H(t)dl = \frac{N_1 i(t)}{l_m} \tag{2.1}$$

where H is the time varying magnetic field strength, N_1 is the number of turns in the primary winding, l_m is the mean flux path and $i(t)$ is the time varying current. The magnetic field strength is decided from these parameters. The number of turns and mean flux length is from the geometry of the coils.

This signal is then fed from a power supply which applies H, to achieve a desired B or H. The current is measured from a low inductance shunt resistor, or the field can be measured by means of field coils. The control computer system then calculates the magnetic field strength of the primary winding's from the measured voltage [28].

$$H(t) = \frac{N_1}{R_n l_m} u_1(t) \Rightarrow H_i = \frac{N_1}{R_n l_m} u_{1i} \tag{2.2}$$

where, R_n is the shunt resistor and u_1 is the primary voltage. This is to control the applied magnetic field strength H. The voltage measurement is digitised by a 14 bit resolution AD converter and adjusted by automatic dynamic adjustments for high precision.

To measure the magnetic flux or the polarisation B, the secondary winding voltage is used. Using Faradays law, the induced voltage is integrated to calculate the B,

$$\frac{dB}{dt} = -\frac{u_2(t)}{N_2 A_m} \Rightarrow B(t) = \frac{1}{N_2 A_m} \int_0^t u_2(t) dt \tag{2.3}$$

where u_2 is the secondary voltage, N_2 is the turns of secondary winding, A_m is the cross section of the electrical steel, and B is the polarisation or magnetic flux density without air flux.

The specific power loss in the material can be calculated using

$$P_{total}[W/kg] = \frac{f}{\rho} \int_0^T H dt \frac{dB}{dt} = \frac{f}{\rho} \int_0^T H dB \tag{2.4}$$

where, P_{total} is the specific power loss, f is the frequency, ρ is the density of the material, H is the magnetic field strength, T the time of a period, and dB is the time varying magnetic flux density.

To control a perfect sinusoidal flux density, the control loop ensures that the voltage at the secondary side has a form factor of 1.111 with an accuracy of 1% according to the IEC standard. The form factor is calculated from the RMS voltage

$$V_{RMS} = \sqrt{\frac{1}{T} \int_0^T \hat{V}^2 Sin(\omega t)^2 dt} \tag{2.5}$$

where T is the period time, ω is the angular frequency in radians per second. The form factor also use the rectified average voltage

$$V_{Average} = \frac{1}{T} \int_0^T \hat{V} Sin(\omega t) dt \tag{2.6}$$

by then dividing the RMS voltage with the rectified average voltage

$$FormFactor = \frac{V_{RMS}}{V_{Average}} \tag{2.7}$$

if the form factor is 1.111 the signal has perfect sinusoidal shape.

2.2.1 Epstein Frame

The Epstein frame is built up of four primary winding's and four secondary winding's, where primary and secondary each are connected in series. The primary winding can also be called magnetizing winding and the secondary winding can be called voltage winding. The measurements are based on the equations described in previous section. As mentioned before the Epstein frame follows the international standard IEC60404-2 [3]. Where the electrical steel under test is has a specific width of 30mm and length of 280mm.

The electrical steel under test is placed in the Epstein frame as in Figure 2.3, where two parallel sides have the rolling direction of the steel and the other two sides have the transverse/cross direction of the steel. The corner is overlapped as in the right side of Figure 2.3. The number of electrical steels must be a multiple of four and the total weight of the test must at least be 240g [3].

The Epstein frame is controlled from the software MPG Expert, where the desired magnetic field strength, magnetic flux density, frequency and shape is chosen. The air flux in the Epstein frame is compensated with a mutual inductor in the center of the winding.

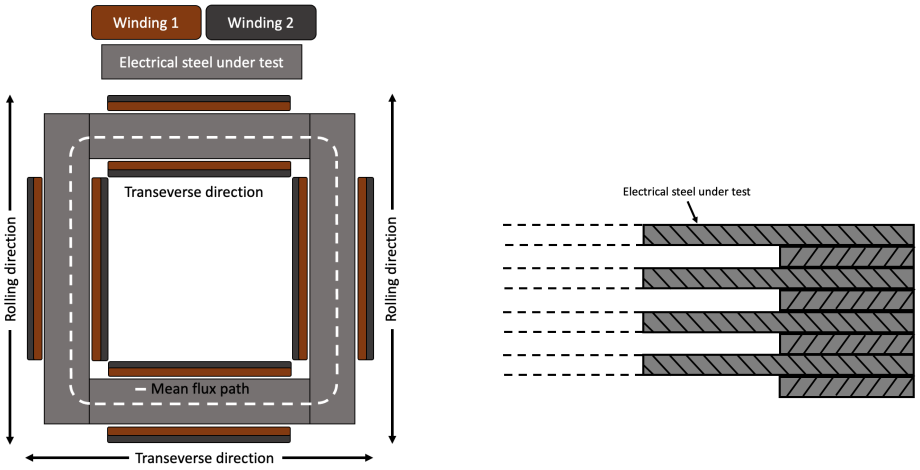

(a) Top view Epstein. **(b)** Side view steel Epstein.

Figure 2.3: Epstein frame, top view and side view.

Since the Epstein is overlapped in the corners there consists some leakage flux there, which is the main disadvantage with the Epstein frame.

2.2.2 Single Strip Tester

Another measurement method that is standardized by the IEC, is the Single Sheet Tester. The Single Sheet Tester follows the standard IEC60404-3 which describes how a measurement should be performed and what accuracy is needed [5]. The

Single Sheet Tester uses large electrical sheets with the minimum length of 500 mm.

In this thesis the measurement sensor is a Single Strip Tester, this sensor is based on the same IEC standard as the sheet tester but is used for smaller strips of the size 280 mm by 30 mm. The Single Strip Tester can also be called a SST.

The SST, as the name states only tests a single sheet of electrical steel, which is pressed between two yokes with very low losses (<1 W/kg at 1.5 T and 50 Hz) of ferromagnetic material.

The SST can be built in two different ways, with the primary and secondary winding around the yoke, or with the primary and secondary around a bobbin and the electrical steel sheet under test. This can be seen in Figure 2.4. Same as the Epstein the SST consist of an inductor that compensates for the air flux.

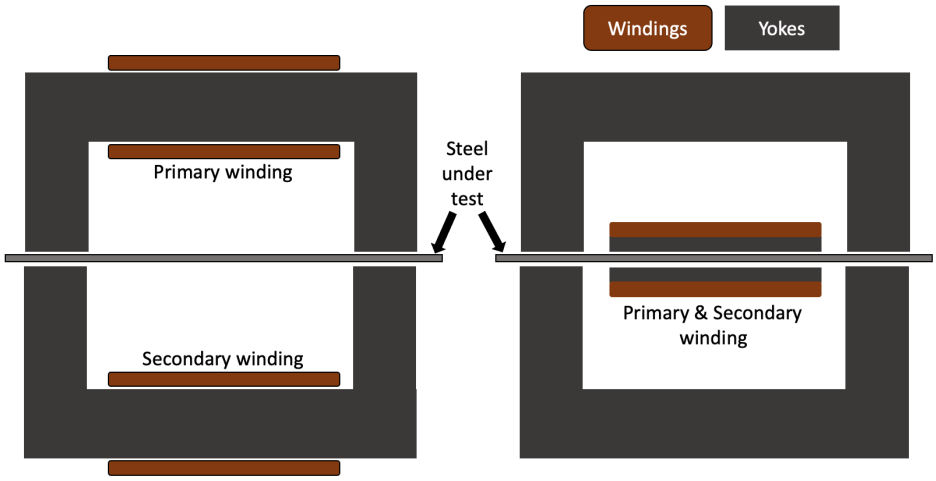

Figure 2.4: Side view, Single Strip Tester measurement device.

Just as the Epstein frame, the SST is controlled from the software MPG Expert.

2.2.3 Other Measurement Methods

There are more measurements methods to measure the magnetic properties of an electrical steel. Such as the Rotational Single Sheet Tester (RSST) and Ring Core (Toroid tester). These will not be used in this thesis work.

2.3 Iron Losses in Electrical Machines

The losses in an EM can be divided into different sections depending on where the losses occur. The losses that occur in the electrical steel is often referred as core

losses or iron losses. These losses can sometimes be split into three categories, hysteresis losses, eddy current losses and excess losses.

This separation of losses is mainly for engineering purpose and the fittings does not justify the physical phenomena [29]. All iron losses come from Joule heating which is from the change of magnetization in the material which creates movements in the magnetic domains and thereby induce eddy currents which produce Joule heating [30].

2.3.1 Hysteresis Losses

When applying a specific magnetic field strength to an electrical steel, the material is highly non-linear and also depends on the past magnetic field strength, this is known as hysteresis and can be seen in Figure 2.5. This results in the typical hysteresis loop of an electrical steel. The integral of the hysteresis loop is known as loss per cycle, as in (2.4).

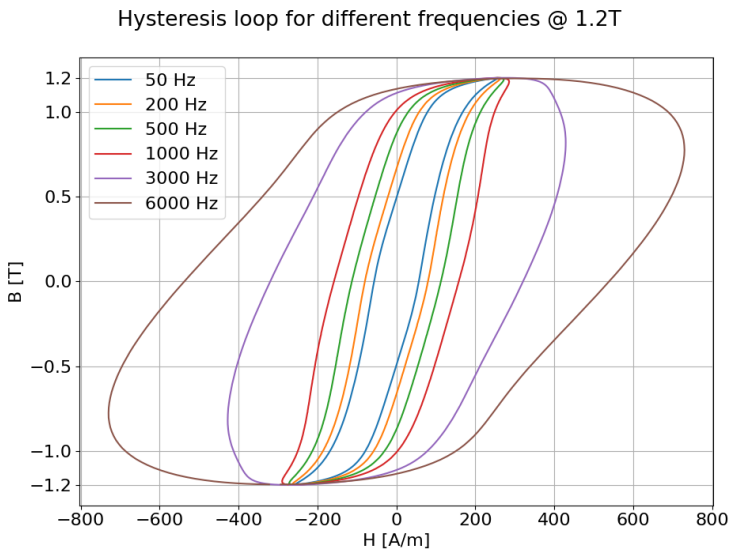

Figure 2.5: Hysteresis loop of NO25-1350H for different frequencies.

A fully demagnetized electrical steel, is built up of domains which have different magnetization but the sum of the magnetization in the electrical steel i zero. When applying an external magnetic field, these domains starts to change its magnetization and aligning with the external magnetic field [31].

As the external magnetic field is increasing, larger domains are created where the magnetization direction is following the external magnetic field. When the external magnetic field starts to reduce, the domains will start to return to its reversible state, but when the external field is reduced to zero the electrical steel is now magnetized, this is known as remanence magnetization.

Continuing reversing the external magnetic field with changed direction, the sum of the electrical steel can now be fully demagnetized but the applied external field is negative, this is called the coercive field.

The hysteresis losses originate from these domain motion and changes. When domains with different magnetization direction get caught between the external field direction and neighbouring direction it could lead to fast jumps in the magnetic flux, these are also called Barkhausen jumps [31]. According to Lenz law, these fast changes could induce eddy currents which would create eddy losses.

2.3.2 Eddy Current Losses

According to Faraday's law a time varying flux will induce a time varying voltage within the electrical steel which in its case create eddy currents circulating [31]. These eddy currents themselves induce a magnetic field which counters the original field as per Lenz law.

Since these eddy currents are dependent on the rate of change of the magnetic flux they increase with frequency and thus increasing the width of the hysteresis loop and the magnetic field strength coercivity (H_c), which can be seen in Figure 2.5. By separating the core into thinner laminations these circulating eddy currents are limited [32].

2.3.3 Excess Losses

For some loss separation models a third component is considered, which is called excess loss. These losses are contributed from the change in the domain walls when the external magnetic field is applied. These changes in the domain walls leads to local changes in B which creates eddy currents which in it turn create Joule losses [31].

Barkhausen jumps create the excess eddy currents and create extra Joule losses [33]. At lower frequency levels excess losses are small compared to hysteresis and eddy current losses so they are usually neglected [32].

2.4 Iron Loss Models

When designing electrical machines, one has multiple different options for choosing iron loss models. There are both models for predicting losses in time domain as well as frequency domain. In this section a few different loss models will be described.

2.4.1 Steinmetz Loss Model

The classical Steinmetz equation (SE) is an iron loss model that can be used for sinusoidal flux distribution [34] and is calculated as

$$p_{loss} = C_m f^{\alpha} \hat{B}^{\beta} \tag{2.8}$$

where p_{loss} is the specific power loss in W/kg, f is the frequency, $\hat{B}$ is the peak flux density, and C_m, α, β are fitting coefficients for the model.

Since the model is only applicable for sinusoidal flux distributions the model has been modified and extended to the Modified Steinmetz Equation [35] (MSE),

$$p_{loss} = C_m f_{eq}^{\alpha-1} \hat{B}^{\beta} f \tag{2.9}$$

where the the new equivalent frequency, f_{eq} can be calculated as

$$f_{eq} = \frac{2}{\Delta B^2 \pi^2} \int_0^T (dB/dt)^2 dt \tag{2.10}$$

here, the ΔB is the difference between max B and min B. This modified version, however has lower precision when the fundamental frequency signal is not as big compared to its harmonics.

Continuing on with more modified versions of the Steinmetz, is the Generalized Steinmetz Equation (GSE) [29], which has an increased DC-bias sensitivity. The GSE can be calculated as

$$p_{loss} = \frac{1}{T} \int_0^T C_m \mid \frac{dB}{dt} \mid^{\alpha} \mid B(t) \mid^{\beta-\alpha} dt \tag{2.11}$$

where C_m, α, β are the fitting coefficients. This model is sensitive to third harmonics in the B due to that the peaks occurs at the same time as the fundamental.

Minor loops, which are created by harmonics in the H and B, increase the losses in the electrical steel. To take into account these minor loops, some modifications were made to the GSE and the improved Generalized Steinmetz Equation [36] was created. This splits the minor and major loops and calculated each separately with

$$p_{loss} = \frac{1}{T} \int_0^T C_m \mid \frac{dB}{dt} \mid^{\alpha} \mid \Delta B \mid^{\beta-\alpha} dt \tag{2.12}$$

where ΔB is the peak to peak flux density for a major or minor loop in the hysteresis loop. A downside with this model is that it does not take the DC bias into consideration due to that the ΔB is just the peak and does not take into consideration the time domain.

2.4.2 Jordan's Loss Model

Another loss separation model is called Jordan's loss model [29], and can be calculated as

$$P_{loss} = k_h f \hat{B}^2 + k_{ec} f^2 \hat{B}^2 = P_h + P_e \tag{2.13}$$

here, the losses are split into two part hysteresis losses P_h, and eddy current losses (dynamic) P_e. The curve fitting coefficients k_h is for the hysteresis, and k_{ec} is for eddy currents. As seen the in the equation, the hysteresis losses are proportional to the frequency while the eddy currents are proportional to the frequency squared.

At 0 Hz and low frequencies only the hysteresis losses are present due to that no eddy currents can be present. This loss model is not as accurate for silicon iron alloy (SiFe), but works good for nickel iron (NiFe) [29].

Based on Maxwell's equations, the coefficient k_{ec} can be calculated [37] as

$$k_{ec} = \frac{\sigma \pi^2 d^2}{6\rho} \tag{2.14}$$

where σ is the conductivity, d is the thickness of the electrical steel, and ρ is the density of the material.

2.4.3 Bertotti's Loss Model

Another model which is similar to the Jordan's model, is the Bertotti's loss model. The model is adding a third term, called excess losses.

$$P = k_h f B_m^2 + k_{ec} f^2 B_m^2 + k_{ex} f^{1.5} B_m^{1.5} = P_h + P_{ec} + P_{ex} \tag{2.15}$$

where k_{ex} is the fitting coefficient for the excess losses. The sum is now the hysteresis loss, eddy current losses and excess losses (P_{ex}) together.

Bertotti [38] added the fitting coefficient for these excess losses which was a statistical model with magnetic objects and domain wall movements, as in

$$k_{ex} = \sqrt{A V_0 \sigma G} \tag{2.16}$$

where A is the cross section area of the material, V_0 is the statistical distribution of the local coercive fields, σ is the conductivity of the material, and G is a dimensionless coefficient of the eddy current damping, $G \approx 0.136$.

2.5 Pulse Width Modulation

Pulse Width Modulation (PWM) compares a desired reference signal to a triangular carrier wave which has a higher frequency compared to the reference signal. This frequency is referred as switching frequency. The PWM signal can be designed in two different ways, using bipolar or unipolar switching. For bipolar switching, when the reference signal is larger than the carrier wave the PWM is positive and when its lower the PWM is negative. This creates very fast polarity switching from positive to negative [39].

For unipolar switching, the PWM signal switches between zero to positive when the reference signal is positive and for second half of period when reference signal is negative the PWM switches between zero and negative values [39].

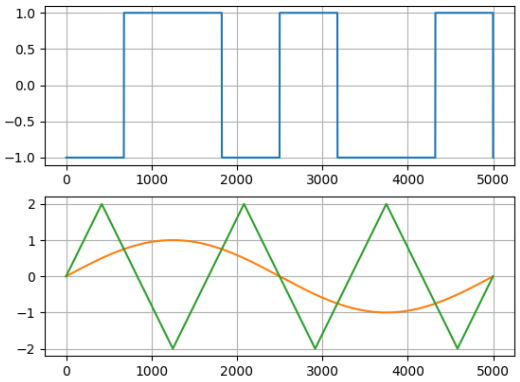

Figure 2.6: $m_f = 3$ and ma = 0.5 PWM signal. Orange: Reference wave, Green: Carrier wave, Blue: PWM

In the frequency spectrum, the signals lower frequency content is removed and the harmonics are surrounded of the integer multiples of the switching frequency.

There are two parameters that commonly determines the shape of the PWM signal. The first parameter, the modulation index of a PWM signal determines if the signal is under-, full- or over-modulated. The modulation index m_a [39] is calculated as

$$m_a = \frac{V_{Reference}}{V_{Carrier}} \tag{2.17}$$

where $V_{Reference}$ is the peak reference sinusoidal signal and $V_{Carrier}$ is the peak carrier wave signal.

The three different region of modulation index can be explained as

1. $m_a > 1$, Over modulation
2. $m_a = 1$, Full modulation

3. $m_a < 1$, Normal modulation

If the m_a is over modulated, the PWM signal look more like a square wave and the higher frequency content is shifted to lower order harmonics. Over modulated is not desired due to these lower order harmonics which are harder to filter out.

The second parameter is frequency modulation ratio m_f [39] which corresponds to the switching frequency in relation to the fundamental frequency. So for a m_f of 3, the carrier wave has a frequency 3 times the fundamental frequency. The m_f can be calculated as,

$$m_f = \frac{f_s}{f_1} \tag{2.18}$$

where f_s is the switching frequency, f_1 is the fundamental. A normal modulated PWM signal with a m_f of 3 can be seen in Figure 2.6

3

Experimental Testing and Measurement Setup

3.1 Electrical Steel Samples

All the measurements were done with a modified version of the electrical steel NO25-1350H [4] from Surahammar and all electrical steel used in this report is referred to this. The virgin BH curve and specific power loss from the data sheet can be seen in Figure 3.1.

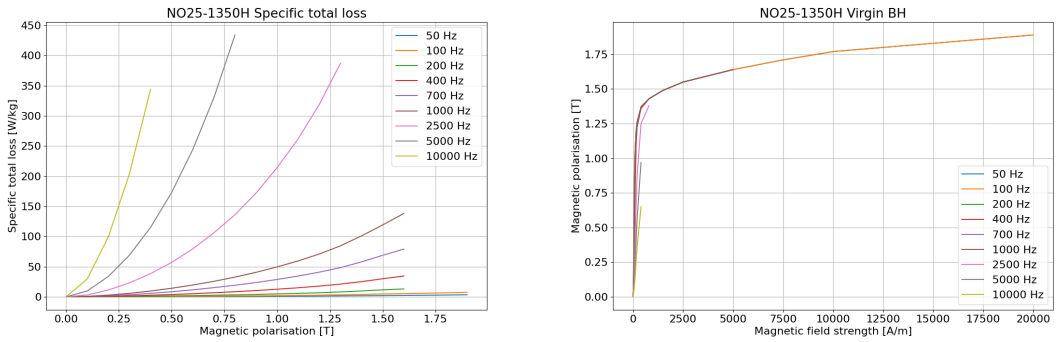

(a) Specific power loss curve. **(b)** Virgin BH-curve.

Figure 3.1: Plotted data from NO25-1350H data sheet.

To test the cut degradation a few different steel samples with different amount of laser cuts was developed. Since the Epstein needs several steel sheets as explained in 2.2.1, the SST and Epstein have different cut sample types due to the practicality of loading the samples in the Epstein.

The steel samples in this report is only cross/transverse direction steel, due to availability.

The steel samples in this thesis is cut using a TruLaser Cell 7040 from TRUMPF [40], with an applied pressure of 11 bar, power of 600W and a speed of 1320 mm/min. As described in Section 2.1.1.2, the cutting degradation of steel is dependent on type of cutting, and more specific for laser the speed, power and pressure. So the degradation in this thesis is tied to the laser specifications above.

3.1.1 Epstein Frame Test Samples

For the Epstein frame, the test consisted of 6 different samples. These samples can be seen in Figure 3.2, the standard Epstein sample (STD) of 30mm by 280mm is there as size reference. From sample A-F the number of cuts increase from 2 to 12 cuts, all while still keeping the same effective cross section. The total number of samples loaded into the Epstein frame for each cut sample was selected to be 20.

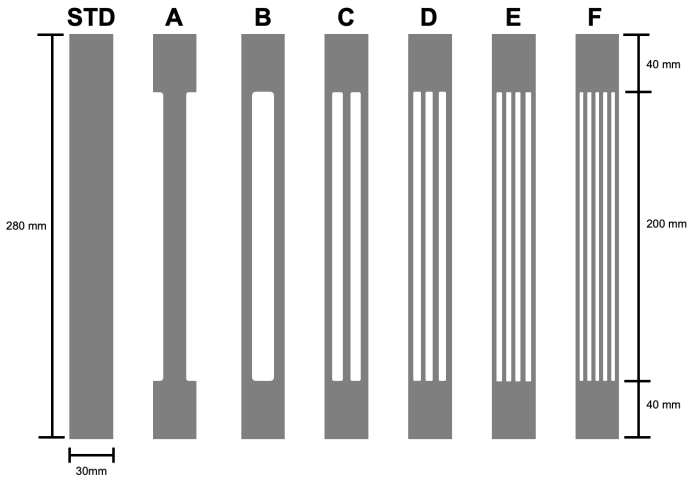

(a) Top view of Epstein cut samples.

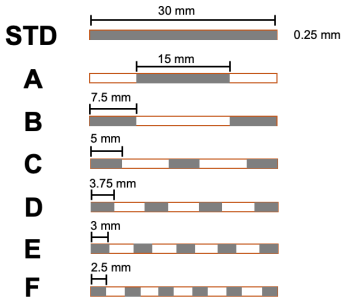

(b) Mid-point cross section view of Epstein cut samples.

Figure 3.2: Descriptive view of cut test samples used for measurements.

From the IEC standard IEC6404-2 [3], the effective mass of the test specimen is calculated from the effective magnetic length, total material length and material weight, in order to take into account where the flux passes through, since it wont go all the way out into the corners of the material.

$$m_{eff} = \frac{l_m}{4l} \cdot m \tag{3.1}$$

where m_{eff} is the effective mass, l_m is the effective magnetic path, l is the length of one sample, and m is the total mass in kg. The effective magnetic path is the same but the effective mass has changed, which can be seen in Figure 3.3.

Since the test material is no longer the standard size of 30mm, some sort of effective mass of the material had to be calculated which is under the effective magnetic path, since this is what the equipment calculates the magnetic flux density and specific power loss from. By setting that the $l = l_m/4$ one can then only take the total mass into consideration to decide the active mass under test,

$$l = \frac{l_m}{4} \Rightarrow m_{eff} = m \tag{3.2}$$

The effective mass is then calculated using the volume of the sample which is underneath the l_m, and the density of the material. Using the volume and density of

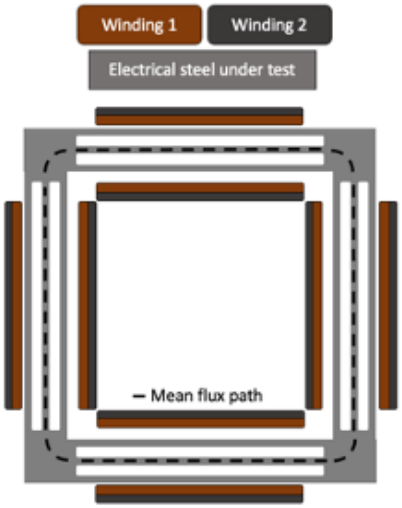

Figure 3.3: The effective magnetic path is the same but the effective total mass has changed.

the material under the effective magnetic path the active mass could be calculated as

$$Volume = t_x \cdot w_x \cdot l_x \tag{3.3}$$

where t_x is the thickness of the material, w_x is the width of the material, and l_x is the length of the material. The x is the for each section underneath l_m.

Table 3.1: Epstein sample total weight and weight difference from sample A.

Sample	STD	A_{ref}	B	C	D	E	F
Total weight [g]	313.86	199.61	197.48	196.73	195.24	196.12	193.79
Weight diff. [%]	N/A	0	-1.07	-1.44	-2.19	-1.75	-2.92
No. Cuts	2	2	4	6	8	10	12
Width [mm]	30	15	7.5	5	3.75	3	2.5

The active mass of the material for the Epstein frame was then calculated to be 153.9 grams which will be used for all samples. This weight compared to its actual measured weight which can be seen in Table 3.1. In the same table, the difference compared to the reference sample A can also be seen, with a max difference of about 3% for sample F. Knowing this information this can be considered when comparing the different samples later.

The cross section in IEC6404-2 [3] is calculated from mass of the material

$$A = \frac{m}{4l\rho_m} \tag{3.4}$$

which resulted in an effective cross section of 21.54 mm^2. The same effective weight

and cross section is kept for all samples from A to F.

3.1.2 SST Test Samples

For the SST measurements, a different set of steel samples was tested. These samples were cut all the way through the material, as can be seen in Figure 3.4, and the total surface area was the same for all samples.

Since the total surface area was the same as a standard steel sample, 30x280mm, no extra calculations was needed for these measurements. These samples were only possible to test in the SST since it only requires one sample between the yokes, and it would not be practically possible create 20 of these samples to the Epstein.

Since the samples are different and the measurement method is different the Epstein tests and SST tests should be compared with caution. The main result comparison of the two tests was to see that they followed the same degradation curves, but actual H, μ_r and P_s can not be compared directly.

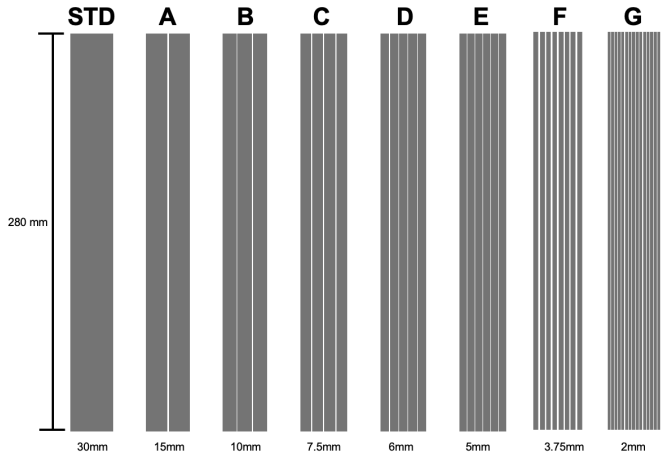

(a) Top view of SST cut samples.

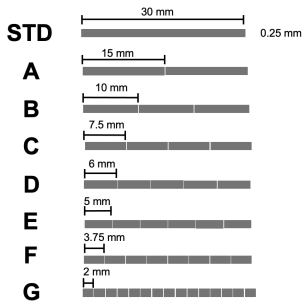

(b) Cross section view of SST cut samples.

Figure 3.4: Descriptive view of SST cut test samples used for measurements.

The total weight of the different samples, and the weight difference can be seen in Table 3.2. Sample G which is the smallest sample, with a width of 2mm, has the highest weight difference of 8%, the smaller the sample width the harder it is to keep accurate.

Table 3.2: SST samples total weight and weight difference from sample STD.

Sample	STD_{ref}	A	B	C	D	E	F	G
Total weight [g]	15.55	15.54	15.21	15.37	15.20	15.19	14.7	14.23
Weight diff. [%]	0	-0.06	-2.19	-1.16	-2.25	-2.32	-5.47	-8.49
No. Cuts	2	4	6	8	10	12	16	30
Width [mm]	30	15	10	7.5	6	5	3.75	2

3.2 Epstein Test Setup

The measurement setup for this report consists of four different Epstein winding configurations. The different limits for the winding's are concluded in Table 3.3. Each winding setting could handle different fundamental frequencies, magnetic field strength and flux density.

Table 3.3: Epstein frame lab setup.

Winding No.	Frequency limit	H limit	B limit
700/700	DC, AC 3-150 Hz	5-30,000 A/m	0.001-2 T
200/200	150-2000 Hz	Max 5000 A/m	0.005-1.8 T
60/60	1-5 kHz	5-3000 A/m	0.001-2 T
20/20	2.5-20 kHz	Max 1000 A/m	0.001-2 T

3.3 SST Test Setup

The SST test setup in this report is with its limits is specified in Table 3.4. The SST only consists of one winding which had a wide range.

Table 3.4: SST lab setup.

Winding No.	Frequency limit	H limit	B limit
90/90	50-10,000 Hz	1-10,000 A/m	0.001-2 T

3.4 MPG Expert PWM

Two parameter settings are needed for the PWM signal in the software MPG Expert. First is the parameter, number of pulses or Fha, which is the same as the frequency modulation ratio in (2.18).

$$Fha = m_f \tag{3.5}$$

The second setting to control the PWM signal is mark to space ratio (Vr). Vr is can be calculated from the inverse of the modulation index m_a from (2.17), which is

$$Vr = \frac{1}{m_a} \tag{3.6}$$

So by setting Vr to 2, the modulation index would be 0.5 and the PWM would operate in the normal modulation. While setting Vr to 0.5 would indicated a modulation index of 2 which corresponds to a over modulation and the harmonic content

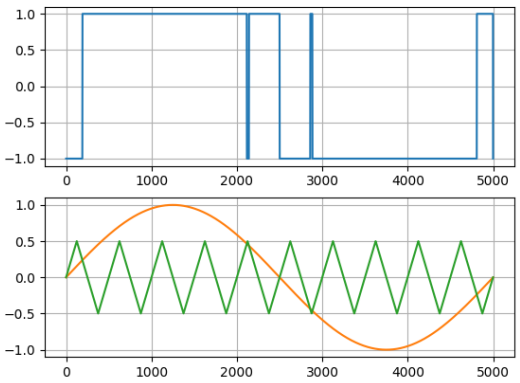

Figure 3.5: Fha = 10 and Vr = 0.5 PWM signal, over modulation. Orange: Reference wave, Green: Carrier wave, Blue: PWM

is shifted to lower frequencies. This can be seen in Figure 3.5 where a over modulation is applied.

4

Equipment Testing, Repeatability and Sensitivity to Parameters

4.1 Determine Repeatability of Measurements

To get a better understanding of the accuracy of the measurements using Epstein and SST a repeatability test was performed. The test was performed both on the SST and Epstein for multiple frequencies and different steps with B as reference.

Using standard deviation of each point and relative standard deviation, the result could be analyzed and take conclusions. The standard deviation was calculated using

$$SD = \sqrt{\frac{1}{N}\sum_{i=1}^{N}(x_i - x_{mean})^2} \tag{4.1}$$

where, SD is the standard deviation, N is the number of tests, x_i is the measured point and x_{mean} is the mean of the measured points. The relative standard deviation can then be calculated with

$$RSD = \frac{SD}{x_{mean}} * 100 \tag{4.2}$$

where RSD is the relative standard deviation.

4.1.1 Repeatability of SST Measurements

The repeatability test for the SST was performed over two different frequencies, 50 Hz and 1000Hz. The test was performed using steps in B and as high as the SST would allow for that specific frequency.

The specified B values and number of tests per frequency is shown in Table 4.1. Each test was performed a total of 30 times, and after every 10 tests the steel was removed from the SST and rested for 5 minutes. The steel that was used here was the STD steel from Figure 3.4 and the weight can be seen in Table 3.2.
Once all the tests were performed, the relative standard deviation and the scattering of the measurements was analyzed. Where the relative standard deviation was calculated using equations (4.1) and (4.2). The result for 1000Hz is summarized in table 4.2.

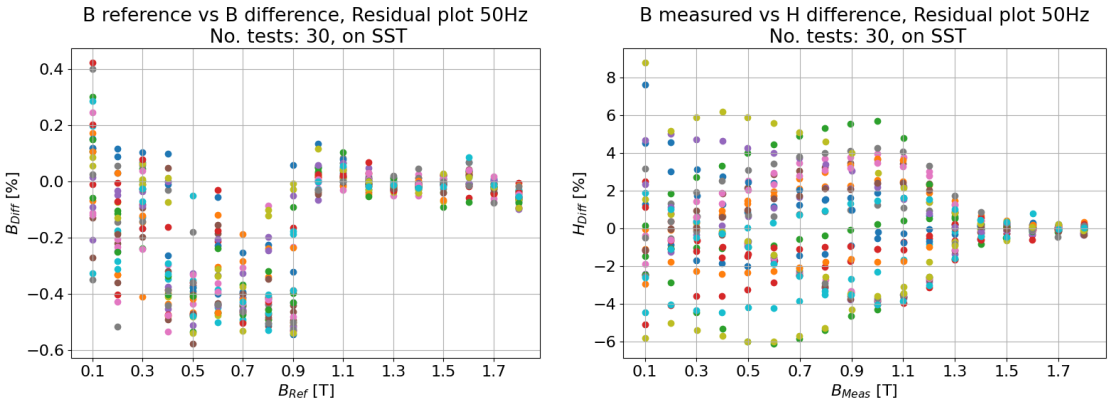

(a) B_{ref} vs $B_{diff}[\%]$ scatter plot. **(b)** B_{ref} vs $H_{diff}[\%]$ scatter plot.

Figure 4.1: Residual plots for SST measurements of 50 Hz

Table 4.1: SST repeatability test.

Frequency [Hz]	No. Tests	B_{start} [T]	B_{step} [T]	B_{stop} [T]
50	30	0.1	0.1	1.8
1000	30	0.1	0.1	1.4

Table 4.2: SST repeatability test RSD result.

Frequency: 1000 Hz			
B [T]	B_{RSD} [%]	H_{RSD} [%]	Ps_{RSD} [%]
0.1	0.04	4.59	4.14
0.2	0.06	4.3	3.21
0.3	0.04	4.35	2.75
0.4	0.03	4.26	2.41
0.5	0.02	4.15	2.14
0.6	0.03	3.93	1.87
0.7	0.04	3.66	1.63
0.8	0.04	3.28	1.4
0.9	0.03	2.76	1.14
1.0	0.04	2.16	0.89
1.1	0.04	1.54	0.68
1.2	0.16	1.13	0.42
1.3	0.17	1.82	0.43
1.4	0.05	0.66	0.26

The result for 50Hz is summarized in Table A.1 in the Appendix. Another way of confirming the accuracy of the measurements was to use scatter plots and see the

difference from the reference value for the B and difference from the mean values for the H. This can be seen in Figure 4.1, where on the x axis the reference steps is plotted from 0.1 T to 1.8 T, and the difference for each measurement point can be seen on the y axis. The difference in reference and measured value of B is very low, meaning a good measure of repeatability.

The SST performed well during the repeatability test and no noticeable problems was found. The full result regarding the SST repeatability test can be seen in Appendix A.

4.1.2 Repeatability of Epstein Measurements

The repeatability test was also performed for the Epstein frame. As described in chapter 2.2.1, the Epstein measurement setup is consisting of 4 different winding settings, each of them able to handle different fundamental frequencies of the flux density. To ensure the accuracy of the Epstein, all of the different winding settings was tested. The different frequency and winding setup can be seen in Table 4.3, where each test consist of steps in B from 0.1 T to highest allowed value. These tests were performed 50 times each for each winding except winding 20, which was performed 30 times due to the high losses at the higher frequency which results in high heat, and thereby taking long time between each measurement.

After 10 consecutive tests, the steel samples were removed and rested for 5 minutes. This was repeated until all 50 tests were completed. The steel used for this test was the 20 samples of STD steel from Figure 3.2 with the weight as in Table 3.1.

Table 4.3: Epstein repeatability test.

Frequency [Hz]	Epstein winding	No. Tests	B_{start} [T]	B_{step} [T]	B_{stop} [T]
50	700	50	0.1	0.1	1.9
100	700	50	0.1	0.1	1.9
400	200	50	0.1	0.1	1.6
1000	60	50	0.1	0.1	1.4
2500	20	30	0.1	0.1	1.3

By looking at the relative standard deviation (RSD) as in the SST tests, some conclusion of accuracy could be drawn. The result from the repeatability tests can be seen in Appendix A.

4.1.2.1 Sensitivity to Settings

The Epstein with winding 200, 60 and 20 performed excellent with RSD around 0.04% for B. For the Epstein 700 larger variations was found. As seen in Figure 4.2, around 1.4 T when the electrical steel starts to saturate, the measured B deviates from the reference B. Looking at the figure, 45 out of the 50 tests where lower

measured value compared to the reference value.

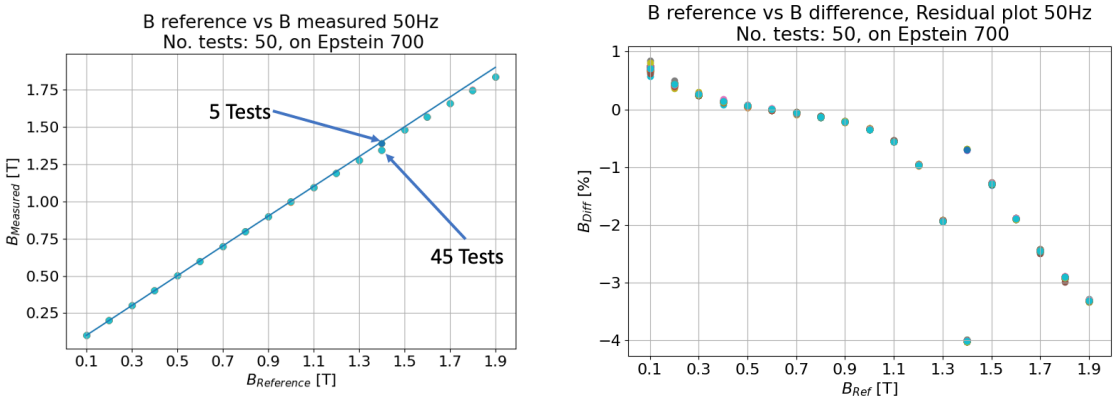

(a) B_{ref} vs $B_{Measured}$ scatter plot. **(b)** B_{ref} vs $B_{diff}[\%]$ scatter plot.

Figure 4.2: Scatter plots for Epstein 700 measurements of 50 Hz

Analyzing the results further, the 5 out of the 50 tests that was closer to the reference value all had a sinusoidal voltage at the secondary winding and a form factor of around 1.111 which is desired. The 5 tests out of the sequence were number 20, 29, 35, 39, and 41. In Figure 4.3, the test number 20 and 21 can be seen. Where test 20 has a sinusoidal polarisation and test 21 has a distorted polarisation.

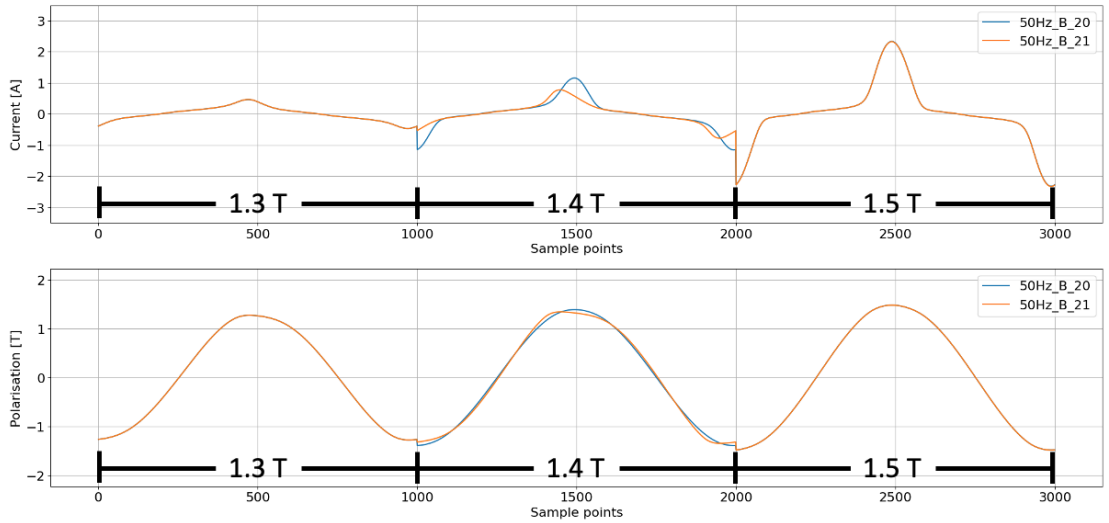

Figure 4.3: Current and polarisation of EP700 at 50 Hz, with reference 1.3T, 1.4T, 1.5T.

Since the electrical steel samples were removed every 10th test, this seems like a randomized consequence. By analyzing further the controller setting for the Epstein 700 had to be tuned. This is because the current was not allowed enough harmonics to keep the secondary voltage a perfect form factor. By changing settings in the

controller for the Epstein 700, the accuracy problem was fixed, which can be seen in Figure 4.4.

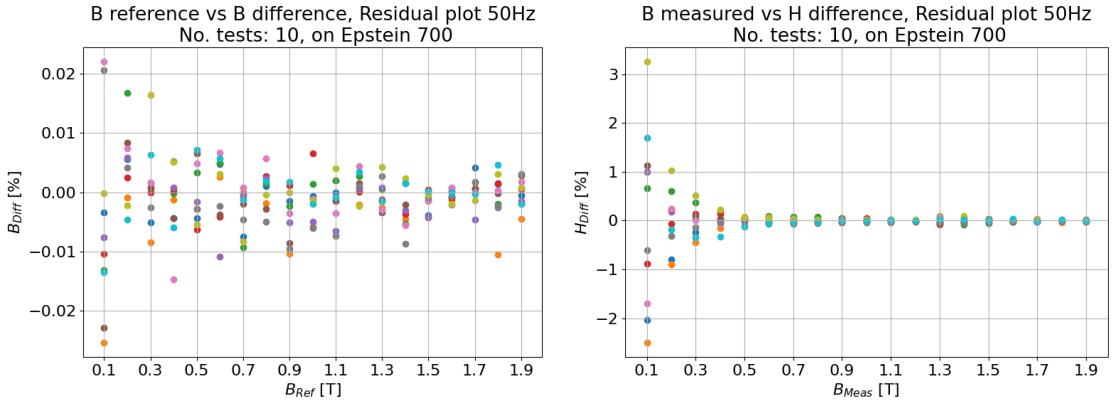

(a) B_{ref} vs $B_{diff}[\%]$ scatter plot. **(b)** B_{ref} vs $H_{diff}[\%]$ scatter plot.

Figure 4.4: Scatter plots for Epstein 700 measurements of 50 Hz, after regulator settings fixed.

The conclusion from the repeatability test was that at least 5 tests should be performed for a reliable measurement result. By taking 5 measurements and then comparing the results and removing any outliers, then taking the average of the results an accurate measurement could be accomplished.

4.2 Recreation of Data Sheet

To try both using H and B as reference steps for Epstein frame, and to test the comparability to others measurement, the data sheet for NO25-1350H [4] was recreated. The steps of B from the data sheet was 0.1T to 1.9T with step size 0.1T. And the steps in H was from 20 to 20000 A/m, with different step sizes that can be seen in the data sheet [4]. These steps was recreated for different frequencies as well, 50 Hz, 100 Hz, 200 Hz, 400 Hz, 700 Hz, 1000 Hz, 2500 Hz, 5000 Hz, and 10000 Hz. See the data sheet for exact measurement points [4]. For some frequencies even higher steps of B and H was possible.

The steps in H is used to create the virgin BH-curve, while the steps in B is used for the specific power loss curve which can be seen in Figure 3.1.

The results from the measured tests can be seen in Figure 4.5, for the lower frequency levels, 50Hz and 100Hz, the difference at higher B is significantly larger, as much as 24% increase. For the higher frequencies 200Hz-10kHz the measured results is closer to the data sheet. All the measured power loss in the electrical steel was also larger compared to the data sheet, with up to 33 % increase which can be seen in Figure 4.6

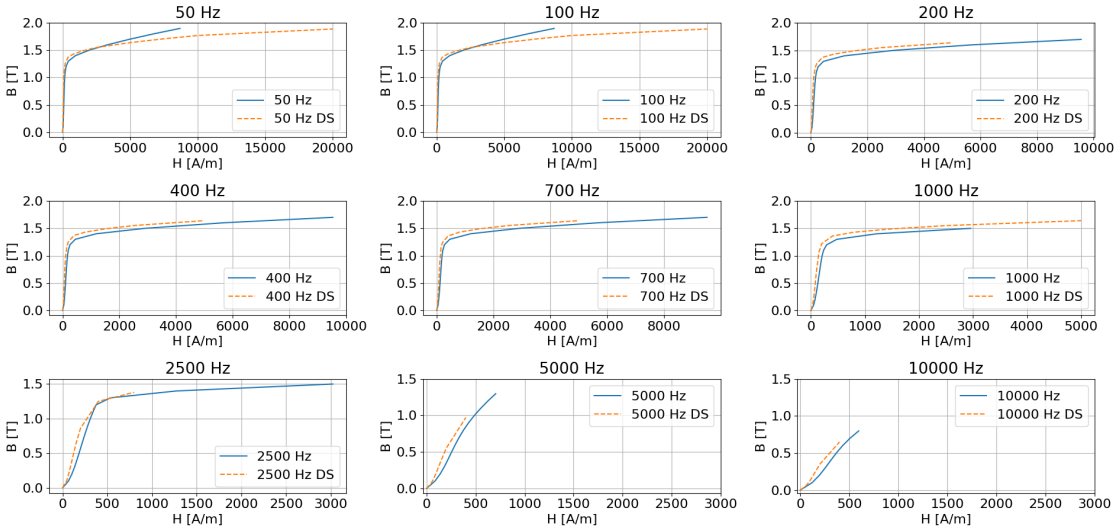

Figure 4.5: Virgin BH curve for different frequencies. Dashed: Data sheet, Solid: measured

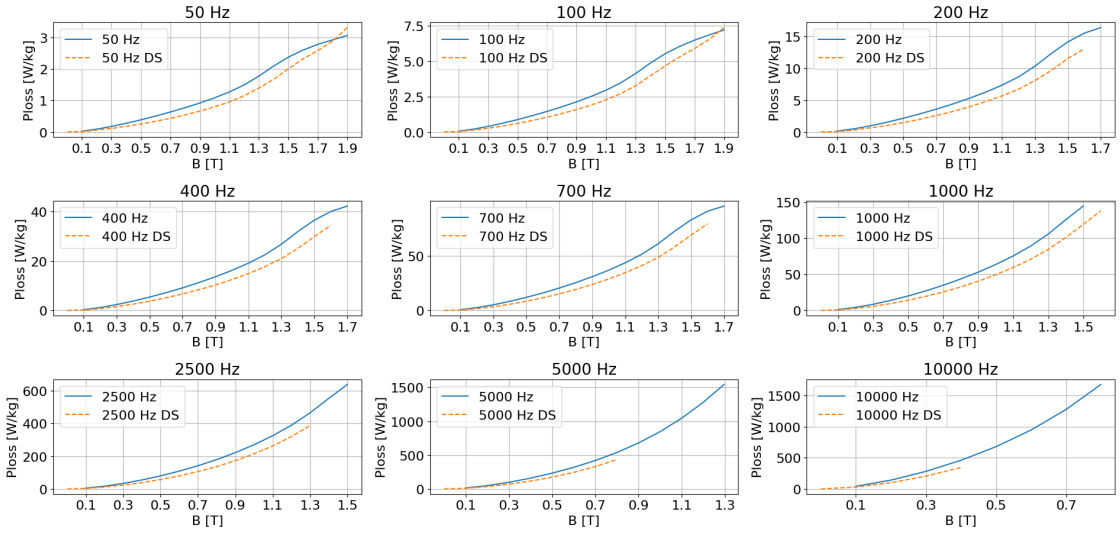

Figure 4.6: Specific power loss curve for different frequencies. Dashed: Data sheet, Solid: measured

The result may however not have to be considered wrong. First, the steel used in this thesis is a modified version of the N025-1350H, so the magnetic properties is not exactly the same. Second, the measured steel in this test was only cross direction steel. When performing the industry standard measurement with Epstein for example a data sheet, the steel is both rolling direction as well as cross direction as explained in 2. This being said, continuing with measurements one should take this result into consideration.

4.3 Epstein and SST Comparison

Since the Epstein and SST have different cut samples due to the practicality of loading the samples, a good test would be to see how a standard sample, STD in 3.2, would compare between SST and Epstein measurement.

The SST has a wide frequency range, and the Epstein uses different winding's for different fundamental frequencies, it would be a good test to check one fundamental frequency per winding and compare with the SST. The frequencies tested was 50, 400, 2500 and 10000 Hz. The measurements showed very similar trend so the results from the 400 Hz frequency will be shown here.

In Figure 4.7, the virgin BH curve and the resulting permeability is shown. It can be seen that the relative permeability with SST is lower for all measured points compared to the Epstein, but most drastic around the peak of the permeability.

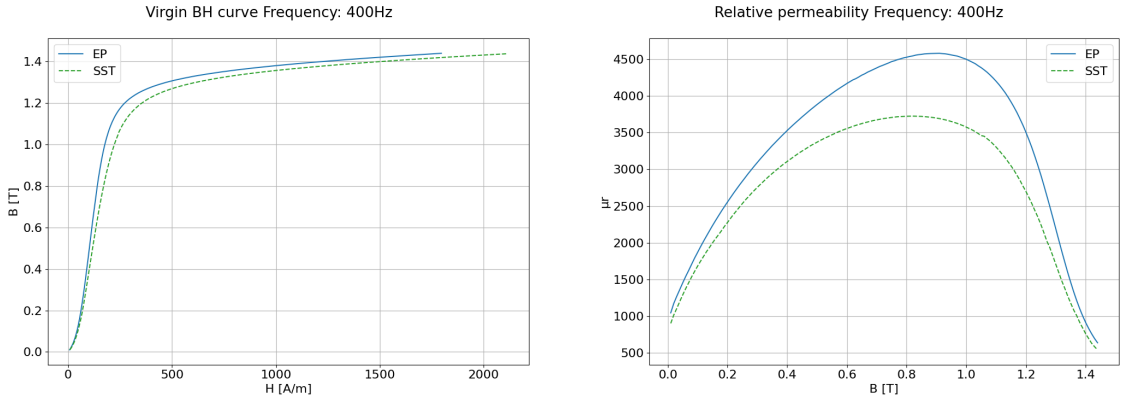

(a) Measured Virgin BH curve 400 Hz. Solid: Epstein, Dashed: SST.

(b) Measured Permeability curve. Solid: Epstein, Circle: SST.

Figure 4.7: Comparison of SST and Epstein using a standard sample STD at 400 Hz.

Instead looking at the difference in percentage between the SST and Epstein as in Figure 4.8, it can be seen that the largest relative difference is around 1.2-1.3 Tesla. The difference in these results might be because of the amount of material that is excited. Since the SST only needs one steel lamination the material might get saturated earlier and the flux is going through the air instead. Which could also be the reason for the lower permeability.

The last figure is looking at the measured specific power loss in the material. This can be seen in Figure 4.9, where the difference between the Epstein and SST can also be seen.

Conclusion from these tests are that the Epstein and SST is very hard to compare with one another. To say which equipment is more accurate is also very hard to say.

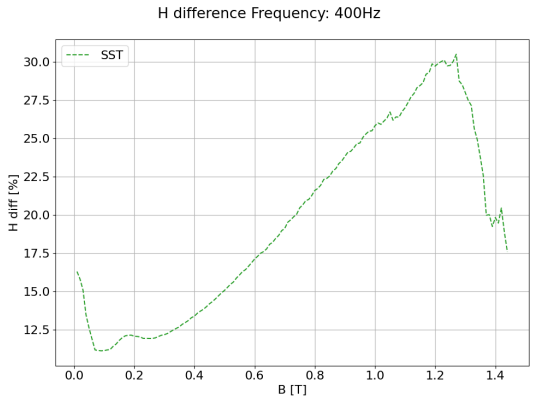

(a) $(H_{SST} - H_{EP})/H_{EP}$, between Epstein and SST at 400 Hz.

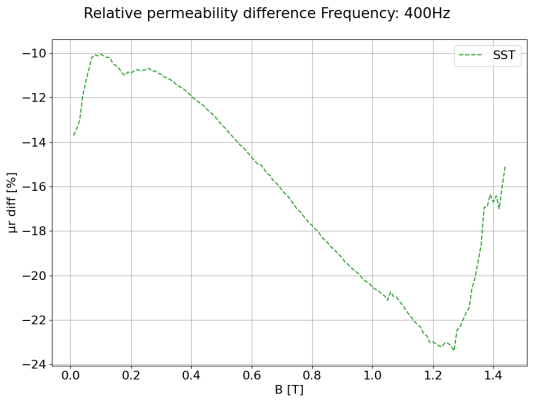

(b) $(\mu_{rSST} - \mu_{rEP})/\mu_{rEP}$, between Epstein and SST at 400 Hz.

Figure 4.8: The difference between SST and Epstein measurements at 400 Hz.

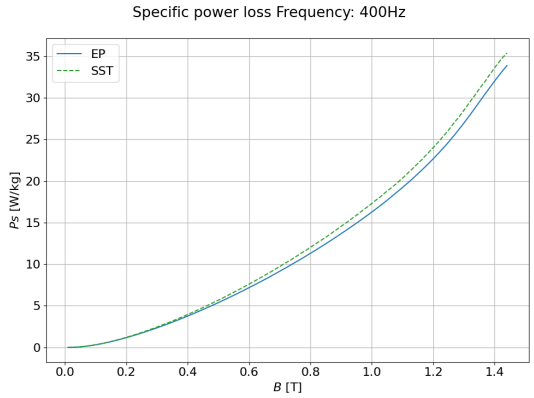

(a) Measured Specific power loss. Solid: Epstein, Dashed: SST.

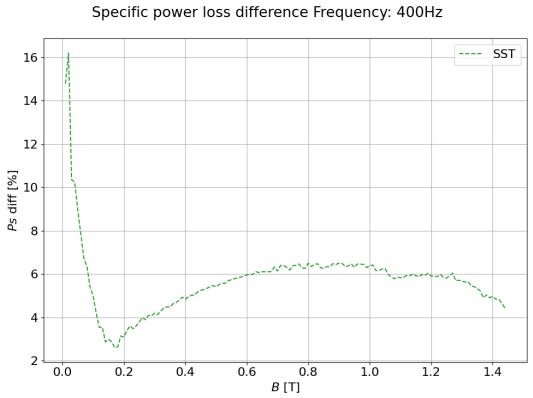

(b) $(P_{SST} - P_{EP})/P_{EP}$, between Epstein and SST at 400 Hz.

Figure 4.9: The difference between SST and Epstein measurements at 400 Hz.

But the result at lower B levels would be expected to be closer to each other, while the higher B levels might differentiate more. When comparing the SST and Epstein later in this thesis, its important to remember that even using the standard sized sample the result is different. But using the SST to check that the same pattern is happening in the Epstein and SST samples could be possible since one is comparing the increase from reference measurements.

4.4 Loss Separation for Sinusoidal Feeding

To get a better understanding of the different iron losses that happens in the electrical steel, and to try some iron loss models, a test was performed comparing the Jordan's loss model (2.13), and Bertotti's loss model (2.15).

4.4.1 Jordan's Loss Model

Starting with Jordan's loss model, the test was performed with reference steps in B between 0.5 and 1.2 T to be in a more "linear" region of the permeability. It was measured over different frequencies from 5 Hz up to 1000 Hz. By using (2.13) and dividing both sides with f a linear relation between power loss in Ws/kg and frequency can be found,

$$\frac{P_{loss}}{f} = k_h \frac{f}{f}\hat{B}^2 + k_{ec}\frac{f^2}{f}\hat{B}^2 \tag{4.3}$$

$$\frac{P_{loss}}{f} = k_h \hat{B}^2 + k_{ec} f \hat{B}^2 \tag{4.4}$$

By extrapolating (4.3) to 0 Hz, one could determine the hysteresis losses since there would not be any eddy currents at 0 Hz. Then by subtracting the hysteresis losses from the measured specific power loss one could separate the hysteresis and eddy current losses,

$$P_{ec} = P_s - P_{hy} \tag{4.5}$$

Using (4.3) and (4.5) in a linear curve fitting and loss separation which can be seen in Figure 4.10, and the resulted loss separation can be seen in figure 4.11.

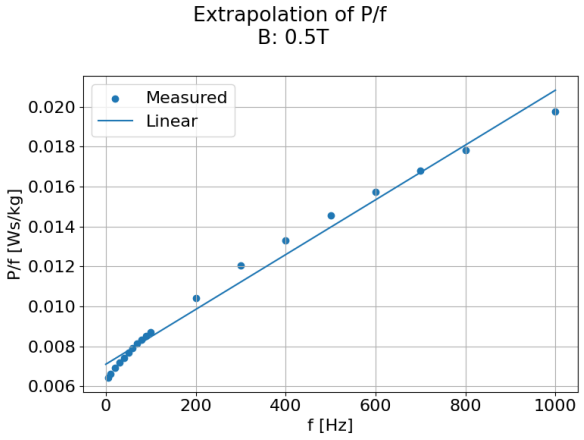

Figure 4.10: Linear regression of P/f and Jordan's loss model.

As seen in Figure 4.10, the measured points of loss at different frequencies are not quite as linear as expected for this loss separation. This leads to that losses for lower

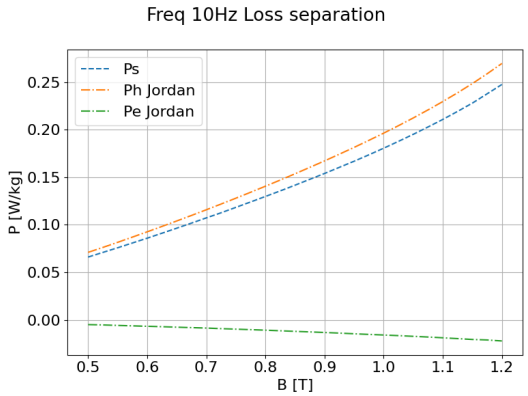

(a) Loss separation 10 Hz.

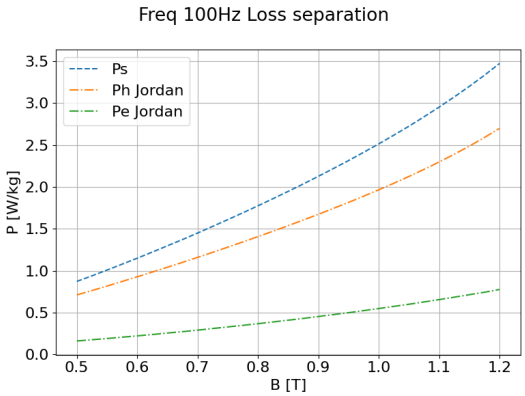

(b) Loss separation 100 Hz.

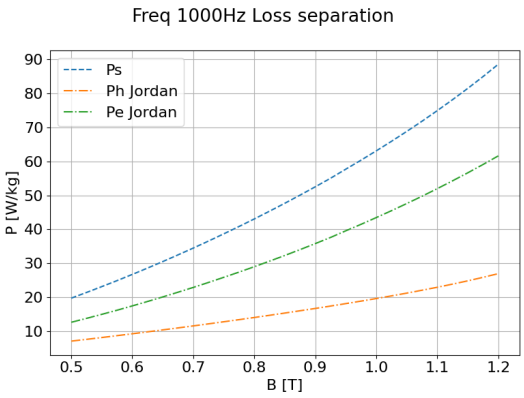

(c) Loss separation 1000 Hz.

Figure 4.11: Loss separation for different frequencies using Jordans model. Dashed is specific power loss in W/kg, Orange is hysteresis loss, and green is eddy current loss.

frequencies the hysteresis loss part is larger than the measured total loss, leading to negative eddy current loss. Which can be seen in Figure 4.11.
This also correlates to what was mentioned in Chapter 2, that the Jordan model does not quite align with SiFe steel while it is more accurate for NiFe steel.

4.4.2 Bertotti's Loss Model

The second loss separation test was with the Bertotti's loss model. Using the same data as for the Jordan's loss model, and the equation (2.15), dividing both sides with frequency

$$\frac{P_{loss}}{f} = k_h \frac{f}{f}\hat{B}^2 + k_{ec}\frac{f^2}{f}\hat{B}^2 + k_{ex}\frac{f^{1}.5}{f}\hat{B}^{1.5} \tag{4.6}$$

$$\frac{P_{loss}}{f} = k_h \hat{B}^2 + k_{ec} f \hat{B}^2 + k_{ex}\sqrt{f}\hat{B}^{1.5} \tag{4.7}$$

one can see a relation that is not linear anymore by also depending on square root of frequency. Using same method as before, extrapolating to 0 Hz one could find

the hysteresis part of the losses. The fitting factor k_{ec} for the eddy currents is calculated as in (2.14). In Figure 4.12 one can see that the fitting is much more accurate compared to the linear fitting.

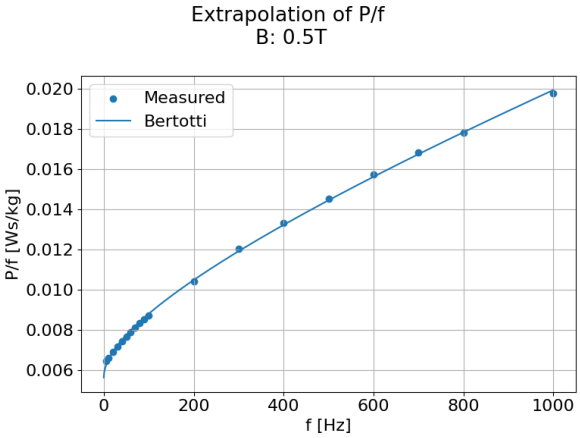

Figure 4.12: Curve fitting of P/f and Bertotti's loss model.

The loss separation can then be seen in Figure 4.13, where compared to the Jordan model, the eddy currents are no longer negative for lower frequencies and it also correlates to the theory that the eddy currents and excess losses are increasing as frequency is increasing.

Using this curve fitting results in a different k_h, k_{ec}, k_{ex} for each B level, this is complicated for certain FEM based programs that specifies the k coefficients per frequency and not per B level.

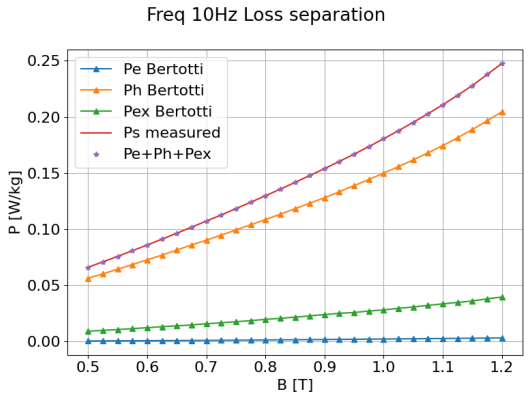

(a) Loss separation 10 Hz.

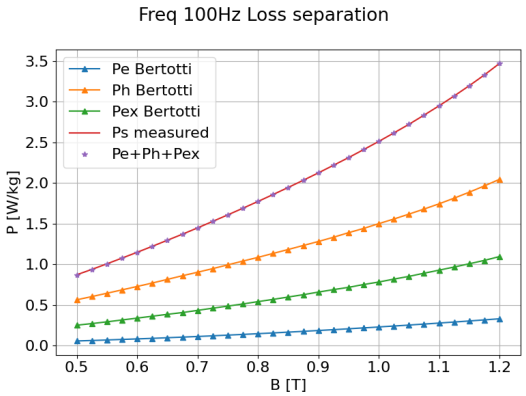

(b) Loss separation 100 Hz.

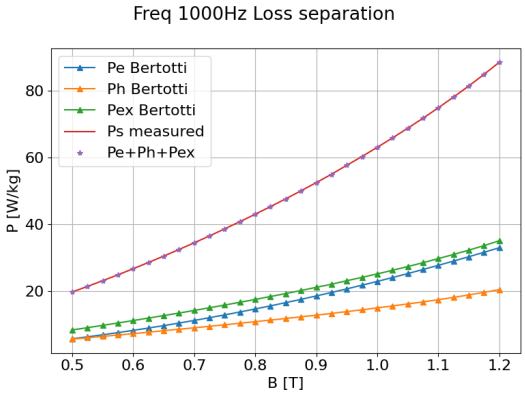

(c) Loss separation 1000 Hz.

Figure 4.13: Loss separation for different frequencies using Bertotti's model. Dashed is specific power loss in W/kg, Orange is hysteresis loss, Blue is eddy current loss and Green is excess loss.

4.5 Specifying PWM Signal in MPG Expert

As mentioned in earlier in Chapter 2.5, the PWM signal in the control software MPG-Expert can be setup in many different ways. Since the comparison of sinusoidal flux density is to be compared with a PWM feeding, a specific PWM shape had to be chosen. A test was performed, to decide three parameters of the PWM,

1. Switching technique, Bipolar or Unipolar.
2. Fh, Constant switching frequency or constant pulse ratio.
3. Vr, over-, full- or normal-modulated.

So a test sequence of different fundamental frequencies and B levels was completed as in Table 4.4. For each point sequence in the table, 12 different PWM signals was tested, which is summarized in Table 4.5.

Table 4.4: Unipolar and Bipolar testing.

Fundamental frequency [Hz]	B_{Start} [T]	B_{Step} [T]	B_{Stop} [T]
50	0.1	0.1	1.9
400	0.1	0.1	1.6
1000	0.1	0.1	1.4
2500	0.1	0.1	1.3

Table 4.5: Unipolar and Bipolar testing.

	Vr = 0.5	Vr = 1.0	Vr = 1.5
Fh = 10	Uni. & Bip.	Uni. & Bip.	Uni. & Bip.
Fh = 20	Uni. & Bip.	Uni. & Bip.	Uni. & Bip.
Fh = 30	Uni. & Bip.	Uni. & Bip.	Uni. & Bip.
Fs = 20 kHz	Uni. & Bip.	Uni. & Bip.	Uni. & Bip.

By introducing a PWM voltage over the primary winding in the Epstein, which can be seen as a large inductance, the current could theoretically be calculated from the inductance current equation

$$i_L = \frac{1}{L} \int V_L dt \tag{4.8}$$

where i_L is the inductance current, L is the inductance of the winding, and V_L is the voltage across the winding. The switching of voltage across the inductance would generate some ripple in the current, where the amplitude of the ripple depends on how much accumulation of voltage, or integral of voltage as in (4.8). This can be seen in Figure 4.14, at point 0, the voltage switches to negative polarity, leading to a decrease of current. At point 1 the voltage switches back to positive leading to

the current increasing, all the way to point 2 when it switches polarity again.

This ripple in current, leads to a ripple in magnetic field strength, which leads to a ripple in the magnetic flux density. This introduces more losses in the material, as the magnetic domains in the material has to realign with the external magnetic field which takes energy. So following this ripple in B and H, leads to the so called minor loops in the hysteresis loop of the material. Since we are introducing new smaller loops, this is increasing the area of the total hysteresis loop, meaning more losses from (2.4).

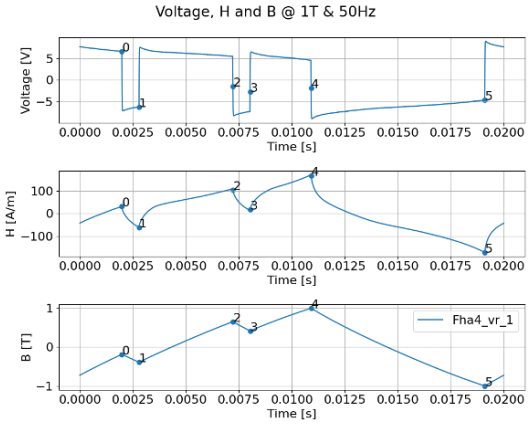

(a) Top: Voltage switching, Middle: H ripple, Bottom: B ripple.

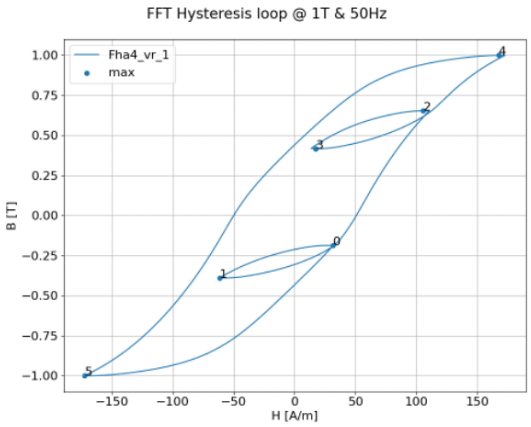

(b) Hysteresis loop with minor loops.

Figure 4.14: Visualization of how PWM introduce ripple in current and flux density, which leads to minor loops.

The width of the minor loop depends on the ripple magnitude in H, while the height of the minor loop depends on the ripple magnitude in B. At lower switching frequency, the loops have larger area, but fewer. At higher switching frequency its the inverse, minor loops have smaller area, but increased amount.

4.5.1 Unipolar Switching

The generated unipolar PWM signal which is sent to the amplifier can be seen in Figure 4.15. Here the result of increasing Vr and Fha can be observed. At the top left corner in the figure, the PWM is over modulated and has very low switching frequency, the result is some quasi square wave, with very little switching. This low switching leads to no minor loops which can be seen in the top left of Figure 4.16.

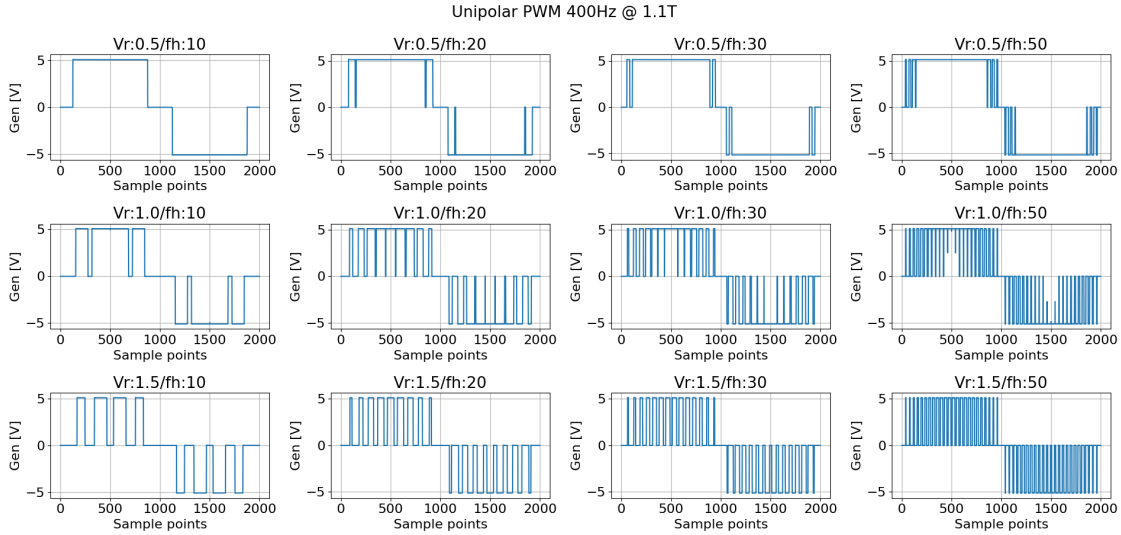

Figure 4.15: Unipolar PWM signal to amplifier for different Fha and Vr. Top: Over modulation, Middle: Full modulation, Bottom: Normal modulation.

As we increase the switching frequency, by look more to the right in the figure, it can be seen that more switching is introduced and thereby ripple in B and H leading to minor loops. Looking more closely at the normal modulation in Figure 4.16, it can be seen that the minor loops actually does not create full loops. This is due to that the unipolar does not change polarity leading to these edges instead. This is still more area compare to a pure sinusoidal, meaning more losses, but it is less compared to bipolar.

The highest Fha of 50 and normal modulation leads to more ripple, but the amplitude of the ripple is decreased due to the very fast switching, as mentioned with the Figure 4.14.

In Figure 4.17, the time averaged specific power losses can be seen. Where the different modulation techniques and Fha are compared to a reference square wave and sinusoidal wave. Similar conclusions can be drawn for Fha changing, the higher the switching frequency the lower the losses.

In same figure, moving from over modulation to normal modulation, means more losses due to more switching. All unipolar PWM leads to more losses compared to sinusoidal and square wave, but the over modulation has the closest losses to sinusoidal. The same loss conclusion can be seen over all fundamental frequencies

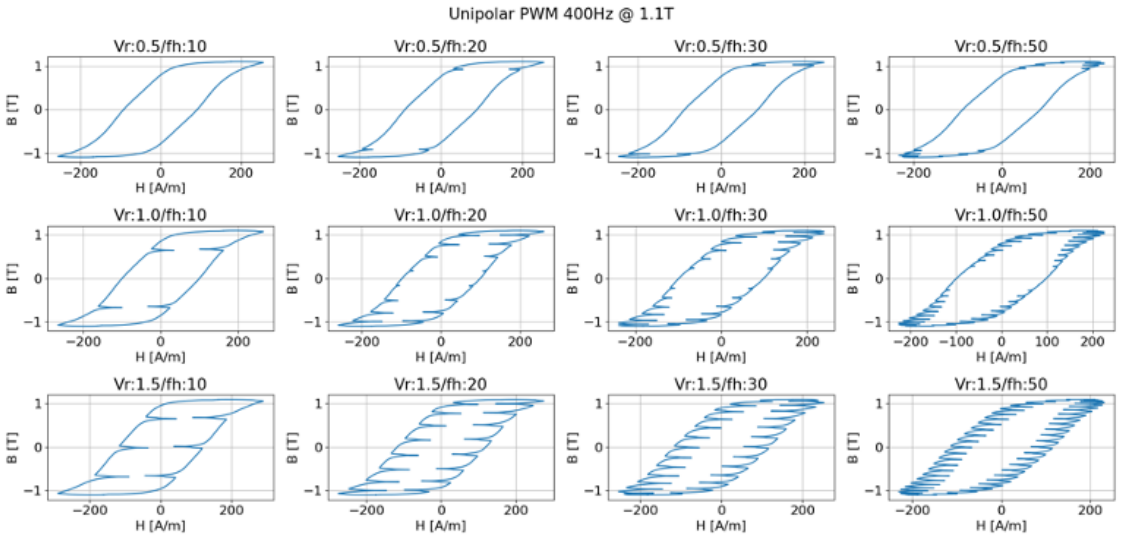

Figure 4.16: Unipolar BH curves for different Fha and Vr. Top: Over modulation, Middle: Full modulation, Bottom: Normal modulation.

tested in Table 4.4.

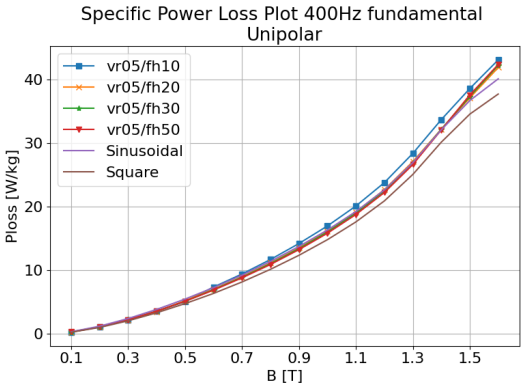

(a) $Vr = 0.5$, over modulation. Compared to sinusoidal and square wave.

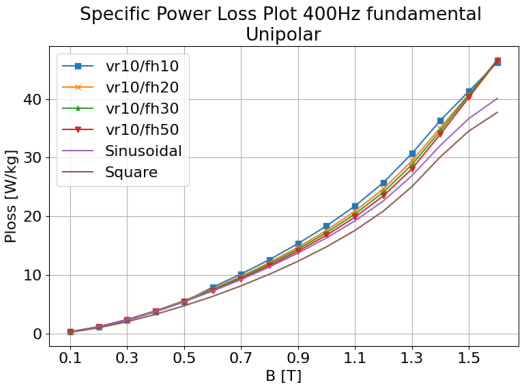

(b) $Vr = 1$, full modulation. Compared to sinusoidal and square wave.

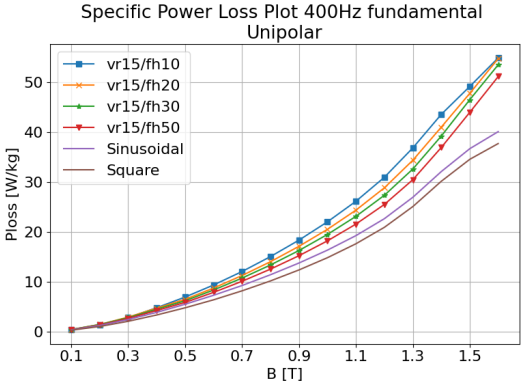

(c) $Vr = 1.5$, normal modulation. Compared to sinusoidal and square wave.

Figure 4.17: Specific power loss for different modulations and different pulse ratios, for unipolar switching.

4.5.2 Bipolar Switching

The same test was performed for bipolar PWM switching. Here the generated voltage signal which is sent to the amplifier can be seen in Figure 4.18. Where over modulation is in the top row, full modulation is in the middle row, and normal modulation is in the bottom row. Since its bipolar, the voltage switches polarity every pulse, as described earlier this will introduce more ripple in the current.

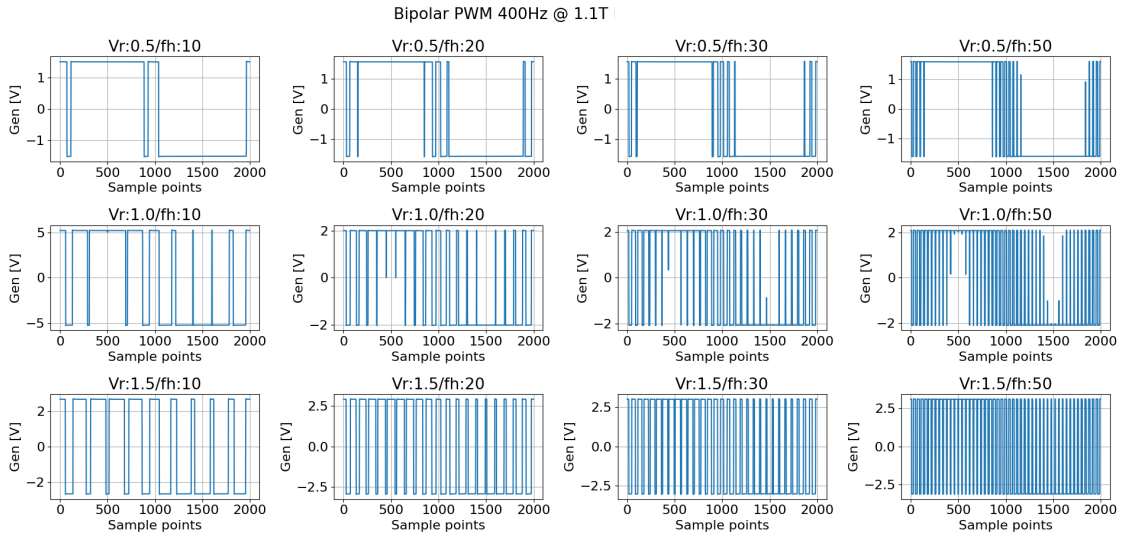

Figure 4.18: Bipolar PWM signal to amplifier for different Fh and Vr. Top: Over modulation, Middle: Full modulation, Bottom: Normal modulation.

The resulting hysteresis loops can be seen in Figure 4.19. The over modulated signal with Fha 10, leads to two minor loops. As the modulation moves from over modulation to normal modulation, more minor loops are introduced and thereby more losses. Looking instead at the higher switching frequency, Fha 50 and normal modulation, it can be noticed that the area under a minor loop is reduced drastically but the amount has increased. The height of the minor loop in this case is very small due to the small ripple in the flux density.

Analyzing the time average losses in the material instead, in Figure 4.20, the same conclusions as for the unipolar signal can be drawn. The over modulated signal has more similar losses to the sinusoidal reference. While the normal modulation has increased losses. As switching frequency is increasing the losses is reducing, still more compared to the reference sinusoidal.

Comparing the worst case losses in bipolar, Vr 1.5 and Fha, with the same signal in unipolar, the bipolar has more losses. This is the case for all the fundamental frequencies tested in Table 4.4.

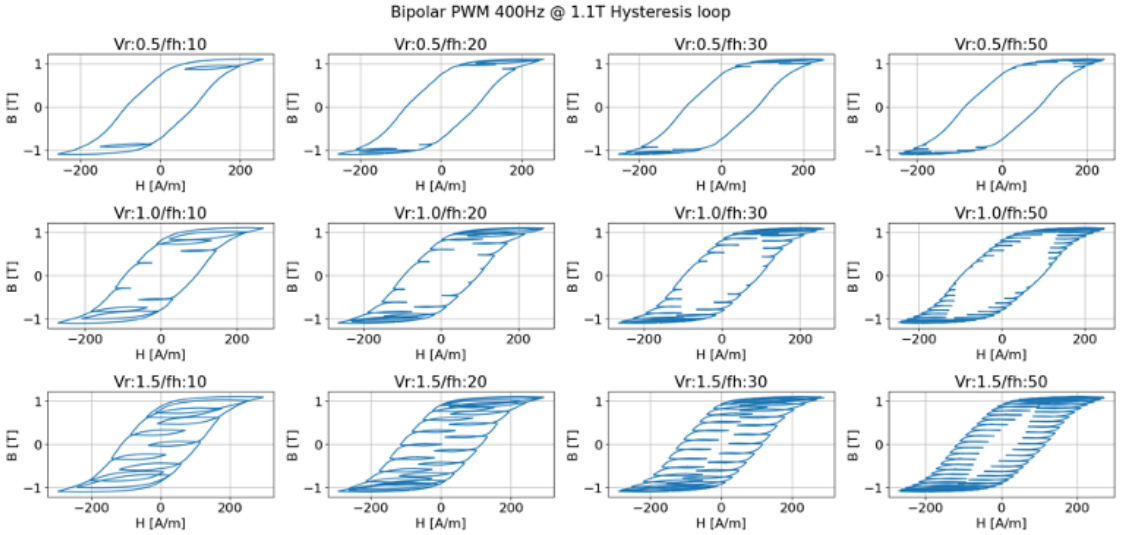

Figure 4.19: Bipolar BH curves for different Fh and Vr. Top: Over modulation, Middle: Full modulation, Bottom: Normal modulation.

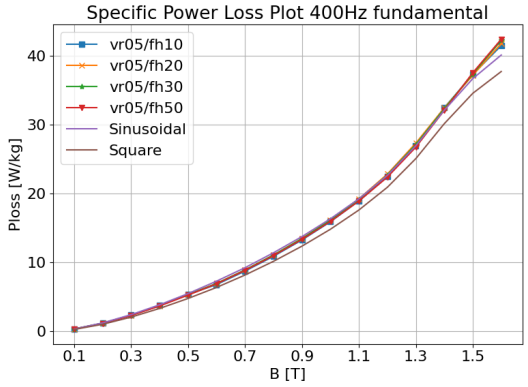

(a) Over modulation.

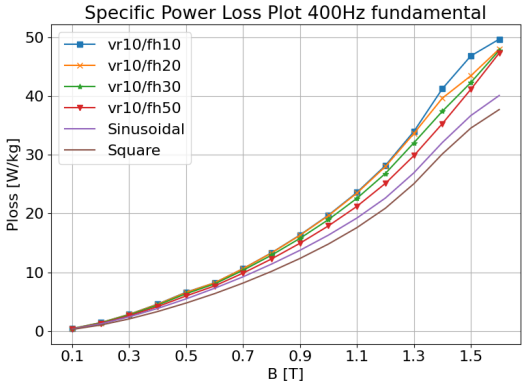

(b) Full modulation.

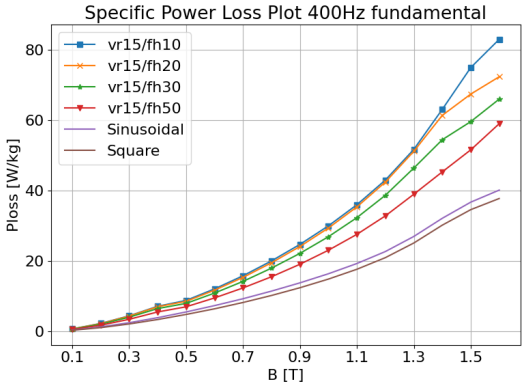

(c) Normal modulation.

Figure 4.20: Specific power loss for different modulations for different pulse ratios, bipolar switching.

5

Cut Effects with Sinusoidal Flux Density

5.1 Epstein Frame Testing

The testing of different cut samples was performed with two different sets of samples, as described in Chapter 3, one set for the Epstein frame and one set for the SST. All tests were performed using B as reference values and a step size of 0.1 Tesla. For each sample the B was increased to equipment's limitation for frequency, current and voltage.

Each sample should undergo same test sequence of different B levels and frequency levels. The desired test sequence for the sinusoidal flux density and Epstein frame can be seen in Table 5.1. The stop level of the magnetic flux density is due to the limitations of the equipment at those specific frequency points.

Table 5.1: Epstein sample test sequence.

Frequency [Hz]	Epstein winding	B_{start} [T]	B_{step} [T]	B_{stop} [T]
10	700	0.1	0.1	1.9
50	700	0.1	0.1	1.9
100	700	0.1	0.1	1.9
200	200	0.1	0.1	1.4
400	200	0.1	0.1	1.4
700	200	0.1	0.1	1.4
1000	60	0.1	0.1	1.2
2500	60	0.1	0.1	1.2
5000	20	0.1	0.1	0.9
10000	20	0.1	0.1	0.7

Using the test setup described above, the degradation in this thesis is divided into two different parts, magnetic field strength degradation H_{deg} and specific power loss degradation Ps_{deg}. Starting with H_{deg} for sinusoidal flux distribution.

5.1.1 Magnetic Field Strength Degradation

Using the data gathered from the sinusoidal flux density test, by looking at the virgin BH curve of the different frequencies and cut samples, one could right away notice that for the same level of B the different samples needed an increased amount of H. This can be seen in Figure 5.2, where 100 Hz and 400 Hz virgin BH curves have been visualized.

All the results have been analyzed but to reduce the amount of figures shown here only 100 Hz and 400 Hz will be shown. The full result figures can be seen in Appendix B.

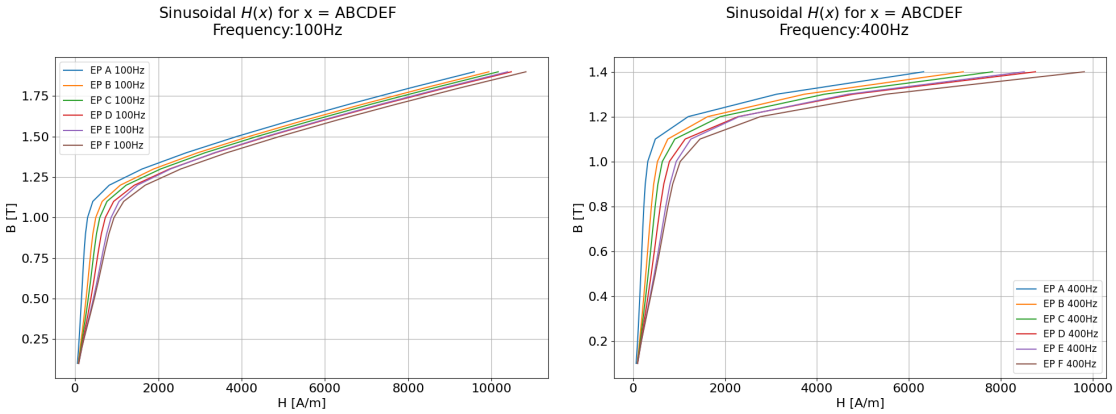

(a) $H_{Measured}$ vs B_{ref} at 100 Hz. **(b)** $H_{Measured}$ vs B_{ref} at 400 Hz.

Figure 5.1: B/H Curves for different cut samples and frequency. Where A-F is steel samples.

To relate the measured values to some sort of degradation, one could see how much extra H is needed for the same B level by taking

$$H_{deg} = \frac{H(x)}{H(A)} \tag{5.1}$$

where x is each sample from A to F, $H(A)$ is the reference sample, and H_{deg} is field strength of $H(x)$ compared to measured H for sample A. Using this equation the H_{deg} is plotted over different B levels and samples. Which can be seen in Figure 5.2. In this figure, 100 Hz and 400 Hz, can be seen, but the same degradation trend can be seen for all the frequencies mentioned in Table 5.1.

First observation that can be noticed in Figure 5.2, is that as sample width is decreasing, the H_{deg} is increasing, with sample F having the largest H_{deg}.

The second observation is that the largest increase of H happens between 0.3-1.1 Tesla, which is when the relative permeability is at largest. The μ_r can be seen in Figure 5.3. This seems reasonable since the reference sample A has its largest permeability around these values, and with the relation between $\hat{B}$ and $\hat{H}$ as in

$$\hat{B} = \mu_r \cdot \mu_0 \hat{H} \tag{5.2}$$

where μ_r is the relative permeability and μ_0 is the permeability of free space, the $\hat{B}$ and $\hat{H}$ indicates that it is calculated from the peak values. The largest degradation of the material would be at the highest permeability of the reference material.

The third observation is that at higher Tesla levels, when the material gets saturated, the degradation is not as severe, about 20% increase compare to 100-200%. This is the same for all fundamental frequencies tested.

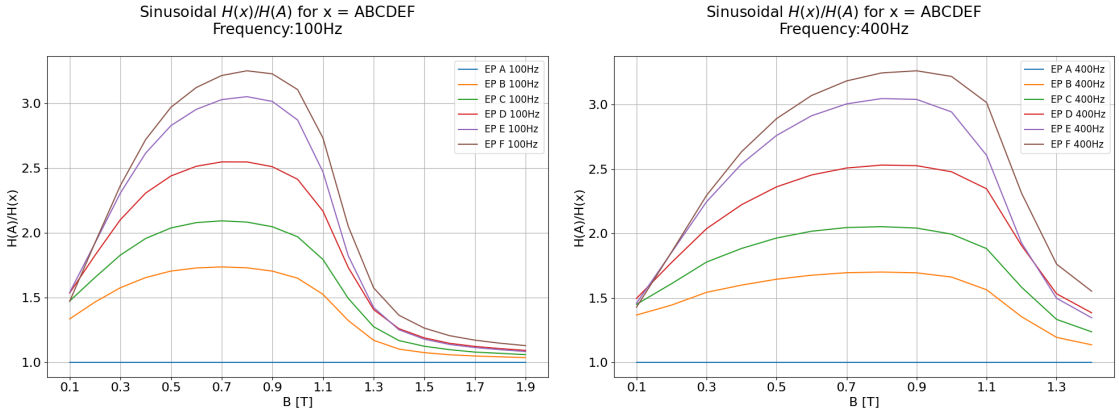

(a) B_{ref} vs H_{deg} at 100 Hz. **(b)** B_{ref} vs H_{deg} at 400 Hz.

Figure 5.2: H_{deg} for 100 Hz and 400 Hz. Where A-F is steel samples.

In Figure 5.3 where the μ_r can be seen, it can be noticed that as the sample width is decreasing, the μ_r has a much flatter curve and is more and more degraded. Just as in Figure 5.2, at higher B levels (1.3-1.9T) and as the material gets saturated the μ_r is the same for all samples.

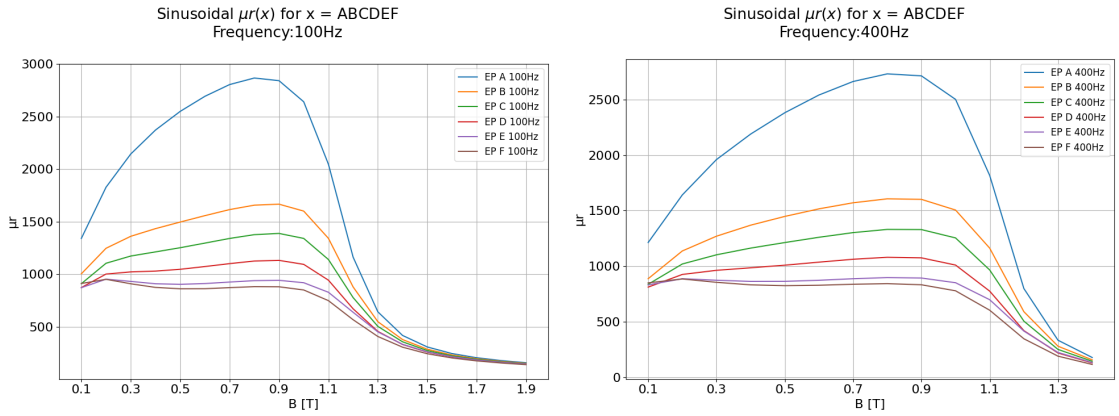

(a) B_{ref} vs μ_r at 100 Hz. **(b)** B_{ref} vs μ_r at 400 Hz.

Figure 5.3: μ_r for different cut samples and frequency. Where A-F is steel samples.

Another way of visualizing the degradation is to determine a parameter which relates the the distance from the cut edge of the samples, by dividing the width of each sample. This can done by using

$$DistfromCE = \frac{w_x}{2} \tag{5.3}$$

where CE is the distance from cut edge, w_x is the width for each sample from Table 3.1.

Using (5.3) the different distance from CE is summarized in Table 5.2. The measured and calculated values for the different samples is the time averaged values, so this "distance from cut edge" is just a simplification for visualization and not the actual values of B and H at that specific distance. But this gives an easier way of describing the degradation compared to referencing the samples as A to F, now it is described as mm from cut edge instead.

Table 5.2: Distance from cut edge calculations.

Test Sample [x]	A	B	C	D	E	F
No. Cuts	2	4	6	8	10	12
Width [mm]	15	7.5	5	3.75	3	2.5
Dist. CE [mm]	7.5	3.75	2.5	1.875	1.5	1.25

In Figure 5.4, the H_{deg} can now be seen versus the CE, the figure shows the H_{deg} for different B levels. What can be seen in this figure is that the H_{deg} has more of a exponential increase at highest degradation between 0.3-1.1 T. At very low B levels and at saturation levels the H_{deg} is more linear and not as severe. When reviewing literature regarding degradation with laser cutting, the same degradation is set over all B levels, this does not seem as accurate looking at this degradation. The degradation seems to depend on the B level.

When implementing the degradation into some FEM based program one could curve fit the degradation from cut edge for each B level. Then this would relate to the increase of H at this specific distance from the cut edge, which would correlate to some sort of degradation model.

Relative permeability is a measure of how well the magnetic material is functioning. The relative permeability is calculated from the peak of H and B, so when looking at degradation of H peak, which have been done so far, the degradation of relative permeability follows the same trend but inverse. However, a different interesting observation could be to look at the harmonic content in the H and B signal, not only the peak values. In Figure 5.5, the degradation for the H can be seen both in the frequency domain as well as the time domain.

To achieve a perfect sinusoidal B field, a distorted H field has to be applied. The frequency domain of the B signal only contains a fundamental content because its

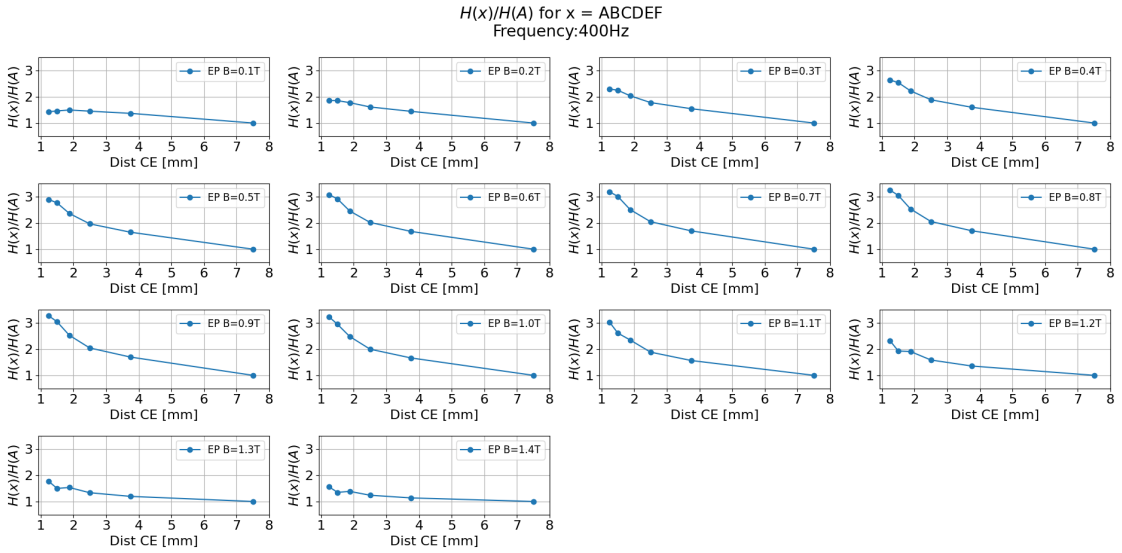

Figure 5.4: H_{deg} vs mm from cut edge, for different B levels.

controlled to be perfect sinusoidal with no harmonics. The harmonic content of the H signal is significantly lower compared to the fundamental.

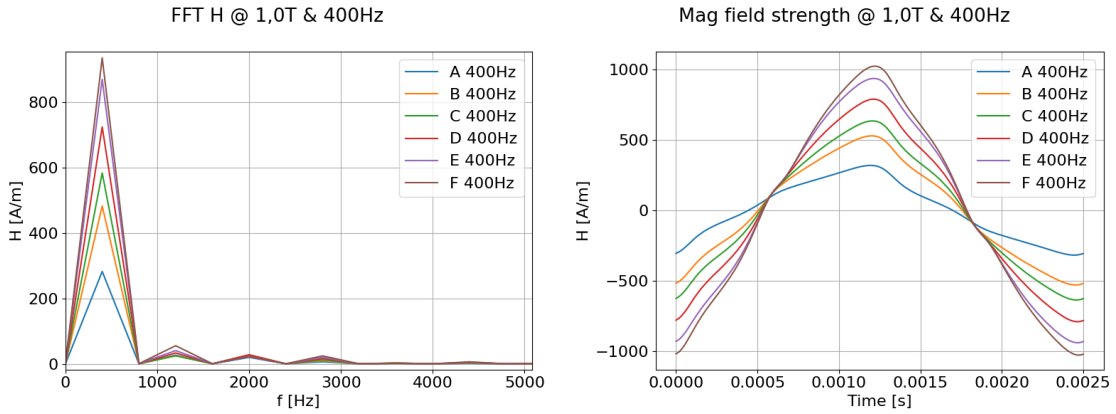

(a) H for different cut samples in frequency domain for 400 Hz fundamental.

(b) H for different cut samples in time domain for 400 Hz fundamental.

Figure 5.5: The H in frequency and time domain, for a 1.2 T sinusoidal B.

In Table 5.3 the fundamental component degradation of H can be seen. Comparing this with the overall degradation, it can be noted that the peak is about the same and at the same B levels. This will be an important comparison later when investigating the PWM signal. The PWM signal contains more harmonics, higher harmonic amplitude, and especially the harmonic around its switching frequency.

Looking at the degradation at the different fundamental frequencies can be seen in Table 5.4. In the table which is specifically for 0.7 T, it can be seen that as the fundamental frequency is increasing the degradation is actually decreasing. This

Table 5.3: H_{1x}/H_{1A} where x is samples A-F, for fundamental H_1 signal. For sinusoidal flux at 400 Hz and different B levels.

Flux density [T]	A	B	C	D	E	F
0.1	1.0	1.35	1.42	1.45	1.41	1.39
0.2	1.0	1.42	1.56	1.68	1.73	1.72
0.3	1.0	1.51	1.72	1.93	2.08	2.1
0.4	1.0	1.57	1.82	2.11	2.36	2.42
0.5	1.0	1.62	1.91	2.26	2.59	2.69
0.6	1.0	1.66	1.98	2.38	2.78	2.91
0.7	1.0	1.69	2.03	2.46	2.92	3.07
0.8	1.0	1.7	2.06	2.52	3.01	3.19
0.9	1.0	1.71	2.07	2.56	3.07	3.27
1.0	1.0	1.71	2.07	2.56	3.08	3.31
1.1	1.0	1.67	2.02	2.53	2.95	3.27
1.2	1.0	1.52	1.82	2.24	2.43	2.82
1.3	1.0	1.3	1.5	1.77	1.81	2.12
1.4	1.0	1.19	1.33	1.52	1.51	1.75

change will be discussed later in this chapter.

Table 5.4: Degradation H_{1x}/H_{1A} where x is samples A-F, at the fundamental frequency for B = 0.7 T and different tested frequencies.

Frequency	A	B	C	D	E	F
10 Hz	1.0	1.77	2.13	2.58	3.05	3.21
50 Hz	1.0	1.76	2.12	2.57	3.03	3.19
100 Hz	1.0	1.74	2.1	2.54	2.99	3.16
200 Hz	1.0	1.73	2.09	2.55	3.03	3.19
400 Hz	1.0	1.69	2.03	2.46	2.92	3.07
700 Hz	1.0	1.63	1.94	2.34	2.77	2.91
1000 Hz	1.0	1.58	1.87	2.23	2.62	2.77
2500 Hz	1.0	1.43	1.64	1.92	2.21	2.33
5000 Hz	1.0	1.31	1.48	1.67	1.91	2.0
10000 Hz	1.0	1.23	1.35	1.49	1.65	1.71

Another way of showing the severity of H_{deg} could be with a contour plot as in Figure 5.6, here its easy to see the same result with the highest degradation around 0.8 T and that at saturation levels the degradation is not as severe. The same trend follows for all frequencies from 10Hz-10kHz which can be seen in Appendix B.

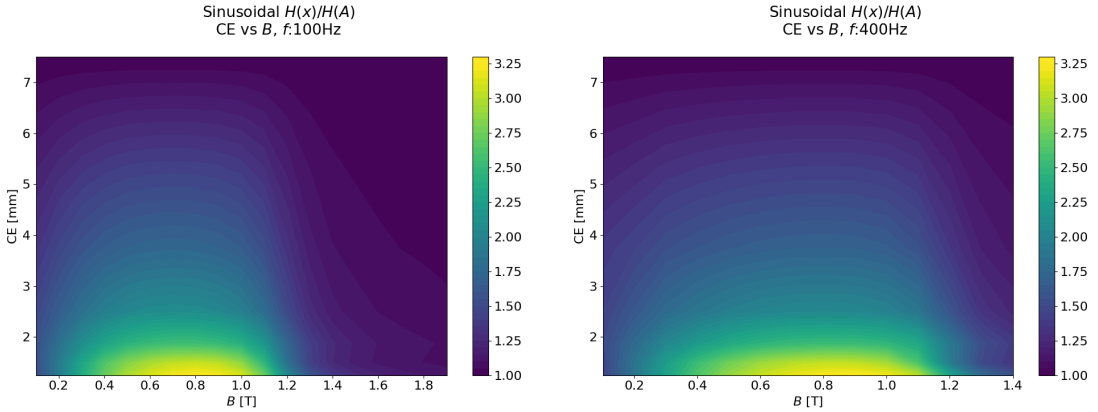

(a) B vs CE at 100 Hz. **(b)** B vs CE at 400 Hz.

Figure 5.6: B vs mm from cut edge, where intensity is H_{deg}.

It is also interesting to see at which frequencies the degradation is the highest, in Figure 5.7 the B levels of 0.5 T and 0.7 T is selected and plotted the full frequency range of 10 Hz to 10 kHz. What is noticed in this plot is that the highest degradation happens at lower frequencies. This might come from the fact that at higher frequencies the eddy currents are more severe leading to skin effect and thus the flux is pushed further to the edges and using the degraded material even though its higher permeability in the center [14].

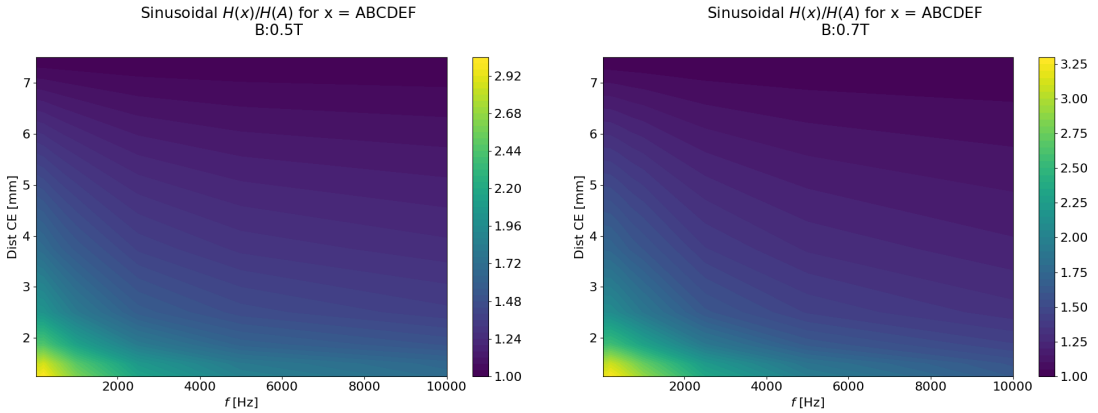

(a) f vs CE at B=0.4T. **(b)** f vs CE at B=0.7T.

Figure 5.7: mm from cut edge vs frequency, where intensity is H_{deg}.

By zooming in at the frequencies between 10-2500 Hz, as in Figure 5.8, it is clear to see that the highest degradation happens between 10-500 Hz. The higher frequencies has high degradation as well, but the highest is at the lower frequencies.

The max H_{deg} for each frequency measured and specific B level is summarized in Table 5.5. What can be noticed in the table is that as mentioned earlier, its higher

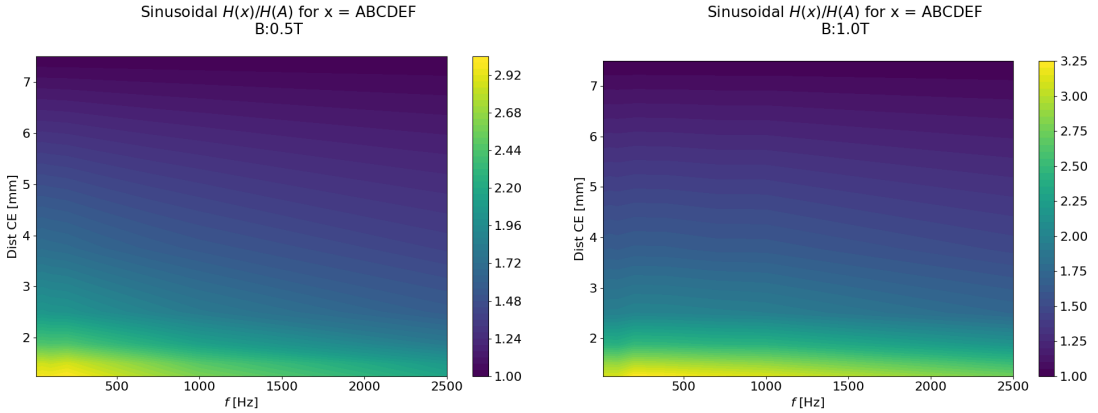

(a) f vs CE at B=0.5T. **(b)** f vs CE at B=1.0T.

Figure 5.8: Frequency vs mm from cut edge, where intensity is H_{deg}.

degradation at lower frequencies, with highest at 200 Hz and 0.8 T. Most degradation is around 0.8 T. There is a quite larger spread for the most narrow sample F, from 1.71 to 3.31. This an almost double increase between the two frequencies.

Table 5.5: Epstein Sinusoidal flux density H_{deg} max at different samples. Where red marks the highest H_{deg} for specific sample.

f [Hz]	B: H_{deg}^{max}	C: H_{deg}^{max}	D: H_{deg}^{max}	E: H_{deg}^{max}	F: H_{deg}^{max}
10	1.73 @ 0.7 T	2.09 @ 0.7 T	2.55 @ 0.7 T	3.05 @ 0.8 T	3.24 @ 0.8 T
50	1.74 @ 0.7 T	2.10 @ 0.7 T	2.56 @ 0.7 T	3.06 @ 0.8 T	3.25 @ 0.8 T
100	1.74 @ 0.7 T	2.09 @ 0.7 T	2.55 @ 0.7 T	3.05 @ 0.8 T	3.25 @ 0.8 T
200	1.73 @ 0.7 T	2.09 @ 0.7 T	2.58 @ 0.8 T	3.11 @ 0.8 T	3.31 @ 0.8 T
400	1.70 @ 0.8 T	2.05 @ 0.8 T	2.53 @ 0.8 T	3.05 @ 0.8 T	3.26 @ 0.9 T
700	1.65 @ 0.9 T	1.99 @ 0.9 T	2.45 @ 0.9 T	2.95 @ 0.9 T	3.17 @ 0.9 T
1000	1.64 @ 1.0 T	1.95 @ 1.0 T	2.43 @ 1.0 T	2.87 @ 0.9 T	3.11 @ 1.0 T
2500	1.54 @ 1.1 T	1.82 @ 1.1 T	2.27 @ 1.1 T	2.52 @ 1.0 T	2.86 @ 1.1 T
5000	1.31 @ 0.4 T	1.46 @ 0.5 T	1.64 @ 0.6 T	1.86 @ 0.8 T	2.03 @ 0.9 T
10000	1.26 @ 0.4 T	1.39 @ 0.3 T	1.52 @ 0.4 T	1.66 @ 0.5 T	1.71 @ 0.5 T

In Figure 5.9 and Figure 5.10, hysteresis loop can be seen for different frequencies, steel samples, and B levels. For lower frequencies, it can be noticed that the hysteresis loop has a very sharp peak, this is due to the phase angle between the H and B. As frequency increases, the loops have a more dull shape. The width of the loop is also increasing as the eddy currents are increasing with the increase of frequency.

The degradation can be seen from the tilting of the hysteresis loops, since to reach the same B level, more H is needed. An interesting point is around 0.1 T, where all the loops are crossing each other, this could perhaps be linked back to the lower

degradation at very low B levels introduced before. This will be discussed more in a later chapter.

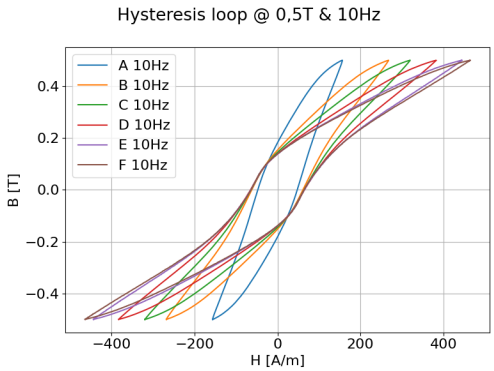

(a) B=0.5T, f=10Hz.

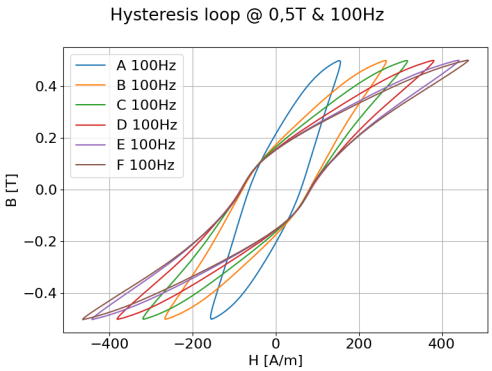

(b) B=0.5T, f=100Hz.

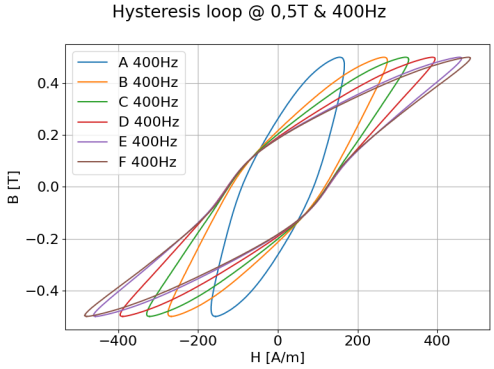

(c) B=0.5T, f=400Hz.

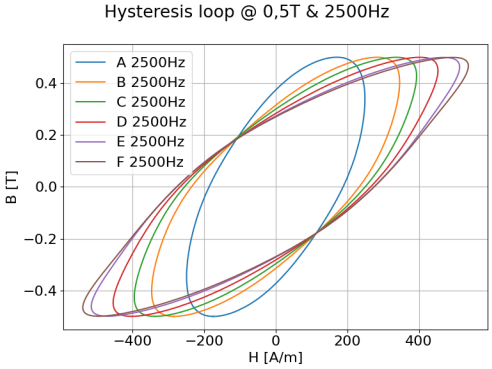

(d) B=0.5T, f=2500Hz.

Figure 5.9: Hysteresis loop for the different samples A-F and different frequencies.

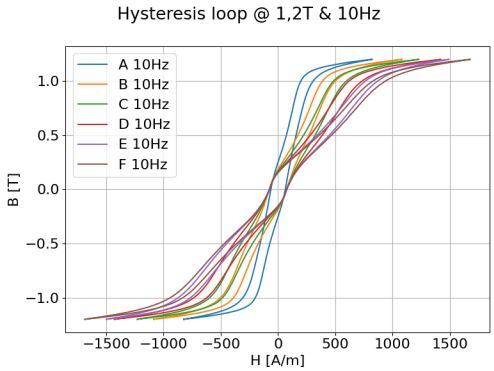

(a) B=1.2T, f=10Hz.

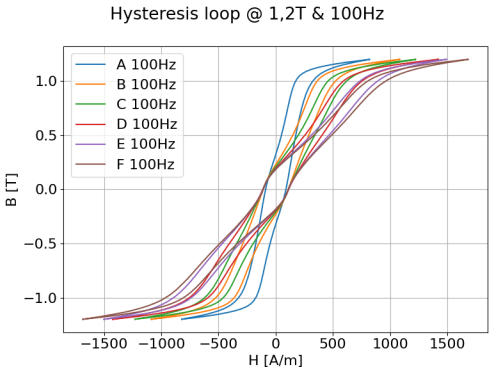

(b) B=1.2T, f=100Hz.

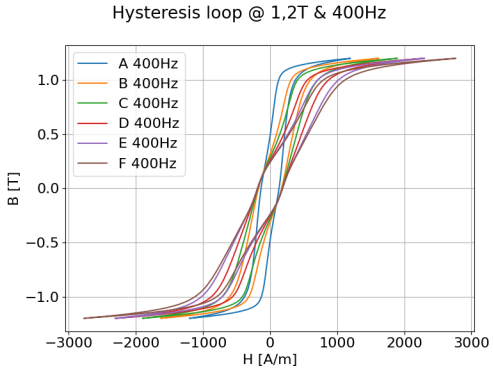

(c) B=1.2T, f=400Hz.

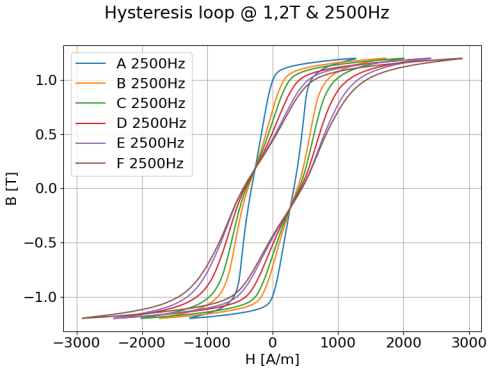

(d) B=1.2T, f=2500Hz.

Figure 5.10: Hysteresis loop for the different samples A-F and different frequencies.

5.1.2 Specific Power Loss Degradation

The second degradation to investigate was the specific power loss degradation, or Ps_{deg}. Just as the H_{deg}, the degradation was calculated as

$$Ps_{deg} = \frac{Ps(x)}{Ps(A)} \tag{5.4}$$

where the x is each sample for A to F, compared to the value of sample A. In Figure 5.11 the measured specific power loss can be seen for two of the frequencies measured. The losses increase as the sample width is decreasing.

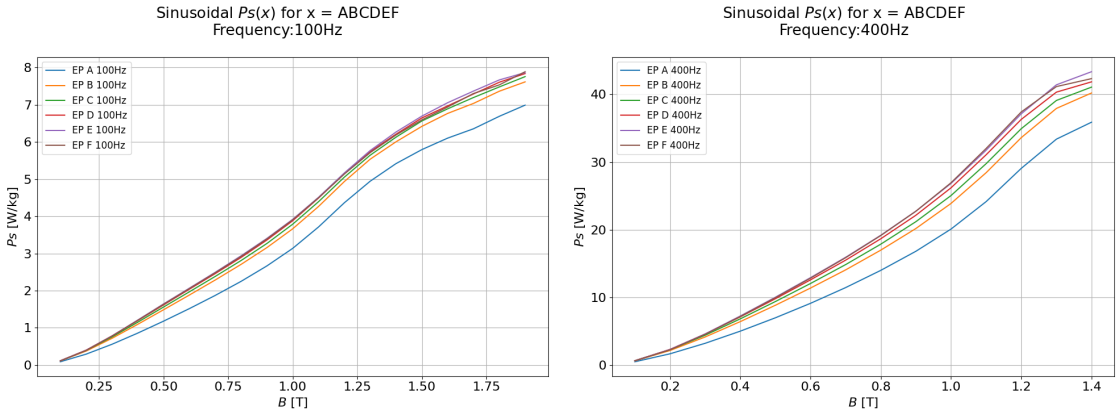

(a) B_{ref} vs $Ps_{Measured}$ at 100 Hz. **(b)** B_{ref} vs $Ps_{Measured}$ at 400 Hz.

Figure 5.11: Ps loss for different cut samples and frequency. Where A-F is steel samples.

Using (5.4) for different B levels, one can see that at lower B levels, the most narrow samples E and F actually has lower losses compared to sample D. The maximum degradation is also not at the highest permeability, instead it occurs at around 0.3-0.4 T. There is still some sort of plateau at the higher B levels around saturation. This same pattern happens over all the measured frequencies.

Moving from different samples to distance from CE again, in Figure 5.13 one can easier see the decrease of degradation at more narrow samples, with some peak around 1.875 mm. Compared to the H_{deg} the Ps_{deg} also is looking more linear than exponential. Why the degradation is lower under 1.875 mm will be discussed in a coming chapter.

Investigating the point 0.3 T which is the highest degradation, in Figure 5.14, the spread of degradation is much more even compared to the same figure for H_{deg}. In the same figure the degradation for 0.7 T can be seen as well, where the degradation is still more evenly spread across the frequencies.

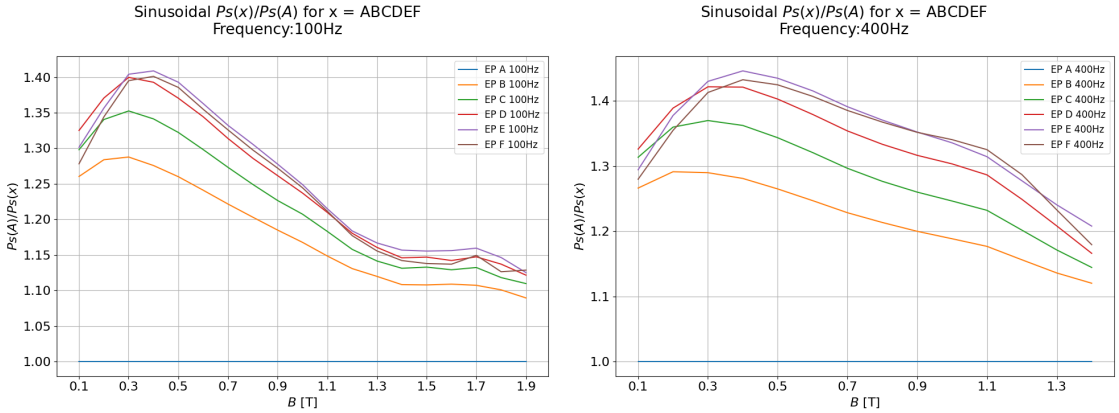

(a) B_{ref} vs Ps_{deg} at 100 Hz. **(b)** B_{ref} vs Ps_{deg} at 400 Hz.

Figure 5.12: Ps_{deg} loss for different cut samples and frequency. Where A-F are steel samples.

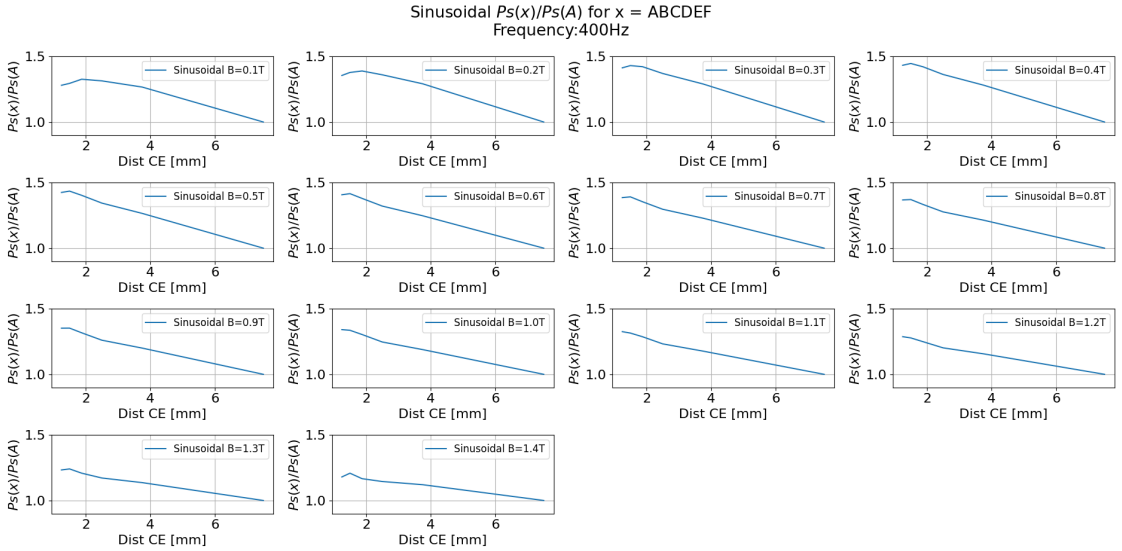

Figure 5.13: Ps_{deg} vs mm from cut edge at 400 Hz, for different B levels.

The resulting degradation is summarized in the Table 5.6, where the maximum degradation is shown for each sample, frequency and at what B level. Looking at the degradation for sample F, the max degradation range over all frequencies tested is between 1.4 to 1.48, comparing this to the H_{deg} which was between 1.7 and 3.3, its quite different.

With this information as a reference for cutting effect degradation, the PWM will be introduced next.

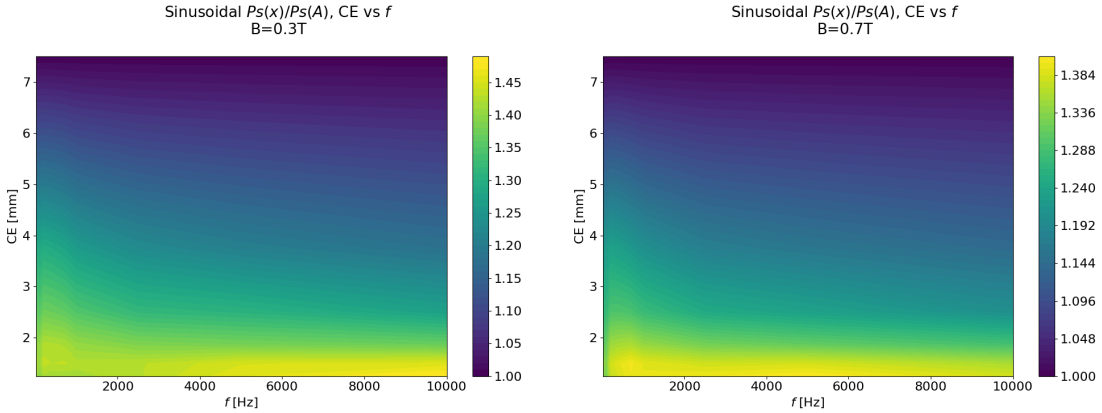

(a) f vs CE at B=0.3T. **(b)** B vs CE at B=0.7T.

Figure 5.14: f vs mm from cut edge, where intensity is Ps_{deg}.

Table 5.6: Epstein Ps_{deg} max at different samples. Where red is the max Ps_{deg} for that specific sample.

f [Hz]	B: Ps_{deg}^{max}	C: Ps_{deg}^{max}	D: Ps_{deg}^{max}	E: Ps_{deg}^{max}	F: Ps_{deg}^{max}
10	1.29 @ 0.3 T	1.36 @ 0.3 T	1.42 @ 0.3 T	1.45 @ 0.4 T	1.45 @ 0.4 T
50	1.29 @ 0.3 T	1.36 @ 0.3 T	1.40 @ 0.3 T	1.42 @ 0.3 T	1.41 @ 0.4 T
100	1.29 @ 0.3 T	1.35 @ 0.3 T	1.40 @ 0.3 T	1.41 @ 0.4 T	1.40 @ 0.4 T
200	1.30 @ 0.3 T	1.37 @ 0.3 T	1.42 @ 0.3 T	1.45 @ 0.4 T	1.43 @ 0.4 T
400	1.29 @ 0.2 T	1.37 @ 0.3 T	1.42 @ 0.3 T	1.45 @ 0.4 T	1.43 @ 0.4 T
700	1.28 @ 0.3 T	1.36 @ 0.3 T	1.42 @ 0.3 T	1.45 @ 0.4 T	1.44 @ 0.4 T
1000	1.26 @ 0.2 T	1.35 @ 0.3 T	1.40 @ 0.3 T	1.44 @ 0.4 T	1.43 @ 0.4 T
2500	1.24 @ 0.2 T	1.32 @ 0.3 T	1.39 @ 0.3 T	1.44 @ 0.4 T	1.44 @ 0.4 T
5000	1.22 @ 0.1 T	1.31 @ 0.3 T	1.38 @ 0.3 T	1.45 @ 0.3 T	1.47 @ 0.4 T
10000	1.18 @ 0.2 T	1.27 @ 0.3 T	1.37 @ 0.3 T	1.46 @ 0.4 T	1.48 @ 0.3 T

5.2 SST Cut Effect Testing, Comparison and Verification

To verify the same cut effect pattern and to check the test samples, a test sequence with the SST samples were created as in Table 5.7. The SST measurement and Epstein frame is hard to compare since its two different measuring methods. With the knowledge from Section 4.3, the results at higher B levels should be ignored, since the result for the standard sample steel did not match.

Table 5.7: SST cut sample test sequence.

f [Hz]	B_{start} [T]	B_{step} [T]	B_{stop} [T]
50	0.1	0.1	1.4
100	0.1	0.1	1.4
200	0.1	0.1	1.4
400	0.1	0.1	1.4
700	0.1	0.1	1.4
1000	0.1	0.1	1.4
2500	0.1	0.1	1.4

From the sample selection in Table 3.1 and in Table 3.2, there is 4 samples that have the same width, 15 mm, 7.5 mm, 5 mm and 3.75 mm. Comparing some of these samples at lower B levels could give some verification of the degradation and that the effective cross section calculated from the effective mass calculated in (3.1), is working correctly.

There would be three different measurements,

1. Epstein samples in Epstein Frame
2. Epstein samples in SST
3. SST samples in SST

Here the Epstein samples in the SST will be referred as $SSTx1$ where x is the specific Epstein sample A,B and D. The Epstein samples in the Epstein frame will still be EPx and the SST samples will be $SSTx$.

Starting with the virgin BH curves for the materials, which can be seen in Figure 5.15, ignoring the result at higher B levels, the curves look very similar with the same angle meaning same relative permeability.

An easier way of analyzing, is checking the difference comparing it to the Epstein's samples in the Epstein frame as reference. This can be seen in Figure 5.16, where its very easy to see that the difference is very stable until about 1.0 Tesla, then it starts increasing. This can be seen for all the frequencies in the measured sequence. The

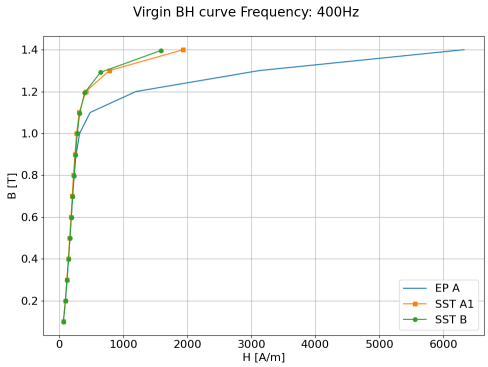

(a) The 15 mm samples H measured at 400 Hz.

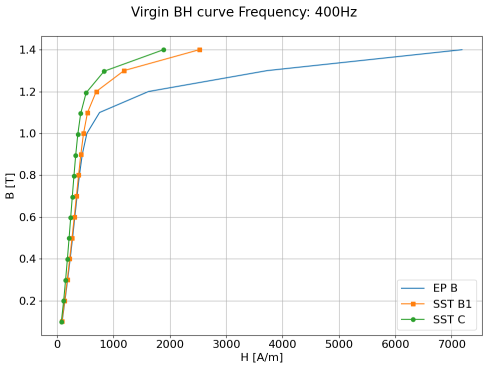

(b) The 7.5 mm samples H measured at 400 Hz.

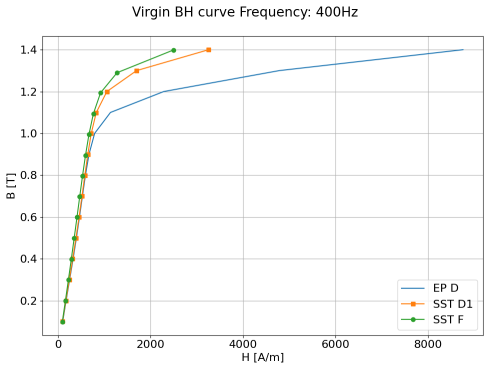

(c) The 3.75 mm samples H measured at 400 Hz.

Figure 5.15: Virgin BH curve of different SST and Epstein samples compared. Blue: Epstein in Epstein, Orange: Epstein sample in SST, Green: SST in SST.

same Epstein steel sample, just measured with SST or Epstein, looks fairly close at lower B levels. It has a difference of about 5 % at these lower B, for the three samples shown.

Knowing this, one could expect an offset from the Epstein measurements, but since the change is pretty constant we would expect about the same degradation at lower B levels.

Looking at the specific power loss instead, which can be seen in Figure 5.17, the different power losses seem to align well around lower B levels again. Looking at the difference for the different samples compared to the Epstein measurement, it can be noted that the result is closer compared to the H values, this might be due to some parameter setting which is used when calculating the H value.

Same as the H values, the 15 mm width sample the SST B has closer values compared to the SST $A1$, but for the 7.5 mm, and 3.75 mm, the $B1$, and $D1$ has closer values. The Ps difference is over all closer, with a value of between -4 % to +2% comparing the Epstein samples.

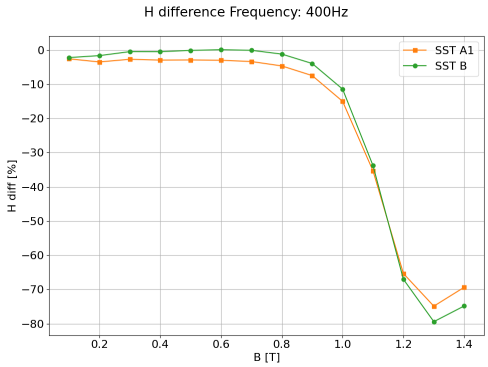

(a) The 15 mm samples H difference in % at 400 Hz.

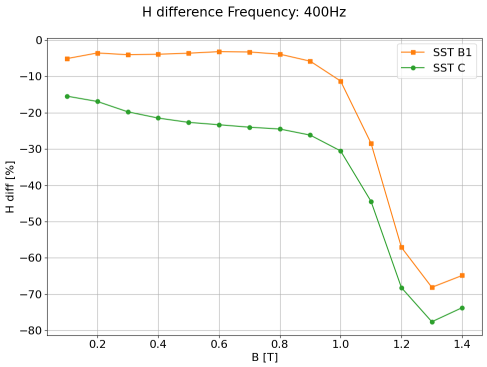

(b) The 7.5 mm samples H difference in % at 400 Hz.

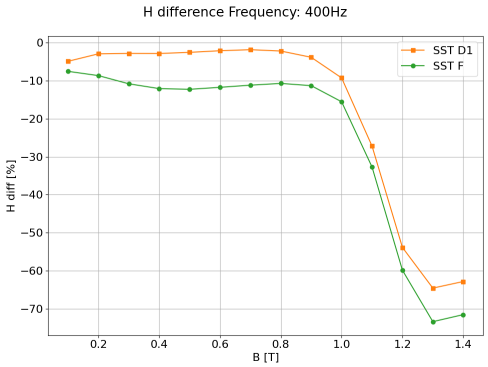

(c) The 3.75 mm samples H difference in % at 400 Hz.

Figure 5.16: The percentage difference of H from comparing to the Epstein sample in the Epstein Frame. Blue: Epstein in Epstein, Orange: Epstein sample in SST, Green: SST in SST.

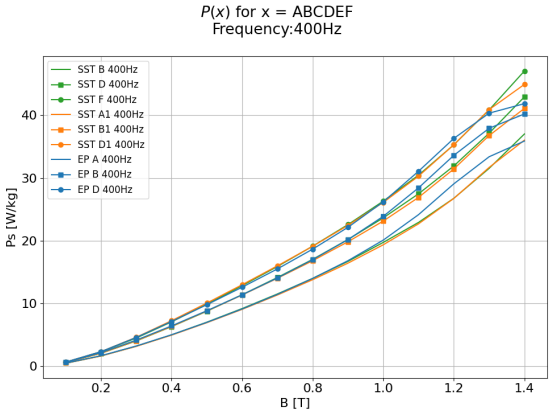

(a) Ps vs B for the sample comparison.

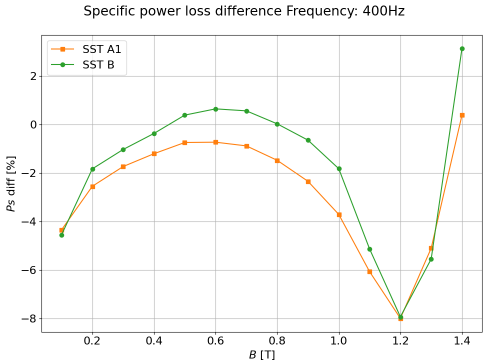

(b) The 15 mm samples Ps difference in % at 400 Hz.

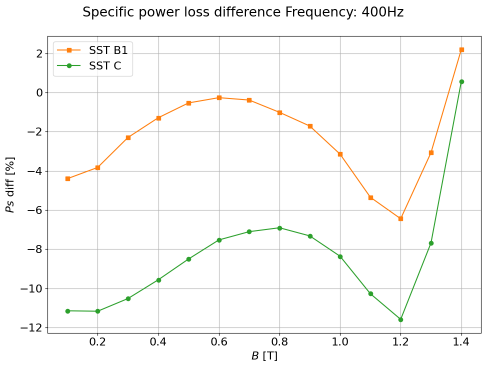

(c) The 7.5 mm samples Ps difference in % at 400 Hz.

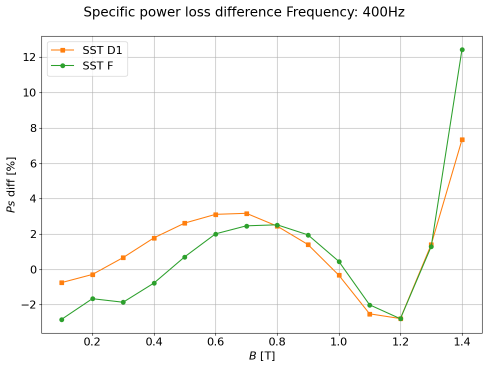

(d) The 3.75 mm samples Ps difference in % at 400 Hz.

Figure 5.17: Ps, and Ps difference for the comparison between SST and Epstein.

5.2.1 H Degradation with SST

Knowing the difference between the SST and Epstein samples, one could look at the degradation for the SST to check if it has the same characteristics as the Epstein. Knowing that the SST has some difference at higher flux densities.

Calculating the same H_{deg} as with the Epstein, just comparing with its reference sample A instead as in

$$H_{deg}^{SST} = \frac{H(x)}{H(A)} \tag{5.5}$$

Looking at the degradation in Figure 5.18, one could notice the same pattern of a curve that looks like the permeability, just that the peak of curve has change to higher flux densities. For the sample G, the measurement might not have been accurate. The material had the width of 2 mm, and due to these very thin strips the material the damage during cutting might have been to severe. There was large burrs on the edges and very delicate to handle. But even taking this into consideration, the same degradation pattern can be seen.

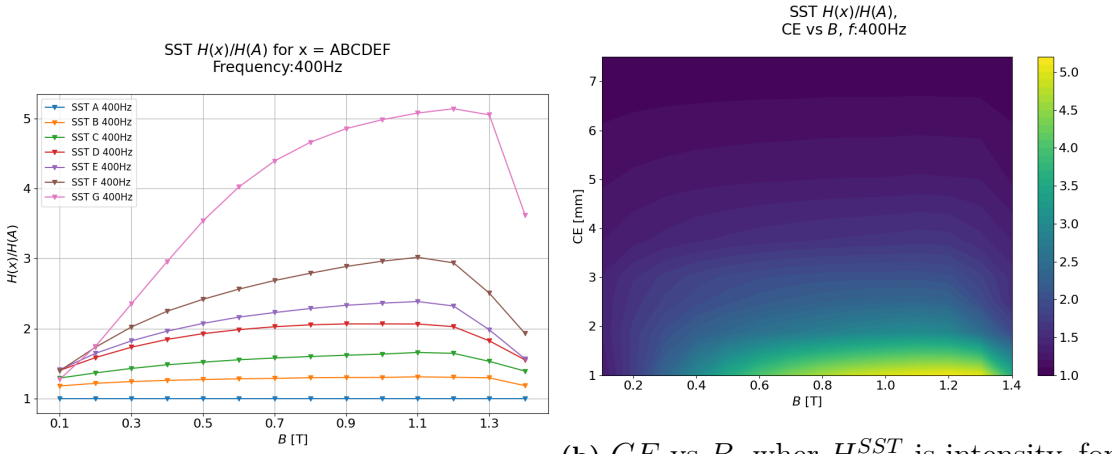

(a) H_{deg}^{SST} vs B for 400 Hz and SST.

(b) CE vs B, wher H_{deg}^{SST} is intensity, for 400 Hz and SST.

Figure 5.18: H_{deg}^{SST} for SST measurements at 400 Hz.

In Figure 5.19 the comparison of the degradation at different distances from cut edges as from (5.3) is depicted. The same degradation is happening at 0.1 Tesla, while also the same exponential degradation versus CE can be seen for the other B levels. The degradation is looking different at higher B levels, which was to be expected. The SST measuring equipment comparison in Section 4.3, showed that there is a difference at higher B levels. The sample G here also shows some different pattern, with peak degradation around 1.2 T, but this is probably also due to that its sample was too narrow as explained earlier.

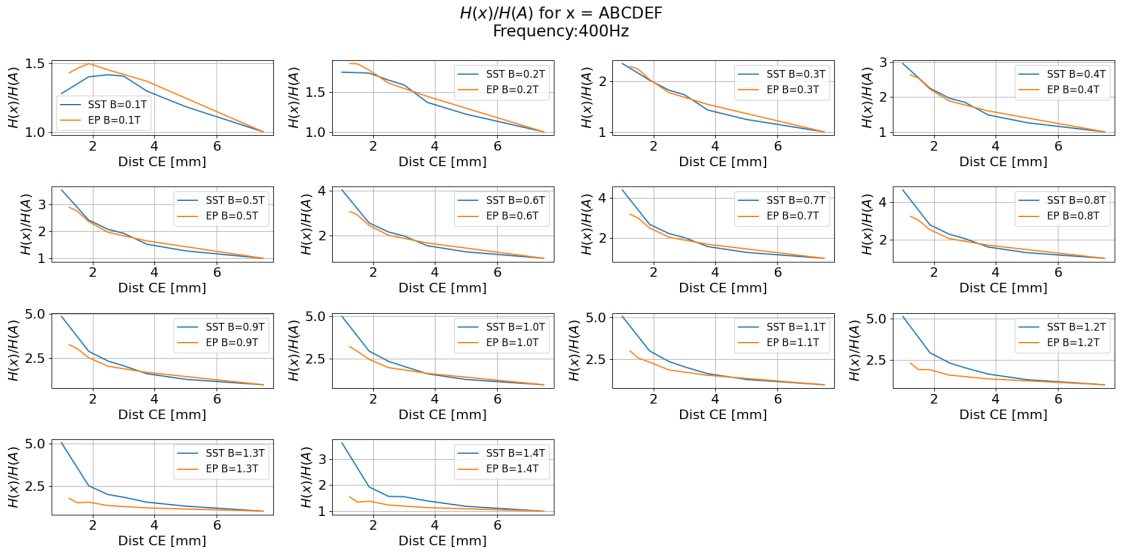

Figure 5.19: H_{deg}^{SST} vs mm from cut edge at 400 Hz, for different B levels.

Instead looking at the specific B level, 0.8 T and 0.9 T in Figure 5.20, to analyse the degradation over different frequencies. This also have the same pattern as for the Epstein, higher degradation at lower frequencies, further strengthening the theory that skin effect pushing the flux further out in the material and counter act the degradation due to cutting.

The H_{deg} for both the Epstein and SST seems very similar which is a good base for when moving onto PWM excitation and for verifying the measurements.

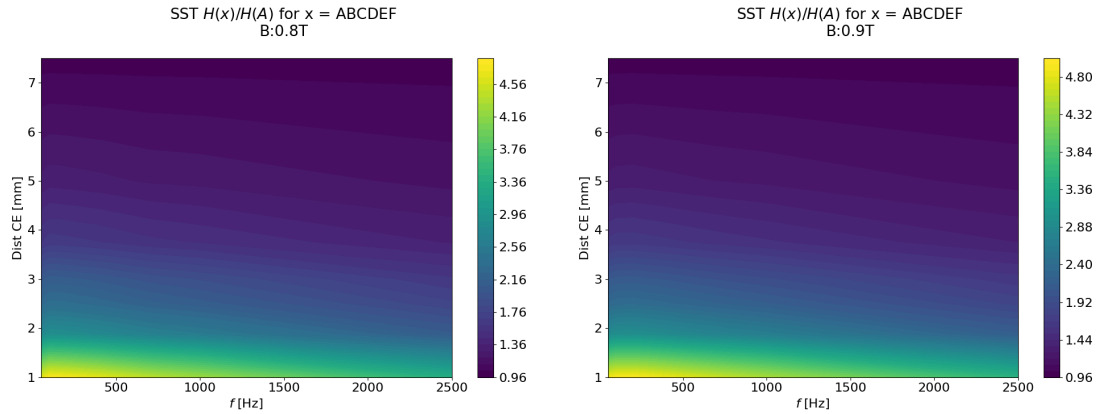

(a) CE vs f at B=0.8T.

(b) CE vs f at B=0.9T.

Figure 5.20: Magnetic field strength degradation at different distances from cut edge and over different fundamental frequencies. Where intensity is H_{deg}^{SST} for SST measurements.

5.2.2 Ps Degradation with SST

The same degradation analyses was performed for the specific power loss, and using the equation

$$Ps_{deg}^{SST} = \frac{Ps(x)}{Ps(A)} \tag{5.6}$$

to determine the degradation. Keeping in mind the sample G could have some doubt regarding the validity of this measurement due to the narrow width. Looking at Figure 5.21, the degradation for the different samples can be seen as well as the degradation for 0.7 T. Ignoring the measurement of the most narrow sample G, there seems to be a degradation peak around 0.4 T, which is about the same as the Epstein measurements. Since the SST was limited at measuring higher B levels, it is hard to confirm the plateau at saturation levels.

Looking at the right side in same figure, the spread across frequencies looks about the same as the Epstein measurement. Also that the intensity, meaning degradation, is increasing evenly across the frequencies.

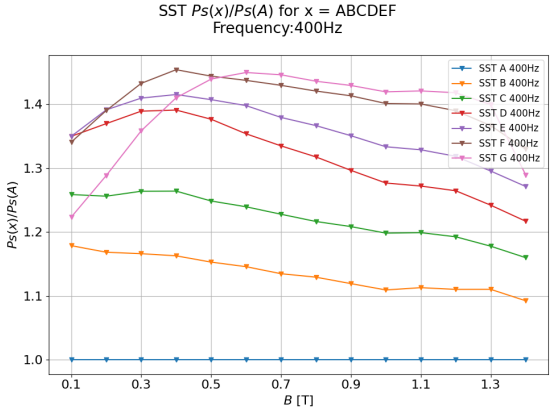

(a) Ps_{deg}^{SST} vs B for SST.

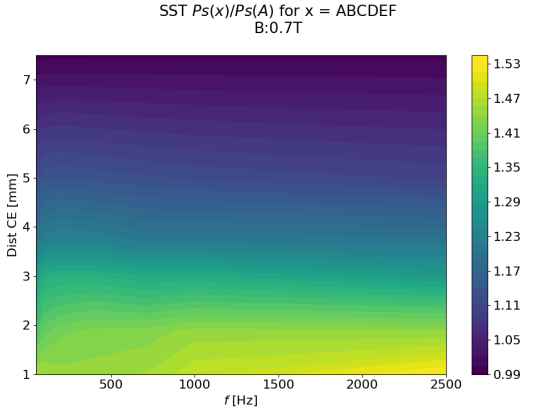

(b) CE vs f at B=0.7T for SST, Ps_{deg}^{SST} is intensity.

Figure 5.21: Ps_{deg}^{SST} for 400 Hz SST measurement.

Moving to the distance from cut edge as in Figure 5.22, one can notice that the Epstein is looking a bit more linear compared to the SST measurements. The degradation is fairly similar with a difference between 10 to 15% increase at worst.

As mentioned in the beginning of this section, the SST and Epstein can never be directly compared, there will be some measurement deviance. But with the methods that is introduced here, one could see some sort of conclusion that even with different cut steel samples, and different measurement methods the degradation is looking fairly similar. This is a good result for moving forward with the PWM excitation and also to verify the models that will be used in the FEM based simulation later.

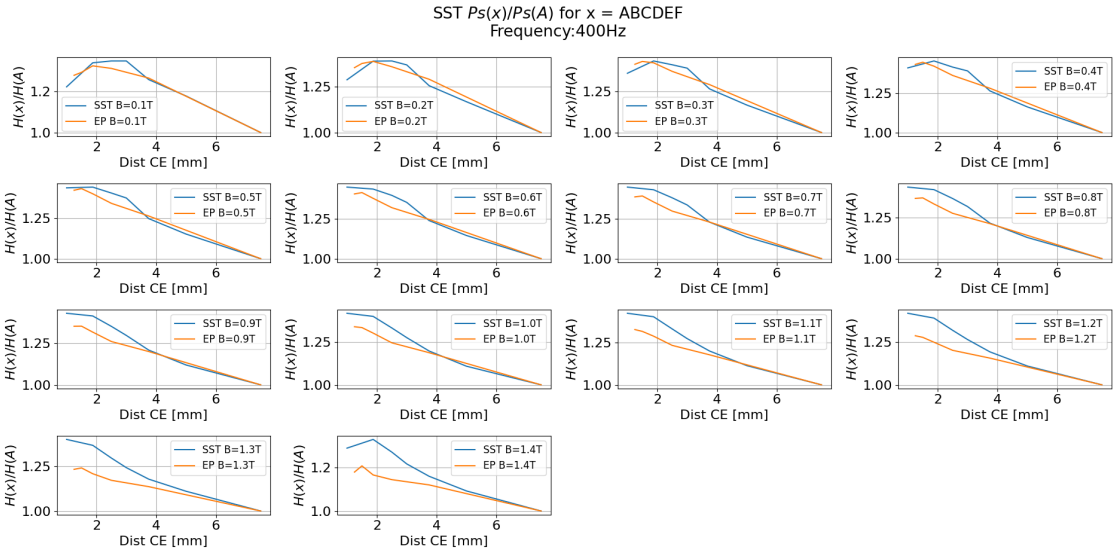

Figure 5.22: Ps_{deg}^{SST} vs mm from cut edge at 400 Hz, for different B levels.

6
Cut Effects with PWM Excitation

6.1 Effect of Cutting with Non-Sinusoidal Flux Distribution

Same as the sinusoidal testing in Chapter 5, the test sequence for each steel sample did steps in B until the equipment's limitation. Compared to Table 5.1, the PWM could not perform at 10, 5000, and 10000 Hz. The B level was also limited more for PWM due to higher H fields. The full test sequence for the PWM can be seen in Table 6.1.

Two more columns have been added to this Table 6.1, Fha and Vr. Taking into account the results from Chapter 4, the Vr is kept at normal modulation for all frequencies, and Fha is kept at a constant switching frequency of 10 kHz, leading to the resulting Fha in the table. The choice of constant switching frequency, is from looking at inverters in electric vehicles, where it is mostly common to have a constant switching frequency. The choice of 10 kHz is due to the limitations in the measurement equipment.

In reality when controlling the electrical machine the Vr would change depending on the machines speed and load, but in order to keep the degrees of freedom down this is an simplification and kept constant. To reduce the amount of figures, only a few of the measured and calculated results will be shown in this chapter, the rest can be seen in Appendix C.

Table 6.1: Epstein PWM sample test sequence.

f [Hz]	Vr	Fha	Epstein winding	B_{start} [T]	B_{step} [T]	B_{stop} [T]
50	1.9	200	700	0.1	0.1	1.9
100	1.9	100	700	0.1	0.1	1.8
200	1.9	50	200	0.1	0.1	1.4
400	1.9	25	200	0.1	0.1	1.4
700	1.9	15	200	0.1	0.1	1.4
1000	1.9	10	60	0.1	0.1	1.2
2500	1.9	4	60	0.1	0.1	1.2

Same as the sinusoidal flux measurements, both H degradation and Ps degradation is investigated. Starting with H degradation.

6.1.1 Magnetic Field Strength Degradation

For the non sinusoidal flux density, there were a few different comparisons that was of interest. The first comparison, was to see the degradation compared to sample A with PWM. The second comparison would be with the measured sample of PWM compared with sample A with sinusoidal excitation. The third and final comparison was to compare cut sample PWM with cut sample sinusoidal, meaning A with A, B with B and so on.

6.1.1.1 With PWM Sample A as Reference

Starting with the same method as for the sinusoidal measurements, looking at the virgin BH curve of the the PWM together with the sinusoidal, the virgin BH curve is created from the peak values of B and H during the measurement. In Figure 6.1, the measured BH curve for 100 Hz and 400 Hz can be seen. In the 100 Hz measurement, the BH curve with PWM signal is very similar to the measured sinusoidal, but as fundamental frequency is increasing the two curves starts to deviate from each other more at lower B levels, before the knee point.

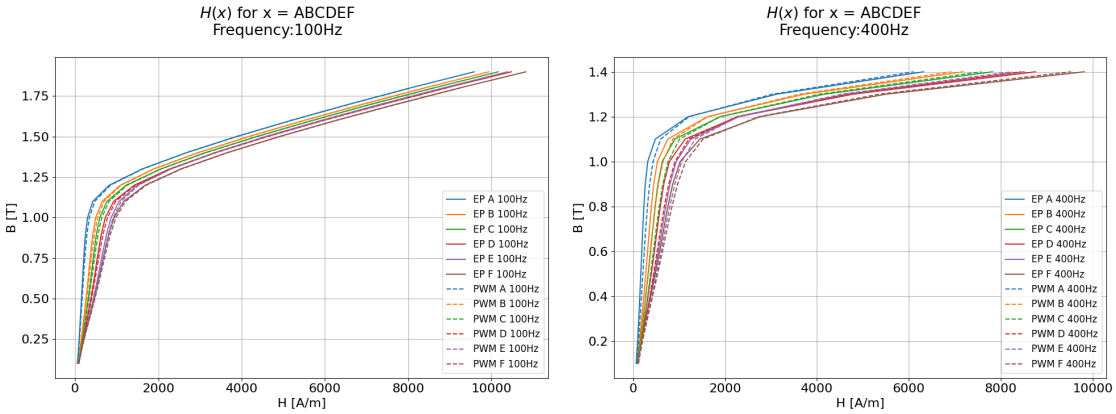

(a) $H_{Measured}$ vs B_{ref} at 100 Hz. **(b)** $H_{Measured}$ vs B_{ref} at 400 Hz.

Figure 6.1: Virgin BH curves for different cut samples and frequency, where A-F is steel samples. Solid: Sine, Dashed: PWM.

Since it is hard to see the difference by just looking at the BH curve, looking at the relative permeability in Figure 6.2, it is easier to see that there is some deviation from the sinusoidal measurement, with lower relative permeability for the PWM signal.

The relative permeability is calculated using (5.2), using the peak B and H measured. The permeability is also deviating less and less when reaching the saturation

region. As fundamental frequency is increasing, the switching frequency stays constant, leading to a lower frequency modulation ratio or Fha, reduces the permeability more and more compared to the sinusoidal permeability.

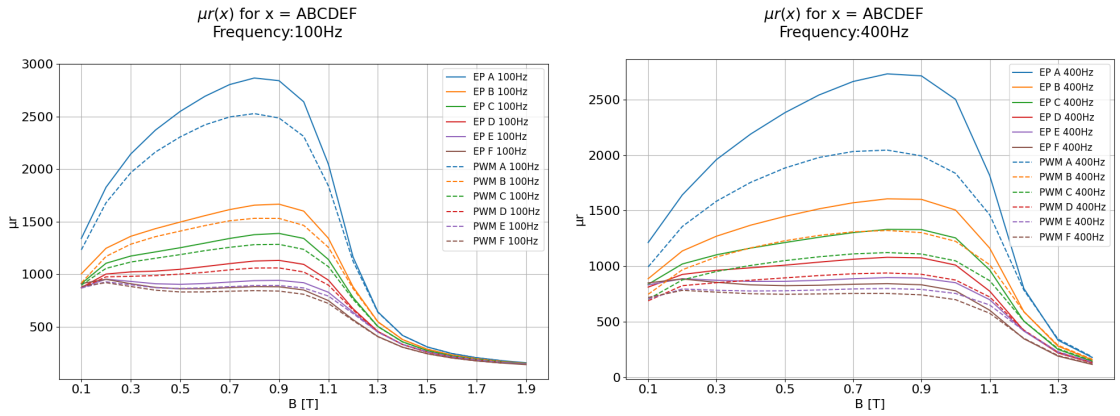

(a) μ_r vs B_{ref} at 100 Hz.

(b) μ_r vs B_{ref} at 400 Hz.

Figure 6.2: Relative permeability for different cut samples and frequency, where A-F is steel samples. Solid: Sine, Dashed: PWM.

Using the same method as for the sinusoidal measurement and degradation, the equation for H_{deg}^{PWM} can be written as

$$H_{deg}^{PWM} = \frac{H^{PWM}(x)}{H^{PWM}(A)} \tag{6.1}$$

where H_{deg}^{PWM} is the degradation with PWM A as reference. Then looking at Figure 6.3 where the degradation is plotted for different B levels. When comparing to its own reference the PWM degradation is actually lower compared to the Sinusoidal degradation. It can also be seen that the degradation follows the same flux density pattern, with the peak around 0.8 T and then plateauing at higher B levels. The same pattern happens as the fundamental frequency is increasing.

Plotting the degradation over distance from CE instead, as in Figure 6.4, the same conclusion can be drawn. The degradation looks similar for different B levels, and at 1.2 T and above the Sinusoidal and PWM actually line up on each other.

Continuing with the peak degradation compared with the measured PWM A sample. The degradation from the CE, calculated with (5.3), this can be seen in Figure 6.5. Just like the sinusoidal degradation the max degradation looks to be around 0.4 T t 1.0 T and is decreasing as distance from CE is increasing.

Looking at the degradation at specific B levels instead, as in Figure 6.6, it can be seen that the degradation is highest at the lower fundamental frequencies, which also correlates to the sinusoidal degradation.

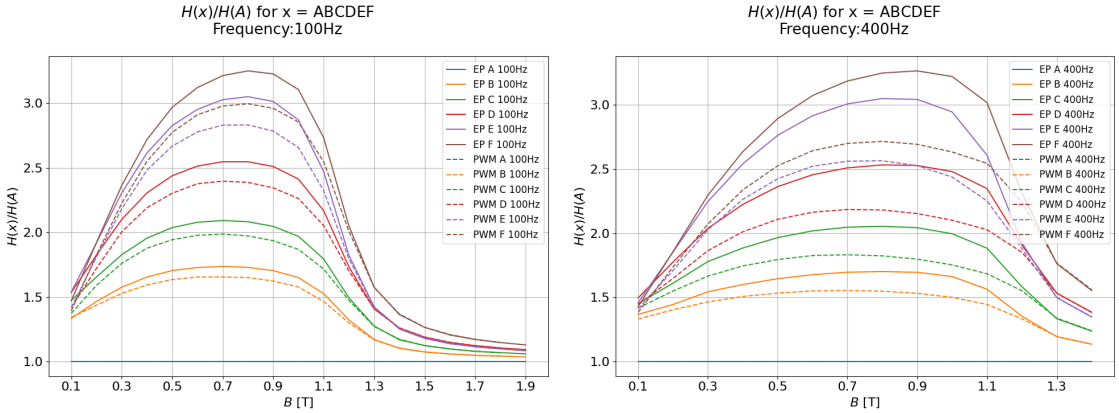

(a) H_{deg}^{PWM} vs B_{ref} at 100 Hz. **(b)** H_{deg}^{PWM} vs B_{ref} at 400 Hz.

Figure 6.3: H_{deg}^{PWM} for different frequencies. Where A-F is steel samples. Solid: Sine, Dashed: PWM.

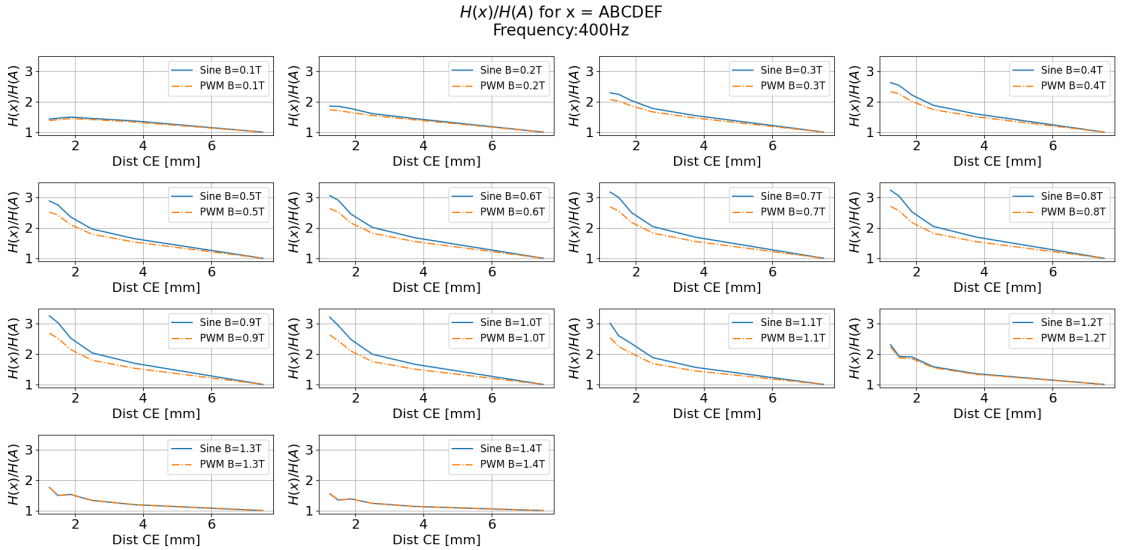

Figure 6.4: H_{deg}^{PWM} vs mm from cut edge for different B levels. Solid: Sine, Dashed: PWM.

Same as for the sinusoidal measurements, the max peak degradation for each sample and at each specific B level can be seen in Table 6.10. Here its easy to see the highest degradation for all samples actually happens at the fundamental frequency of 50 Hz.

When comparing degradation to the sinusoidal measurements, the highest degradation is expected to be at higher frequencies, due to the changing Fha.

Another interesting point from the table, is that the degradation over the different frequencies is pretty wide spread, from 3.11 at 50 Hz, to 2.08 at 2500 Hz. This is something to remember for later when comparing to the sinusoidal reference.

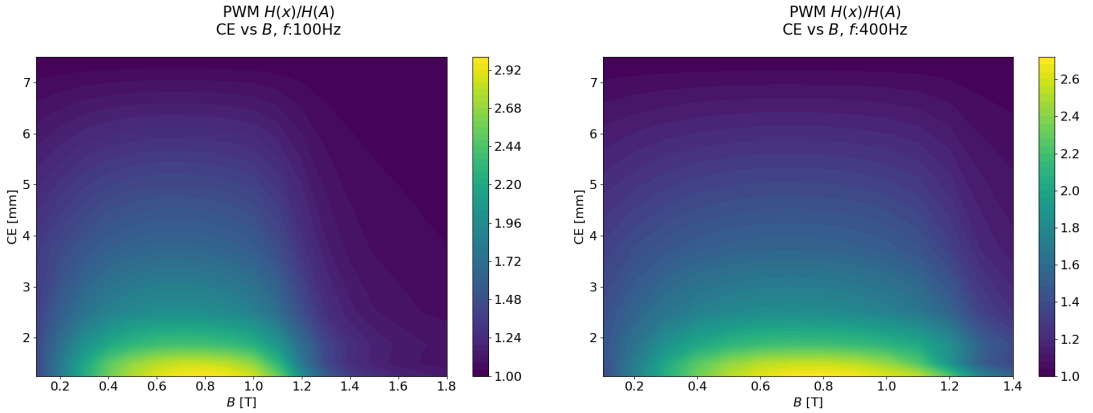

(a) B vs CE at 100 Hz. **(b)** B vs CE at 400 Hz.

Figure 6.5: H_{deg}^{PWM} is intensity, for different frequencies.

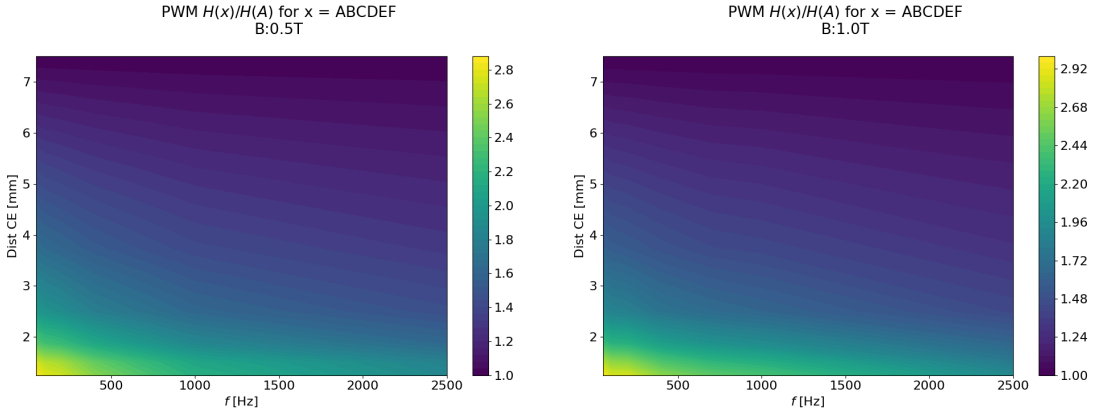

(a) CE vs f at B=0.5T. **(b)** CE vs f at B=1.0T.

Figure 6.6: H_{deg}^{PWM} is intensity for different B levels.

Table 6.2: Epstein H_{deg}^{PWM} max and at what B level. For different samples and frequencies.

f [Hz]	B: H_{deg}^{max}	C: H_{deg}^{max}	D: H_{deg}^{max}	E: H_{deg}^{max}	F: H_{deg}^{max}
50	1.69 @ 0.7 T	2.04 @ 0.7 T	2.47 @ 0.7 T	2.94 @ 0.8 T	3.11 @ 0.8 T
100	1.66 @ 0.6 T	1.99 @ 0.7 T	2.4 @ 0.7 T	2.83 @ 0.8 T	3.0 @ 0.8 T
200	1.62 @ 0.7 T	1.94 @ 0.7 T	2.34 @ 0.7 T	2.79 @ 0.8 T	2.95 @ 0.8 T
400	1.55 @ 0.7 T	1.83 @ 0.7 T	2.18 @ 0.7 T	2.56 @ 0.8 T	2.71 @ 0.8 T
700	1.48 @ 0.7 T	1.73 @ 0.7 T	2.04 @ 0.8 T	2.38 @ 0.8 T	2.52 @ 0.8 T
1000	1.42 @ 0.8 T	1.65 @ 0.8 T	1.95 @ 1.0 T	2.25 @ 0.9 T	2.4 @ 1.0 T
2500	1.34 @ 0.3 T	1.49 @ 0.4 T	1.74 @ 1.2 T	1.86 @ 1.1 T	2.08 @ 1.2 T

A problem discovered when performing the analysis of the PWM measurement was that the software controlling the desired signal in MPG Software controls the peak

signal. So to achieve the desired B peak, a specific H peak was applied. From this the permeability was calculated and other calculations. Problem with this is that the PWM signal contains a lot of harmonics, due to the switching. So to reach the B of 1.1 T for example, then the controller changes the H until the peak of 1.1 T is achieved. This peak B for 400 Hz can be seen in Figure 6.7, where the signal can be seen both in time domain as well as in frequency domain with an FFT.

In the figure the peak value of 1.1 T is achieved, but the actual fundamental signal is lowered compared to the perfect Sinusoidal signal. This, as mentioned before, is due to the harmonics which bring the peak value up to the 1.1 T. Since permeability is calculated from these peaks of H and B the more harmonic content it is hard to do comparison to a perfect sinusoidal signal.

For the B in the Figure 6.7, one interesting point is that the B for the different samples are fairly similar, since this is what is being controlled. It can be seen that the same fundamental component for the steel samples $A - F$ as well as the same harmonic content at the switching frequency, with some small variations. So when looking at the H, the degradation could be analyzed in the frequency domain between the samples, using FFT.

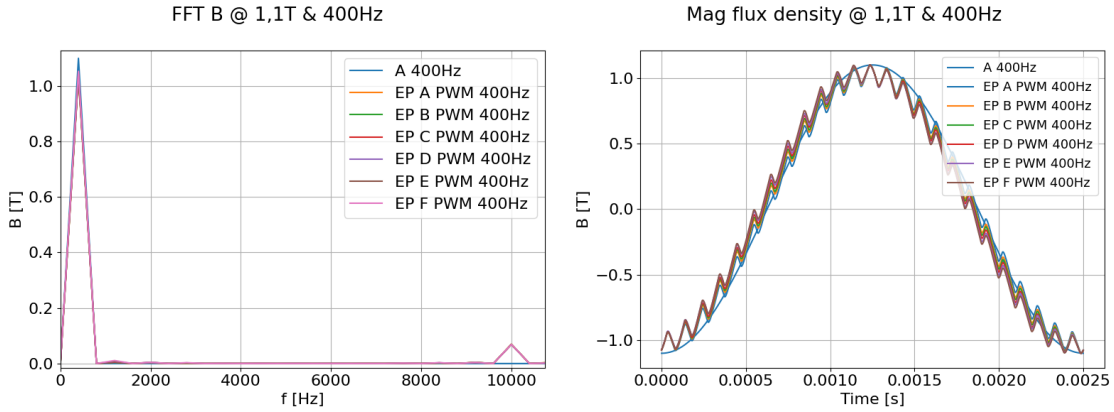

(a) FFT for B at 400 Hz.

(b) Time domain for B at 400 Hz.

Figure 6.7: FFT and time domain for flux density at 400 Hz. Comparing pure sinusoidal with PWM signal.

In Figure 6.8 the H field applied to reach the 1.1 T for the different samples can be seen, both in time domain as well as in frequency domain measured at 400 Hz. In the time domain the H increase as the samples width is decreasing, which has been seen before.

Instead looking in the frequency domain, an interesting conclusion can be drawn. The degradation is not the same at the fundamental component as at the switching frequency component. This means that the ripple magnitude in H for different samples is not increasing as severe as for the fundamental component.

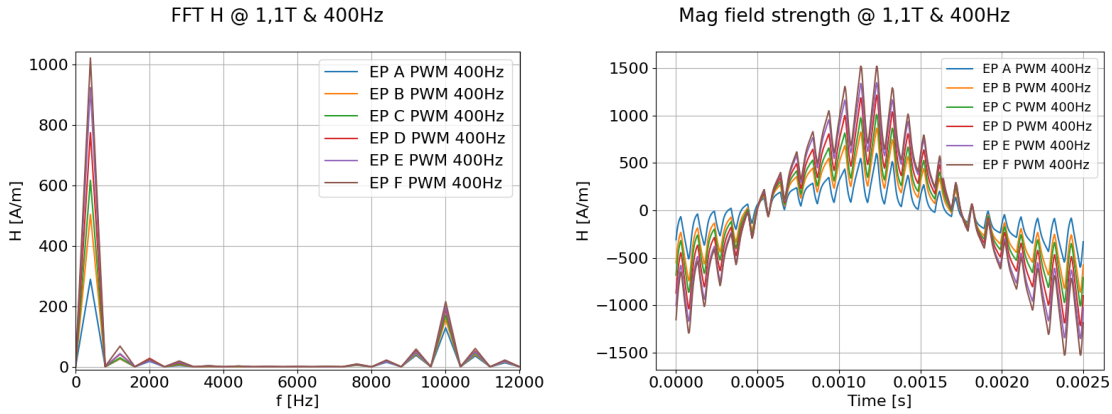

(a) FFT for H at 400 Hz.

(b) Time domain for H at 400 Hz.

Figure 6.8: FFT and Time domain for magnetic field strength at 400 Hz. Comparing pure sinusoidal with PWM signal.

Starting with an analysis of the degradation compared to the fundamental component of H for sample A, this can be seen in Table 6.3. In table, the peak degradation happens around 1.1 T for the fundamental degradation. Comparing this to the peak degradation Figure 6.3, the max degradation seems to have shifted from 0.9 T for the peak and 1.1 T for the fundamental degradation. Keeping this in mind for later discussions.

Table 6.3: H_{deg} for fundamental H_1 signal. Where x is sample A-F, H_1 is content at fundamental.
For non-sinusoidal flux at 400 Hz.

Harmonic	Flux Density [T]	A	B	C	D	E	F
H_{1x}/H_{1A}	0.2	1.0	1.42	1.56	1.64	1.68	1.7
H_{1x}/H_{1A}	0.3	1.0	1.51	1.71	1.9	2.04	2.08
H_{1x}/H_{1A}	0.4	1.0	1.58	1.83	2.11	2.36	2.42
H_{1x}/H_{1A}	0.5	1.0	1.63	1.93	2.28	2.61	2.71
H_{1x}/H_{1A}	0.6	1.0	1.68	2.01	2.41	2.81	2.94
H_{1x}/H_{1A}	0.7	1.0	1.71	2.06	2.5	2.97	3.12
H_{1x}/H_{1A}	0.8	1.0	1.73	2.1	2.57	3.08	3.26
H_{1x}/H_{1A}	0.9	1.0	1.75	2.13	2.62	3.16	3.36
H_{1x}/H_{1A}	1.0	1.0	1.75	2.14	2.65	3.21	3.44
H_{1x}/H_{1A}	1.1	1.0	1.74	2.13	2.67	3.19	3.53
H_{1x}/H_{1A}	1.2	1.0	1.65	2.06	2.59	2.81	3.34

In Figure 6.8, in the frequency domain, 9 different harmonics can be seen and the fundamental, where all harmonics are odd harmonics. To limit the analysis to some extent, only the fundamental (f_1) degradation and the degradation at the switching

frequency (f_s) is analyzed. The content at the f_s is the second highest component of the signal and a significant component. This limitation is due to the time limit in the thesis. But keeping in mind that there is more harmonic content in the H signal and different degradation at each harmonic.

By zooming in at the degradation at the fundamental component of H and the f_s component, as in Figure 6.9, one can notice the degradation for the two different components. The fundamental has significantly larger degradation compared to the content at the f_s. Looking at the degradation at the f_s, comparing it to the sample A harmonic content at the f_s, can be seen in Table 6.4.

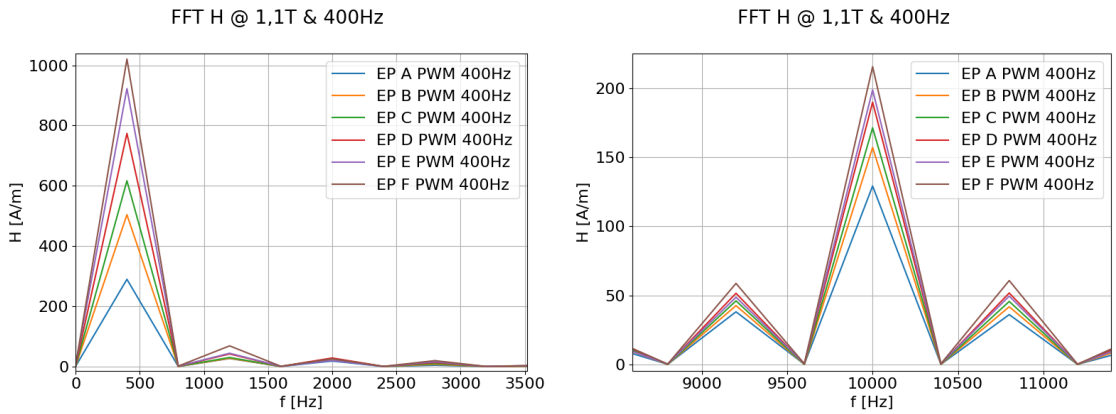

(a) Zoomed FFT for H around fundamental f_1, measured at 400 Hz.

(b) Zoomed FFT for H around switching f_s, measured at 400 Hz.

Figure 6.9: Zoomed FFT of magnetic field strength, around the fundamental and around the switching frequency, showing the degradation.

From the sinusoidal degradation, two different conclusions were drawn. First, that the H degradation depends on the frequency, second that the H degradation depend on the B level in the material. Knowing this, Table 6.4 also shows the B level at harmonic frequency. So for example, at 0.7 T peak, the flux density level at f_S is 0.04 T, shown as B_s in the table. In the table, it can be seen that the degradation is not as severe as the fundamental, as mentioned earlier, with a max degradation of 1.74 at f_s compared to 3.44 at f_1.

Looking at the fundamental degradation of the sinusoidal measurement at 10 kHz, which is the same frequency as the switching frequency in this case, can be seen in Table 6.5. Comparing the fundamental degradation in sinusoidal 10 kHz, the max degradation is around 1.74, which for the PWM measurement at f_s max also calculated to 1.74. Which seems to be some correlation to the degradation for PWM depends on the f_s, and B level. The PWM does however also have that fundamental part of B in the material, which will affect the saturation and degradation in the material.

Table 6.4: H_{sx}/H_{sA} degradation and flux density at switching frequency, at 400 Hz.

B_{Peak} [T]		A	B	C	D	E	F
	B_s[T]	0.02	0.02	0.02	0.02	0.02	0.02
0.3T	H_{sx}/H_{sA}	1.0	1.24	1.33	1.4	1.45	1.46
	B_s[T]	0.03	0.03	0.03	0.03	0.03	0.03
0.4T	H_{sx}/H_{sA}	1.0	1.24	1.33	1.42	1.49	1.51
	B_s[T]	0.03	0.03	0.03	0.03	0.03	0.03
0.5T	H_{sx}/H_{sA}	1.0	1.23	1.32	1.42	1.52	1.54
	B_s[T]	0.04	0.04	0.04	0.04	0.04	0.04
0.6T	H_{sx}/H_{sA}	1.0	1.22	1.32	1.42	1.52	1.55
	B_s[T]	0.04	0.04	0.04	0.04	0.04	0.04
0.7T	H_{sx}/H_{sA}	1.0	1.21	1.31	1.41	1.52	1.55
	B_s[T]	0.05	0.05	0.05	0.05	0.05	0.05
0.8T	H_{sx}/H_{sA}	1.0	1.2	1.3	1.41	1.51	1.56
	B_s[T]	0.06	0.06	0.06	0.06	0.06	0.06
0.9T	H_{sx}/H_{sA}	1.0	1.2	1.3	1.41	1.51	1.56
	B_s[T]	0.06	0.06	0.06	0.06	0.06	0.06
1.0T	H_{sx}/H_{sA}	1.0	1.21	1.3	1.42	1.52	1.59
	B_s[T]	0.07	0.07	0.07	0.07	0.07	0.07
1.1T	H_{sx}/H_{sA}	1.0	1.22	1.33	1.47	1.54	1.67
	B_s[T]	0.07	0.07	0.07	0.07	0.07	0.07
1.2T	H_{sx}/H_{sA}	1.0	1.23	1.37	1.54	1.52	1.74
	B_s[T]	0.07	0.07	0.07	0.07	0.07	0.08

Table 6.5: H_{1x}/H_{1A}, Sinusoidal fundamental degradation where x is sample A-F. For fundamental frequency of 10 kHz.

	A	B	C	D	E	F
0,1T Sine	1.0	1.25	1.35	1.4	1.41	1.4
0,2T Sine	1.0	1.26	1.38	1.49	1.56	1.57
0,3T Sine	1.0	1.26	1.4	1.52	1.64	1.67
0,4T Sine	1.0	1.26	1.4	1.54	1.68	1.72
0,5T Sine	1.0	1.26	1.39	1.54	1.69	1.74
0,6T Sine	1.0	1.24	1.37	1.52	1.68	1.74
0,7T Sine	1.0	1.23	1.35	1.49	1.65	1.71

As mentioned earlier the measurement sequence was performed over a couple of different fundamental frequencies. The switching frequency was however kept constant, therefore an interesting analysis would be to look at the degradation at of the harmonic content at the switching frequency.

In Table 6.6 a few different measurements can be seen, first the B level at the f_s harmonic, second the fundamental degradation compared to sample A, third the switching harmonic degradation compared to sample A, and finally the amount of content at the f_s compared to f_1 related to its own signal. This also shown for different fundamental frequencies.

Starting by looking at the switching frequency content related to the fundamental (H_{sx}/H_{1x}). As the f_1 is increasing, and f_s is kept constant, the Fha is lowered and more content is at lower harmonics. This leads to more content at the f_s. This higher content at the f_s leads to larger B at the f_s. More B at f_s leads to higher degradation, which was noticed in the sinusoidal measurements.

Another interesting analysis that can be seen in the table, is that the fundamental degradation is largest at lower frequencies, and as fundamental frequency is increasing, the fundamental degradation is decreasing, same as in the sinusoidal measurement. The degradation at f_s is increasing as degradation at f_1 is decreasing. This is possibly due to as explained above, the B content at the f_s is increasing.

Table 6.6: Flux density at switching frequency, fundamental degradation component, switching harmonic degradation component, and how large switching harmonic is compared to fundamental. At 1.1T and different frequencies.

	A	B	C	D	E	F
50 Hz, B_s[T]	0.01	0.01	0.01	0.01	0.01	0.01
50 Hz, H_{1x}/H_{1A}	1.0	1.71	2.08	2.57	3.05	3.3
50 Hz, H_{sx}/H_{sA}	1.0	1.15	1.21	1.28	1.29	1.34
50 Hz, H_{sx}/H_{1x}	0.12	0.08	0.07	0.06	0.05	0.05
100 Hz, B_s[T]	0.03	0.03	0.03	0.03	0.03	0.03
100 Hz, H_{1x}/H_{1A} at f_1	1.0	1.72	2.1	2.59	3.09	3.33
100 Hz, H_{sx}/H_{sA} at f_s	1.0	1.16	1.23	1.3	1.32	1.38
100 Hz, H_{sx}/H_{1x}	0.21	0.14	0.13	0.11	0.09	0.09
200 Hz, B_s[T]	0.04	0.04	0.04	0.04	0.04	0.04
200 Hz, H_{1x}/H_{1A} at f_1	1.0	1.74	2.15	2.69	3.21	3.54
200 Hz, H_{sx}/H_{sA} at f_s	1.0	1.2	1.29	1.39	1.43	1.51
200 Hz, H_{sx}/H_{1x}	0.32	0.22	0.19	0.16	0.14	0.14
400 Hz, B_s[T]	0.07	0.07	0.07	0.07	0.07	0.07
400 Hz, H_{1x}/H_{1A} at f_1	1.0	1.74	2.13	2.67	3.19	3.53
400 Hz, H_{sx}/H_{sA} at f_s	1.0	1.22	1.33	1.47	1.54	1.67
400 Hz, H_{sx}/H_{1x}	0.45	0.31	0.28	0.25	0.22	0.21
700 Hz, B_s[T]	0.11	0.11	0.11	0.11	0.11	0.11
700 Hz, H_{1x}/H_{1A} at f_1	1.0	1.69	2.07	2.57	3.06	3.35
700 Hz, H_{sx}/H_{sA} at f_s	1.0	1.22	1.33	1.47	1.55	1.66
700 Hz, H_{sx}/H_{1x}	0.62	0.44	0.39	0.35	0.31	0.31
1000 Hz, B_s[T]	0.17	0.17	0.17	0.18	0.18	0.18
1000 Hz, H_{1x}/H_{1A} at f_1	1.0	1.61	1.96	2.45	2.89	3.19
1000 Hz, H_{sx}/H_{sA} at f_s	1.0	1.23	1.35	1.54	1.68	1.82
1000 Hz, H_{sx}/H_{1x}	0.78	0.59	0.54	0.49	0.45	0.45
2500 Hz, B_s[T]	0.35	0.35	0.35	0.35	0.35	0.35
2500 Hz, H_{1x}/H_{1A} at f_1	1.0	1.41	1.65	2.0	2.28	2.51
2500 Hz, H_{sx}/H_{sA} at f_s	1.0	1.23	1.35	1.51	1.6	1.71
2500 Hz, H_{sx}/H_{1x}	1.15	1.01	0.94	0.87	0.81	0.78

6.1.1.2 With Sinusoidal Sample A as Reference

Comparing the measured PWM signal with the sinusoidal sample A as reference instead, was done with

$$H_{deg}^{Sine} = \frac{H^{PWM}(x)}{H^{Sine}(A)} \tag{6.2}$$

where H_{deg}^{Sine} is the peak degradation. Showing the same frequencies as for the other degradation, 100 Hz and 400 Hz, the H_{deg}^{Sine} can be seen in Figure 6.10. Since all the samples in the figure is compared with the same reference measurement, it can be noticed that the degradation is higher compared to the sinusoidal for all PWM measurements. The second thing that can be noticed, which was also seen for the permeability, is that at the saturation point around 1.3 T, the degradation of PWM and sinusoidal is same for the same steel samples. As the fundamental frequency is increasing, the H_{deg}^{Sine} is increasing more and more due to the changing Fha.

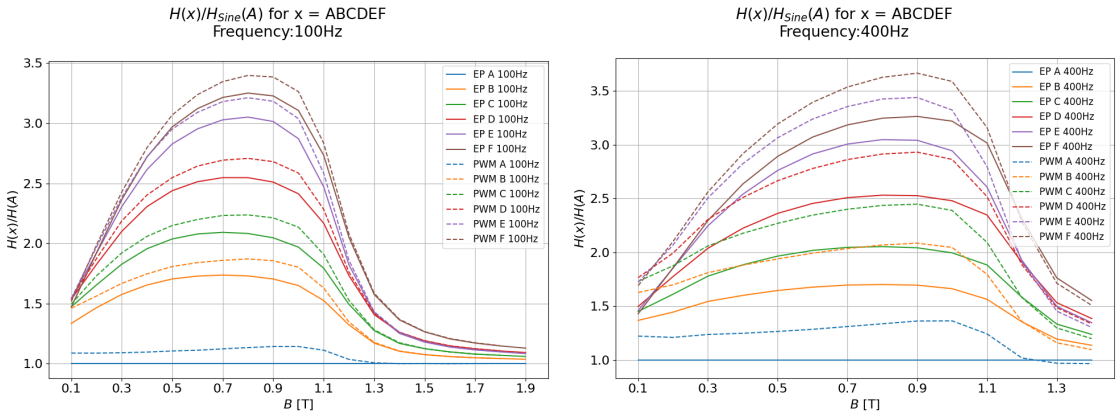

(a) H_{deg}^{Sine} vs B_{ref} at 100 Hz. **(b)** H_{deg}^{Sine} vs B_{ref} at 400 Hz.

Figure 6.10: H_{deg}^{Sine} for different frequencies. Where A-F is steel samples. Solid: Sine, Dashed: PWM.

Plotting the degradation as distance from CE, which can be seen in Figure 6.11, a similar exponential degradation can be noticed but with an offset for the PWM degradation. As mentioned before the degradation at higher B levels is lined up and similar to the sinusoidal degradation.

An interesting difference from the sinusoidal H degradation was that degradation spread was much more even across the different fundamental frequencies when comparing to sinusoidal sample A. In Figure 6.12, the degradation can be seen over different fundamental frequencies, and colour is much more even across the frequencies.

In Table 6.7 the same thing can be seen, here with the maximum degradation for each sample, different fundamental frequencies, and at each B level it occurred.

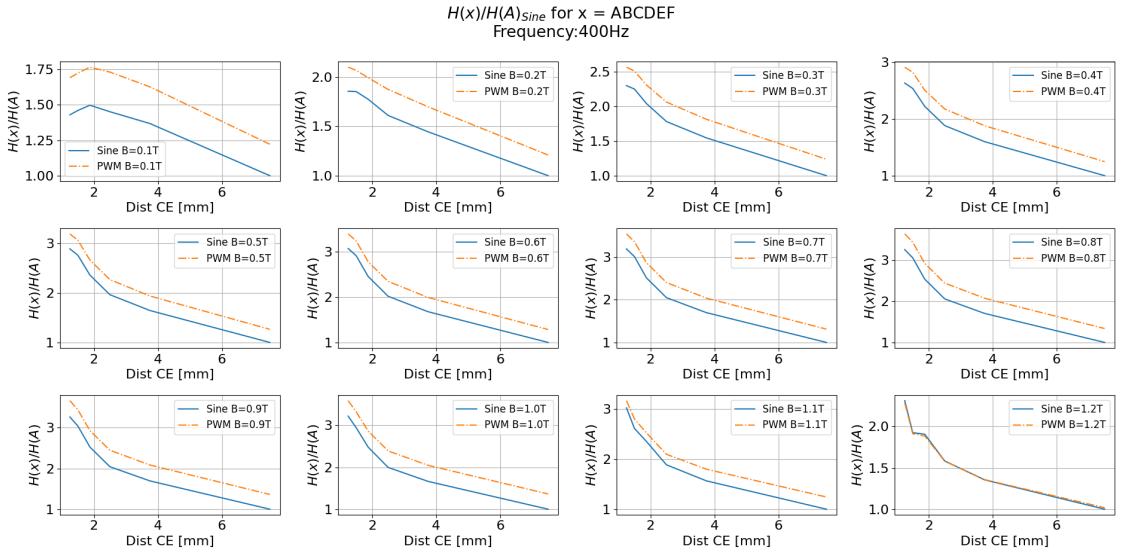

Figure 6.11: H_{deg}^{Sine} vs mm from cut edge for different B levels. Solid: Sine, Dashed: PWM.

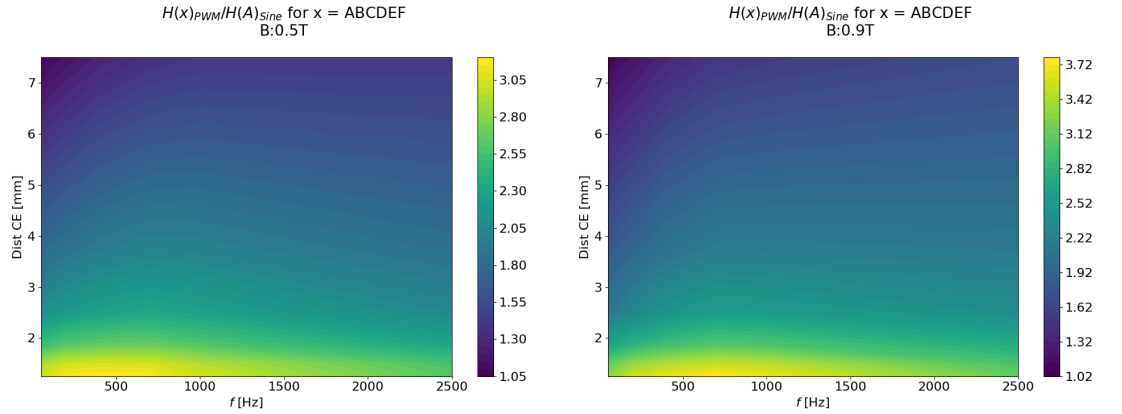

(a) CE vs f at B=0.5T.

(b) CE vs f at B=1.0T.

Figure 6.12: H_{deg}^{Sine} is intensity for different B levels.

Looking at sample F for example, the degradation ranges between 3.33 to 3.76 across different frequencies. The degradation compared to sinusoidal reference is quite drastic as well, at the most narrow sample and maximum degradation its 3.76 times as much H needed to reach same B. This means 3.76 times as much current to reach same point which is significant.

As mentioned earlier, these comparisons where using the peak values of H, but it is also of interest to look at the degradation at the f_1 and at f_s. In Table 6.8, the degradation is compared at f_1 and f_s to the measured sinusoidal content at f_1. The maximum degradation for the f_1 can be seen at 1.0 T, while the maximum degradation for f_s can be seen at 1.1 T. The degradation at the f_s is varying up and down and doesn't have the same increase and decrease of degradation as the f_1. Looking

Table 6.7: Epstein H_{deg}^{Sine} max and at what B level. For different samples and frequencies.

f [Hz]	A: H_{deg}^{max}	B: H_{deg}^{max}	C: H_{deg}^{max}	D: H_{deg}^{max}	E: H_{deg}^{max}	F: H_{deg}^{max}
50	1.07 @ 0.7T	1.8 @ 0.7T	2.17 @ 0.7T	2.63 @ 0.8T	3.14 @ 0.8T	3.33 @ 0.8T
100	1.14 @ 0.8T	1.87 @ 0.8T	2.24 @ 0.8T	2.71 @ 0.8T	3.21 @ 0.8T	3.4 @ 0.8T
200	1.22 @ 0.8T	1.94 @ 0.8T	2.32 @ 0.8T	2.81 @ 0.8T	3.34 @ 0.8T	3.56 @ 0.9T
400	1.36 @ 0.9T	2.09 @ 0.9T	2.45 @ 0.9T	2.93 @ 0.9T	3.44 @ 0.9T	3.67 @ 0.9T
700	1.51 @ 0.9T	2.18 @ 0.9T	2.56 @ 0.9T	3.04 @ 0.9T	3.53 @ 0.9T	3.76 @ 0.9T
1000	1.55 @ 1.0T	2.2 @ 1.0T	2.54 @ 1.0T	3.02 @ 1.0T	3.47 @ 0.9T	3.71 @ 1.0T
2500	1.76 @ 1.0T	2.27 @ 1.0T	2.52 @ 1.0T	2.9 @ 1.0T	3.19 @ 1.0T	3.41 @ 1.0T

at the degradation as distance from CE, the f_s degradation does have some sort of exponential degradation still, just like the f_1 degradation.

In Figure 6.13 the degradation from Table 6.8 can be seen. With a peak around 0.9 T and 1.0 T. Comparing this figure with the peak degradation Figure 6.10, it has similar shape but the maximum peak is shifted some.

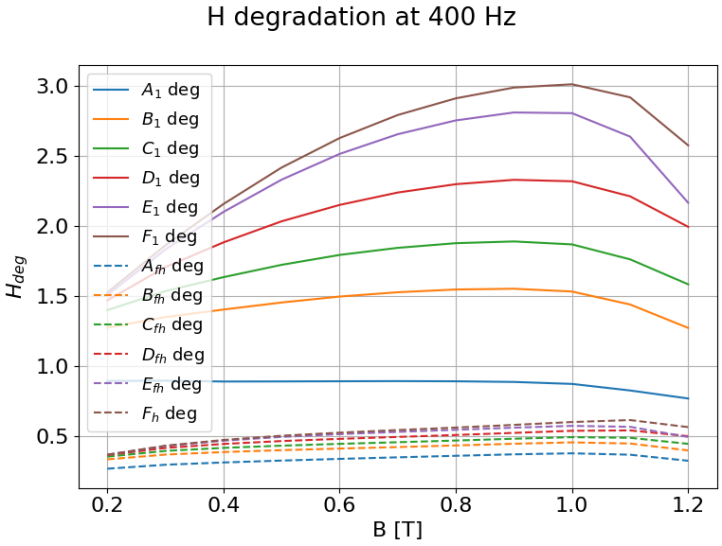

Figure 6.13: Degradation at f_s and f_1 with sinusoidal sample A as reference. Dashed: f_s degradation, Solid: f_1 degradation.

This degradation of the fundamental content and switching frequency content was also compared for all the different fundamental frequencies measured. This was summarized in Table 6.9, which is specific for 1.2 T. What can be noticed here is the fundamental degradation is decreasing as fundamental frequency is increasing, and the opposite for the switching frequency degradation, increasing as fundamental frequency is increasing. This is the same as for the calculations with PWM sample

Table 6.8: H_{deg} for fundamental H_1 and H_s signal.
For non-sinusoidal flux at 400 Hz.

Harmonic	Flux Density [T]	A	B	C	D	E	F
H_{1x}/H_{1A}^{Sine}	0.2	0.9	1.28	1.4	1.47	1.51	1.53
H_{sx}/H_{1A}^{Sine}	0.2	0.27	0.34	0.36	0.37	0.37	0.37
H_{1x}/H_{1A}^{Sine}	0.3	0.9	1.35	1.54	1.71	1.83	1.86
H_{sx}/H_{1A}^{Sine}	0.3	0.3	0.37	0.4	0.42	0.43	0.43
H_{1x}/H_{1A}^{Sine}	0.4	0.89	1.4	1.64	1.88	2.1	2.16
H_{sx}/H_{1A}^{Sine}	0.4	0.31	0.39	0.42	0.45	0.47	0.47
H_{1x}/H_{1A}^{Sine}	0.5	0.89	1.45	1.72	2.03	2.33	2.42
H_{sx}/H_{1A}^{Sine}	0.5	0.33	0.4	0.43	0.47	0.5	0.5
H_{1x}/H_{1A}^{Sine}	0.6	0.89	1.5	1.79	2.15	2.51	2.63
H_{sx}/H_{1A}^{Sine}	0.6	0.34	0.41	0.45	0.48	0.52	0.53
H_{1x}/H_{1A}^{Sine}	0.7	0.89	1.53	1.84	2.24	2.66	2.79
H_{sx}/H_{1A}^{Sine}	0.7	0.35	0.42	0.46	0.5	0.53	0.55
H_{1x}/H_{1A}^{Sine}	0.8	0.89	1.55	1.88	2.3	2.75	2.91
H_{sx}/H_{1A}^{Sine}	0.8	0.36	0.44	0.47	0.51	0.55	0.56
H_{1x}/H_{1A}^{Sine}	0.9	0.89	1.55	1.89	2.33	2.81	2.99
H_{sx}/H_{1A}^{Sine}	0.9	0.37	0.45	0.48	0.53	0.56	0.58
H_{1x}/H_{1A}^{Sine}	1.0	0.87	1.53	1.87	2.32	2.81	3.01
H_{sx}/H_{1A}^{Sine}	1.0	0.38	0.46	0.49	0.54	0.58	0.6
H_{1x}/H_{1A}^{Sine}	1.1	0.83	1.44	1.76	2.21	2.64	2.92
H_{sx}/H_{1A}^{Sine}	1.1	0.37	0.45	0.49	0.54	0.57	0.62
H_{1x}/H_{1A}^{Sine}	1.2	0.77	1.27	1.58	1.99	2.17	2.58
H_{sx}/H_{1A}^{Sine}	1.2	0.33	0.4	0.45	0.5	0.5	0.57
H_{1x}/H_{1A}^{Sine}	1.3	0.98	1.31	1.55	1.88	1.87	2.31
H_{sx}/H_{1A}^{Sine}	1.3	0.28	0.32	0.35	0.39	0.38	0.44
H_{1x}/H_{1A}^{Sine}	1.4	1.2	1.44	1.61	1.84	1.8	2.15
H_{sx}/H_{1A}^{Sine}	1.4	0.24	0.27	0.29	0.32	0.31	0.35

A as reference. This will be discussed further in discussions chapter and conclusions.

Table 6.9: H degradation compared to sinusoidal fundamental sample A, at 1.2 T, and for different frequencies.

	A	B	C	D	E	F
H_{1x}/H_{1A}^{Sine} at 50 Hz	0.89	1.39	1.66	2.01	2.29	2.52
H_{sx}/H_{1A}^{Sine} at 50 Hz	0.1	0.11	0.11	0.12	0.12	0.12
H_{1x}/H_{1A}^{Sine} at 100 Hz	0.83	1.32	1.58	1.93	2.21	2.43
H_{sx}/H_{1A}^{Sine} at 100 Hz	0.17	0.19	0.2	0.22	0.21	0.23
H_{1x}/H_{1A}^{Sine} at 200 Hz	0.81	1.31	1.62	2.04	2.23	2.64
H_{sx}/H_{1A}^{Sine} at 200 Hz	0.22	0.26	0.28	0.3	0.3	0.32
H_{1x}/H_{1A}^{Sine} at 400 Hz	0.77	1.27	1.58	1.99	2.17	2.58
H_{sx}/H_{1A}^{Sine} at 400 Hz	0.33	0.4	0.45	0.5	0.5	0.57
H_{1x}/H_{1A}^{Sine} at 700 Hz	0.67	1.08	1.33	1.67	1.86	2.19
H_{sx}/H_{1A}^{Sine} at 700 Hz	0.4	0.49	0.54	0.62	0.62	0.71
H_{1x}/H_{1A}^{Sine} at 1000 Hz	0.71	1.13	1.41	1.77	1.91	2.27
H_{sx}/H_{1A}^{Sine} at 1000 Hz	0.51	0.65	0.75	0.88	0.89	1.04
H_{1x}/H_{1A}^{Sine} at 2500 Hz	0.65	0.91	1.09	1.35	1.48	1.73
H_{sx}/H_{1A}^{Sine} at 2500 Hz	0.69	0.87	0.97	1.12	1.15	1.31

6.1.1.3 Comparing PWM Sample's with Sinusoidal Sample's

The last comparison for the H degradation, was with comparing sample to sample. This was done using

$$H^x_{deg} = \frac{H^{PWM}(x)}{H^{Sine}(x)} \tag{6.3}$$

where H^x_{deg} is the sample degradation, and x is sample A to F. Looking at this degradation was interesting to see which of the samples had the highest impact of going from sinusoidal B to non-sinusoidal B. The H^x_{deg} for 100 Hz and 400 Hz, can be seen in Figure 6.15. Here the peak is very clear at 1.0 T for both frequencies.

The second conclusion from the figure is that the degradation is worst for sample A, and then degradation is decreasing as sample width is decreasing. So going from sinusoidal to PWM, the most impact is just changing signal. The degradation has lower impact on the more narrow samples with PWM. But as the fundamental frequency is increasing and Fha is decreasing the impact is increasing more, which can be seen comparing 100 Hz to 400 Hz sample F. Sample F has a peak of 1.04 at 100 Hz and 1.12 at 400 Hz.

Confirming what has been noticed before is that at higher B levels, the degradation plateaus and for 100 Hz is close to 1, meaning same measured H for both samples.

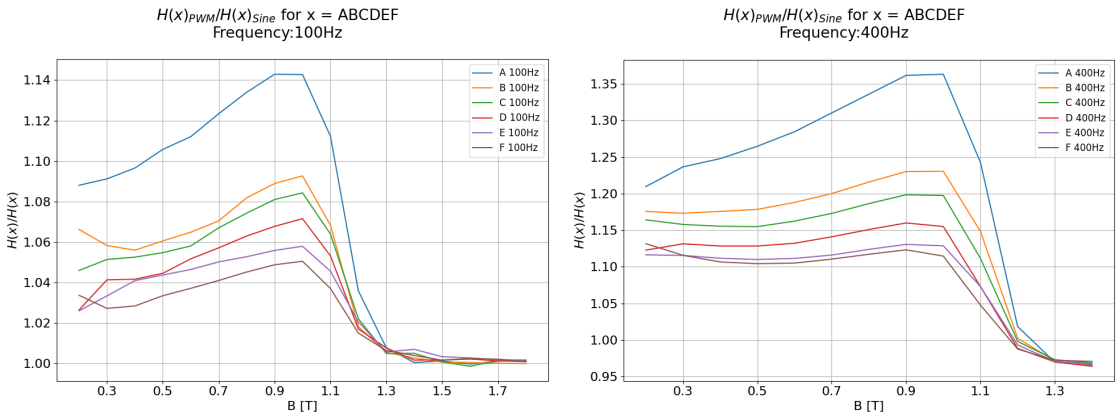

(a) H^x_{deg} vs B_{ref} at 100 Hz. **(b)** H^x_{deg} vs B_{ref} at 400 Hz.

Figure 6.14: H^x_{deg} for different frequencies. Where A-F is steel samples.

The same degradation pattern can be seen in Figure 6.15, where the intensity is the degradation. Around 1.2 T, the color is very consistent and dark meaning no difference between the samples. The degradation max is now at the widest sample, just as mentioned above, and the degradation is decreasing as the distance gets closer to the CE.
Lastly the maximum degradation comparing sample to sample can be seen in Table 6.10. Here, same as before, the maximum degradation for each sample, frequency

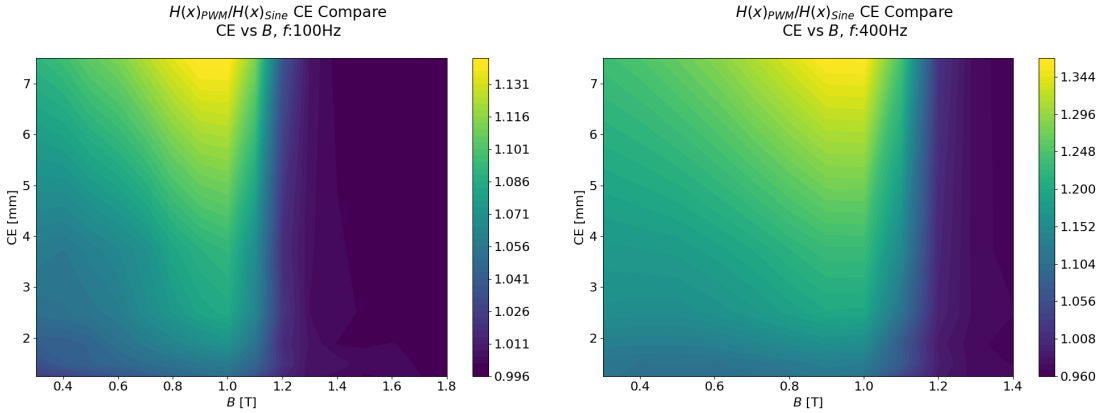

(a) CE vs B at 100 Hz.

(b) CE vs B at 400 Hz.

Figure 6.15: H^x_{deg} is intensity for different frequencies.

and at what specific B level can be seen. In the table, it can be noticed that the degradation is increasing as fundamental frequency is increasing. This is due to the Fha is decreasing and the harmonic content is appearing at closer to the fundamental. This is reducing the performance of the PWM and leading to an increase of degradation comparing sample to sample.

Another point from the table, around 0.1 T the measurement did not seem very reasonable due to control limits, so this point may be disregarded.

Table 6.10: Epstein H_{deg} max at different samples Hx over Hx.

f [Hz]	A: H^{max}_{deg}	B: H^{max}_{deg}	C: H^{max}_{deg}	D: H^{max}_{deg}	E: H^{max}_{deg}	F: H^{max}_{deg}
50	1.07 @ 0.7T	1.04 @ 0.7T	1.05 @ 0.8T	1.04 @ 0.8T	1.03 @ 0.8T	1.03 @ 0.8T
100	1.14 @ 1.7T	1.09 @ 1.7T	1.08 @ 1.7T	1.07 @ 1.7T	1.06 @ 1.7T	1.05 @ 1.7T
200	1.22 @ 0.8T	1.14 @ 0.8T	1.13 @ 0.8T	1.1 @ 0.8T	1.08 @ 0.8T	1.08 @ 0.7T
400	1.36 @ 0.8T	1.23 @ 0.8T	1.2 @ 0.7T	1.16 @ 0.7T	1.13 @ 0.7T	1.12 @ 0.7T
700	1.51 @ 0.8T	1.33 @ 0.8T	1.29 @ 0.8T	1.24 @ 0.7T	1.2 @ 0.8T	1.19 @ 0.7T
1000	1.55 @ 0.7T	1.34 @ 0.7T	1.31 @ 0.7T	1.25 @ 0.7T	1.21 @ 0.7T	1.19 @ 0.7T
2500	1.76 @ 0.8T	1.53 @ 0.8T	1.44 @ 0.8T	1.36 @ 0.7T	1.27 @ 0.8T	1.25 @ 0.7T

6.1.2 Specific Power Loss Degradation

Same as the H degradation, the Ps degradation is divided in three sections, comparing with PWM as reference, with sinusoidal as reference, and comparing sample to sample. Starting with the PWM as reference.

6.1.2.1 With PWM Sample A as Reference

For degradation with PWM signal as reference the degradation was calculated as

$$Ps_{deg}^{PWM} = \frac{Ps_{PWM}(x)}{Ps_{PWM}(A)} \tag{6.4}$$

where Ps_{deg}^{PWM} is the degradation, and x is measured sample A to F. Starting with the measured specific power loss, which can be seen in Figure 6.16. The power loss increase can be noticed quite easily comparing the PWM and sinusoidal, with PWM having drastically larger losses. Which was to be expected, since the switching introduced the minor loops and also increased the eddy currents in the material, higher losses was to be expected.

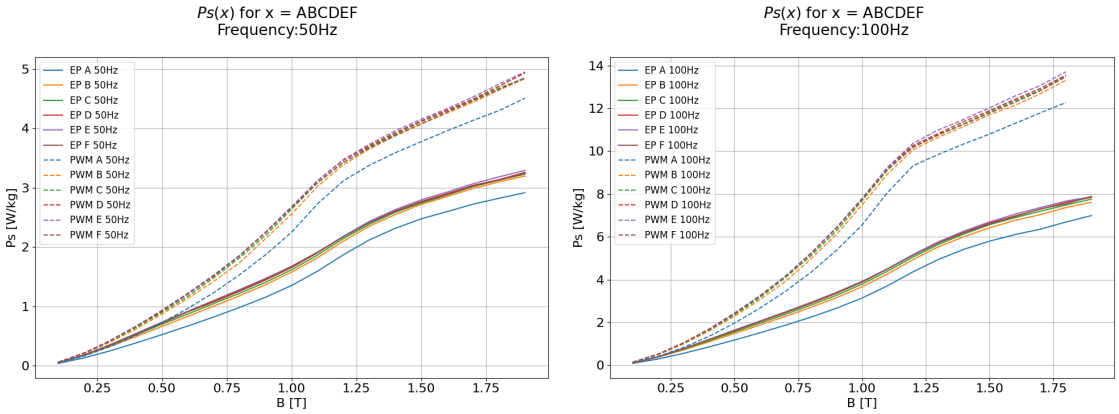

(a) $Ps_{Measured}$ vs B_{ref} at 50 Hz, Dashed: PWM, Solid: Sinusoidal.

(b) $Ps_{Measured}$ vs B_{ref} at 100 Hz, Dashed: PWM, Solid: Sinusoidal.

Figure 6.16: Ps loss for different cut samples and frequency, comparing PWM losses with Sinusoidal.

Then starting to look at the Ps_{deg}^{PWM} in Figure 6.17, first thing to notice is that the PWM degradation compared to its own reference is actually lower compared to the sinusoidal reference. This is the same as for the H_{deg}^{PWM}, this is could be meaning that due to the switching content from the PWM, the material is reaching some sort of degradation saturation, meaning it cannot keep the same degradation when under more magnetic field strength at different harmonics. Another thought could be that the same as for the higher fundamental frequencies with the sinusoidal measurement, the skin effect due to the switching in the PWM leads to skin effect

which uses the material more even though its degraded.

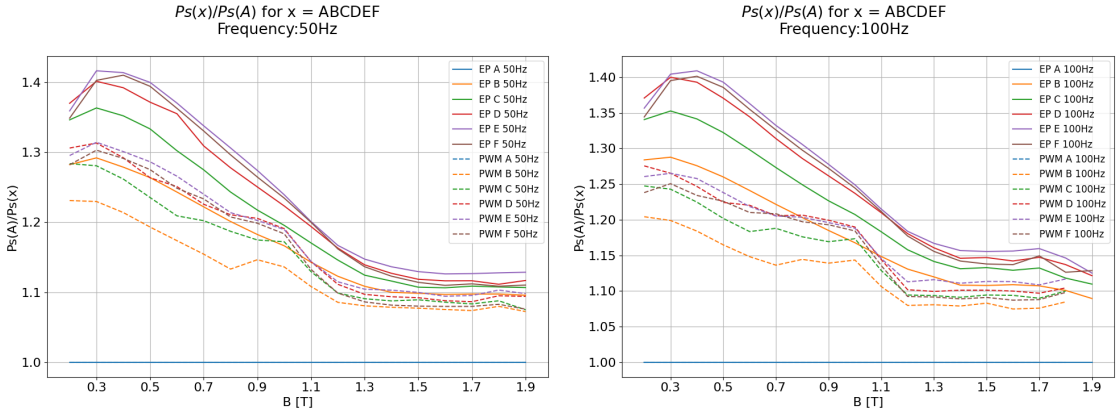

(a) Ps_{deg}^{PWM} vs B_{ref} at 50 Hz, Dashed: PWM, Solid: Sinusoidal.

(b) Ps_{deg}^{PWM} vs B_{ref} at 100 Hz, Dashed: PWM, Solid: Sinusoidal.

Figure 6.17: Ps degradation for different cut samples and frequency, comparing PWM losses with Sinusoidal.

Looking at the degradation at distance from CE, the same conclusions can be drawn. With the lower degradation for the PWM compared to sinusoidal degradation. The degradation does seem to have some sort of linear increase as distance from CE is decreasing. It has the same peak as for the sinusoidal as well, around 0.3 T. The degradation from cut edge here could be used to create some model that could be implemented into the FEM program.

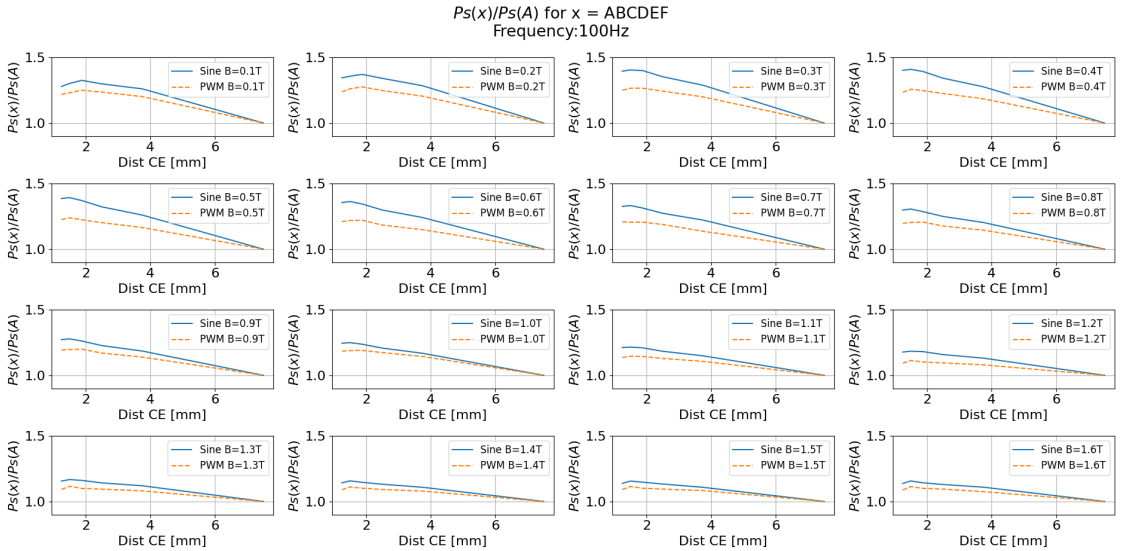

Figure 6.18: Ps_{deg} vs mm from cut edge at 400 Hz, for different B levels.

In Table 6.11 the maximum degradation for the different samples, fundamental frequencies and at what specific B level can be seen. When comparing to PWM as

reference, the maximum degradation seems to be happening at lower fundamental frequencies, except for 1000 Hz. This is an interesting analysis since the degradation is reducing after 1000 Hz.

There is two key factors to this degradation pattern, first is that the PWM effect does seem to have some peak of loss around Fha = 10-15, this is due to the increase in ripple and minor loops. This will be seen in the coming section where the effect of different Fha is analyzed.

The second factor is that since the f_s is kept constant, this is changing the Fha and leading to an even Fha for some of the fundamental frequencies. When Fha is an odd integer, it will create and odd symmetry in the signal as well as a half-wave symmetry and then only odd harmonics will be present in the frequency spectrum, and thereby lower losses. So when when Fha is an even integer it will loose these qualities and thereby an increase of losses.

The measurement at very high B levels have been questioned here as well. Analyzing the points above 1.1 T, the controller does not seem to be able to control the B to a sinusoidal fundamental and larger harmonics are introduced.

Another point in the table is that for some of the measurements the sample E has larger degradation compared to sample F. This is due to that the sample F is so narrow that after some point the material is seen as air.

Table 6.11: Epstein Ps_{deg} max and at what B level. For different samples and frequencies with PWM reference.

f [Hz]	B: Ps_{deg}^{max}	C: Ps_{deg}^{max}	D: Ps_{deg}^{max}	E: Ps_{deg}^{max}	F: Ps_{deg}^{max}
50	1.23 @ 0.3 T	1.28 @ 0.3 T	1.31 @ 0.3 T	1.31 @ 0.3 T	1.3 @ 0.3 T
100	1.2 @ 0.3 T	1.24 @ 0.3 T	1.27 @ 0.3 T	1.27 @ 0.3 T	1.25 @ 0.3 T
200	1.18 @ 0.3 T	1.22 @ 0.3 T	1.25 @ 0.3 T	1.24 @ 0.3 T	1.23 @ 0.3 T
400	1.22 @ 0.3 T	1.28 @ 0.3 T	1.32 @ 0.3 T	1.33 @ 0.4 T	1.32 @ 0.4 T
700	1.2 @ 0.3 T	1.26 @ 0.3 T	1.29 @ 0.3 T	1.31 @ 0.4 T	1.32 @ 1.1 T
1000	1.18 @ 0.3 T	1.26 @ 0.3 T	1.33 @ 1.1 T	1.42 @ 1.1 T	1.48 @ 1.1 T
2500	1.2 @ 0.3 T	1.27 @ 0.3 T	1.34 @ 0.3 T	1.38 @ 0.3 T	1.38 @ 0.3 T

From the table, disregarding the points at 1000 Hz, it can also be seen that the degradation spread is closer compared H_{deg}, with only varying between 1.23 and 1.38 times the reference sample. This can also be seen in Figure 6.19, where the degradation is viewed at distance from CE over different fundamental frequencies. The intensity of the degradation can be seen more evenly spread here.

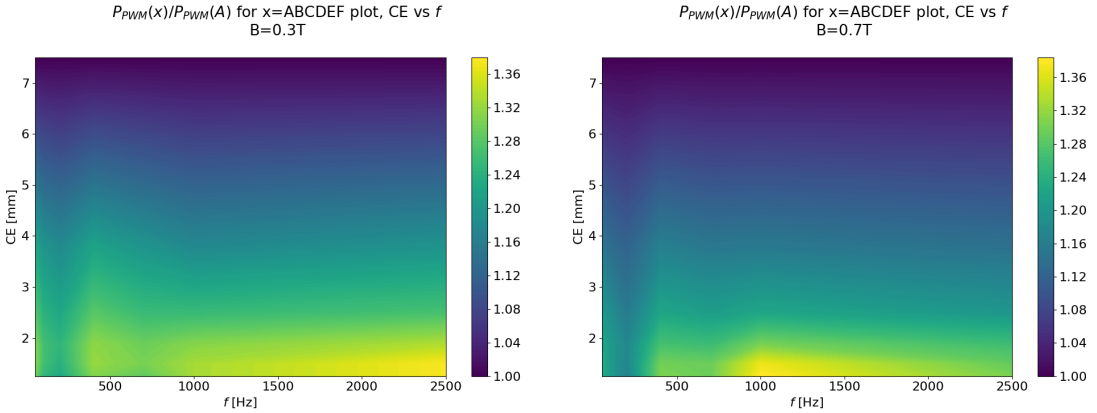

(a) Ps_{deg}^{PWM} vs Distance from CE at 0.3 T.

(b) Ps_{deg}^{PWM} vs Distance from CE at 0.7 T.

Figure 6.19: Ps_{deg}^{PWM} degradation for different cut samples and frequency.

6.1.2.2 With Sinusoidal Sample A as Reference

Second comparison is with the sinusoidal measurement of sample A as reference. Using this will lead to a degradation calculated as following,

$$Ps_{deg}^{Sine} = \frac{Ps_{PWM}(x)}{Ps_{Sine}(A)} \tag{6.5}$$

where Ps_{deg}^{Sine}, and x is the different steel samples A to F. The degradation can be seen in Figure 6.20, where in the left side of the figure the degradation for PWM does look quite different now, with a peak around 1.1 T and then coming to some sort of plateau around 1.5 T.

The right side of the figure is showing the degradation at distance from CE compared over different fundamental frequencies. Here the changing of Fha is very prominent since the largest degradation is happening around 1000 Hz. This is again due to the even harmonic and lower order harmonic.

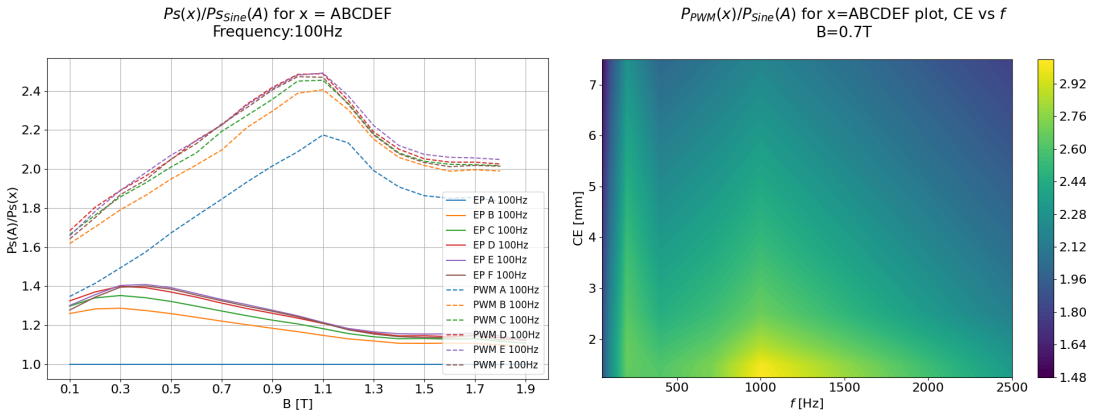

(a) Ps_{deg}^{Sine} vs B for fundamental f of 100 Hz.

(b) Distance from CE vs f where Ps_{deg}^{Sine} is intensity at 0.7 T.

Figure 6.20: Ps_{deg}^{Sine} degradation for different samples, and for compared over different fundamental frequencies.

Turning the view around and looking at the degradation over distance from cut edge instead, the same linear degradation can be seen, but this time with an offset due to the increase of minor loop losses. Using the different degradation here could be used as a model when implementing the degradation in FEM simulations.

In Table 6.12, the maximum degradation for each sample, frequency and specific B level can be seen. The maximum degradation can be seen around 1000 Hz, and 1.1 T. The degradation here is 3.51 which is a significant increase in iron loss. The increase iron loss was to be expected due to the increase in ripple in the B and H.

In Figure 6.22 and Figure 6.23 the hysteresis loops for sinusoidal excitation and PWM excitation can be seen. Here it can be noticed that the minor loops are in-

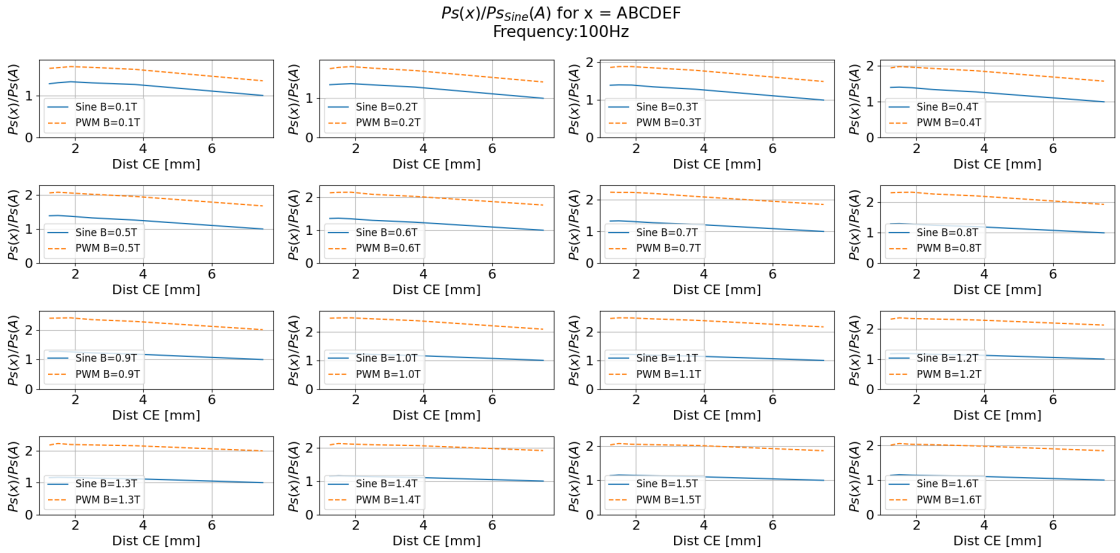

Figure 6.21: Ps_{deg}^{Sine} vs mm from cut edge at 100 Hz, for different B levels.

Table 6.12: Epstein Ps_{deg}^{Sine} max at different samples with as Sine reference, and at what specific B level.

f [Hz]	A: Ps_{deg}^{max}	B: Ps_{deg}^{max}	C: Ps_{deg}^{max}	D: Ps_{deg}^{max}	E: Ps_{deg}^{max}	F: Ps_{deg}^{max}
50	1.71 @ 1.1T	1.9 @ 1.1T	1.95 @ 1.0T	1.98 @ 1.0T	1.98 @ 1.0T	1.97 @ 1.0T
100	2.17 @ 1.1T	2.41 @ 1.1T	2.45 @ 1.1T	2.49 @ 1.1T	2.49 @ 1.1T	2.47 @ 1.0T
200	2.64 @ 1.1T	2.9 @ 1.1T	2.96 @ 1.0T	3.01 @ 1.0T	3.01 @ 1.0T	3.02 @ 1.0T
400	2.25 @ 1.1T	2.56 @ 1.1T	2.68 @ 1.1T	2.8 @ 1.1T	2.88 @ 1.1T	2.92 @ 1.1T
700	2.34 @ 1.1T	2.67 @ 1.1T	2.8 @ 1.1T	2.94 @ 1.1T	3.03 @ 1.1T	3.08 @ 1.1T
1000	2.37 @ 1.1T	2.73 @ 1.1T	2.92 @ 1.1T	3.16 @ 1.1T	3.36 @ 1.1T	3.51 @ 1.1T
2500	1.88 @ 1.1T	2.13 @ 1.1T	2.26 @ 1.1T	2.41 @ 1.1T	2.47 @ 1.1T	2.53 @ 1.1T

creasing as the fundamental frequency is increasing. The result of this changing Fha will be analyzed in the next section.

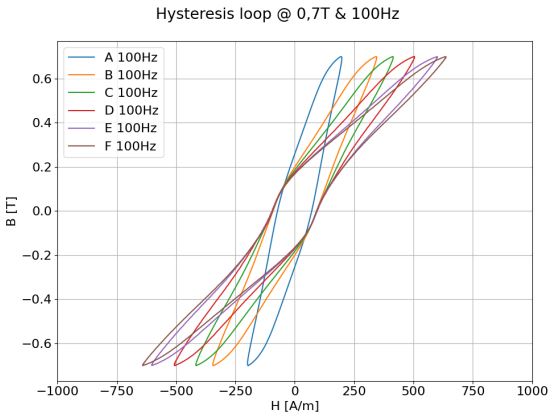

(a) Hysteresis loop for sinusoidal excitation at 0.7 T and 100 Hz.

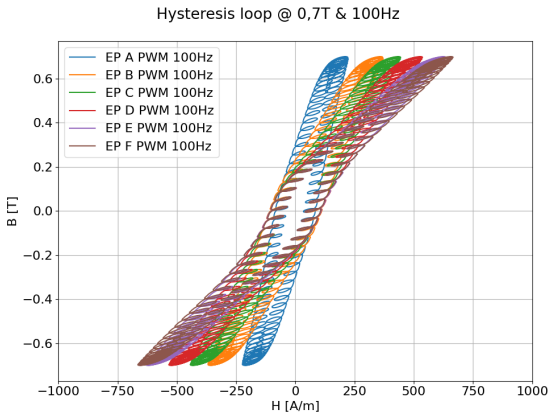

(b) Hysteresis loop for PWM excitation at 0.7 T and 100 Hz.

Figure 6.22: Hysteresis loop for sinusoidal and PWM excitation, for different samples A to F.

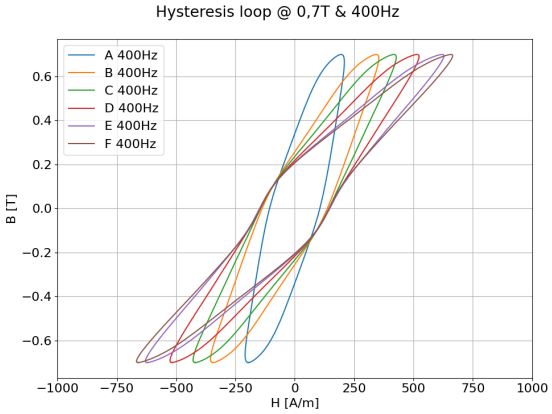

(a) Hysteresis loop for sinusoidal excitation at 0.7 T and 400 Hz.

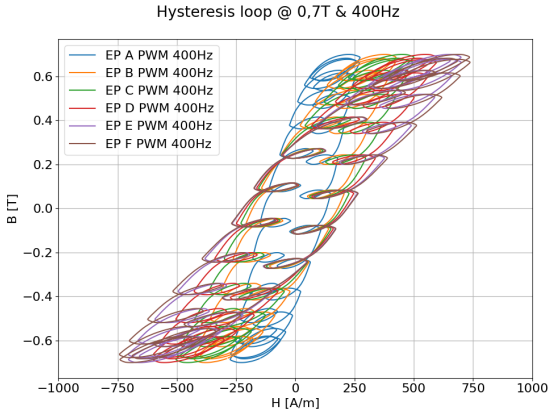

(b) Hysteresis loop for PWM excitation at 0.7 T and 400 Hz.

Figure 6.23: Hysteresis loop for sinusoidal and PWM excitation, for different samples A to F.

6.1.2.3 Comparing PWM Sample with Sinusoidal Sample

The last comparison for the power loss degradation with PWM excitation is the sample to sample comparison. The degradation can be calculated as,

$$Ps(x)_{deg} = \frac{Ps_{PWM}(x)}{Ps_{Sine}(x)} \tag{6.6}$$

where $Ps(x)_{deg}$ is the degradation from sample to sample. In Figure 6.24, the $Ps(x)_{deg}$ can be seen for different B levels to the left and compared at different distance from CE to the right. A key point here is that the largest difference for sample A, and lower as sample width is decreasing. This would mean that the degradation effect is lowered as the PWM is introduced. This is the same conclusion as for the $H(x)_{deg}$.

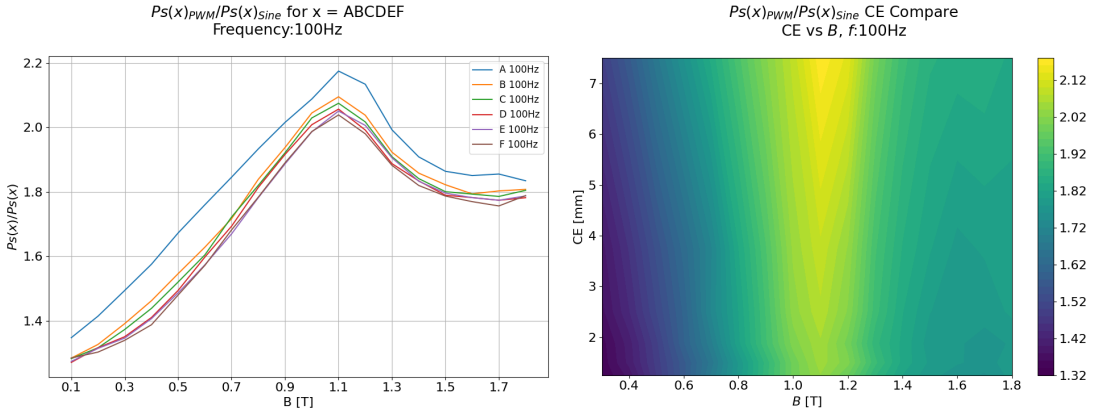

(a) Hysteresis loop for sinusoidal excitation at 0.7 T and 400 Hz.

(b) Hysteresis loop for sinusoidal excitation at 0.7 T and 400 Hz.

Figure 6.24: Hysteresis loop for sinusoidal and PWM excitation, for different samples A to F.

Same as for the other degradation's, Table 6.13 is a summarized table with the maximum degradation for the different samples. At lower fundamental frequencies largest degradation is at sample A. But as fundamental frequencies is increasing and the Fha is decreasing and the degradation is shifting to being more affected and higher at more narrow samples.

Table 6.13: Epstein $Ps(x)_{deg}$ max for different samples, frequencies and at each specific B level.

f [Hz]	A: P_{deg}^{max}	B: P_{deg}^{max}	C: P_{deg}^{max}	D: P_{deg}^{max}	E: P_{deg}^{max}	F: P_{deg}^{max}
50	1.71 @ 1.0T	1.66 @ 1.0T	1.65 @ 1.0T	1.64 @ 1.0T	1.63 @ 1.0T	1.62 @ 1.0T
100	2.17 @ 1.8T	2.09 @ 1.8T	2.07 @ 1.8T	2.06 @ 1.8T	2.05 @ 1.8T	2.04 @ 1.8T
200	2.64 @ 1.0T	2.47 @ 1.0T	2.42 @ 1.0T	2.36 @ 1.0T	2.33 @ 1.0T	2.3 @ 0.9T
400	2.41 @ 1.3T	2.45 @ 1.3T	2.53 @ 1.3T	2.65 @ 1.3T	2.62 @ 1.3T	2.79 @ 1.3T
700	2.52 @ 1.3T	2.53 @ 1.3T	2.56 @ 1.3T	2.63 @ 1.3T	2.61 @ 1.3T	2.71 @ 1.3T
1000	2.45 @ 1.1T	2.52 @ 1.1T	2.61 @ 1.1T	2.73 @ 1.1T	2.79 @ 1.1T	2.95 @ 1.1T
2500	1.97 @ 1.1T	2.03 @ 1.1T	2.09 @ 1.1T	2.13 @ 1.1T	2.09 @ 1.1T	2.13 @ 1.1T

6.2 Effects of Changing Fha

As mentioned before, in EM's there is usually a constant switching frequency and therefore the Fha is changing with our machine increasing speed. The tests before had that constant switching frequency, but the fundamental was changing as well so to be able to see the impact of only changing Fha this test was performed.

The test was performed for two different fundamental frequencies, 50 Hz and 400 Hz, to confirm the changes. The 400 Hz had 6 different Fha points but ranging over B values from 0.3 T to 1.1 T.

The 50 Hz measurement had all odd Fha between 1 and 49 to get a more detailed resolution for Fha, but the measurement was only performed at 0.7 T.

6.2.1 Effects of Fha at 400 Hz

Starting with the 400 Hz measurement, as mentioned before the controller sets the peak value of the desired signal, in this case B. For each of the different steel samples, the FFT of the B is almost identical. This means that as the steel samples width is decreasing and is more affected by the degradation in the material, the increase in H is still resulting in same B. Since it is the B that is controlled by the controller, the very similar B is expected for all steel samples, and what is changing is the H.

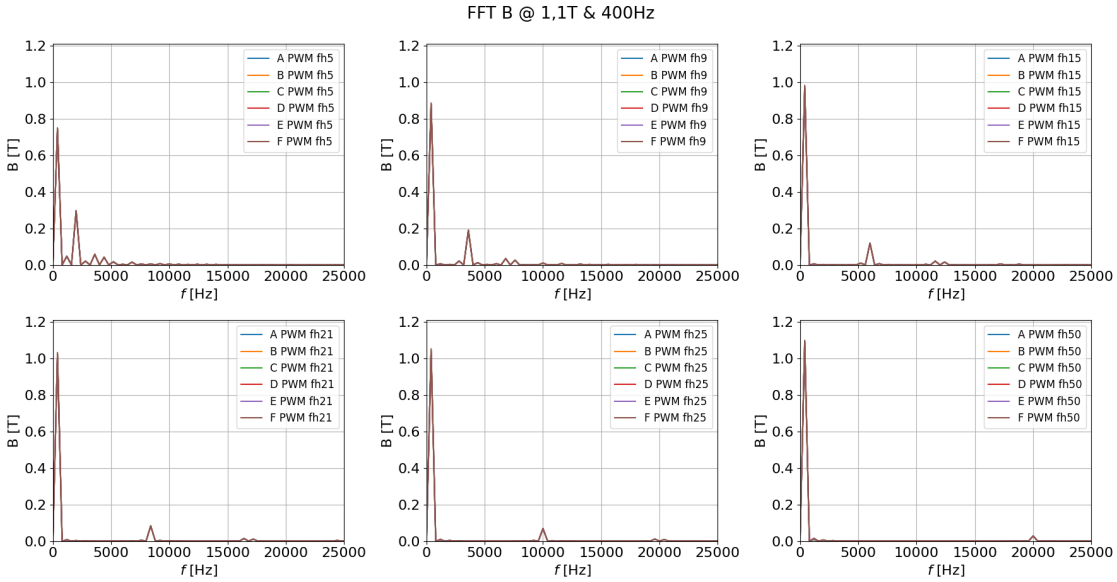

Figure 6.25: FFT of $B = 1.1$ T, for different Fha, where the legend in each figure shows the Fha number.

The FFT of B in Figure 6.25 is for a peak value of 1.1 T. To achieve this B, the H applied across the samples can be seen in Figure 6.26, here the signal is in time

domain. What can be seen in this figure is that as Fha is increasing, the number of ripples is increasing but the amplitude in ripple is decreasing, as explained in Section 4.5. Here the interesting point is the different degradation at fundamental versus at switching frequency for the different steel samples.

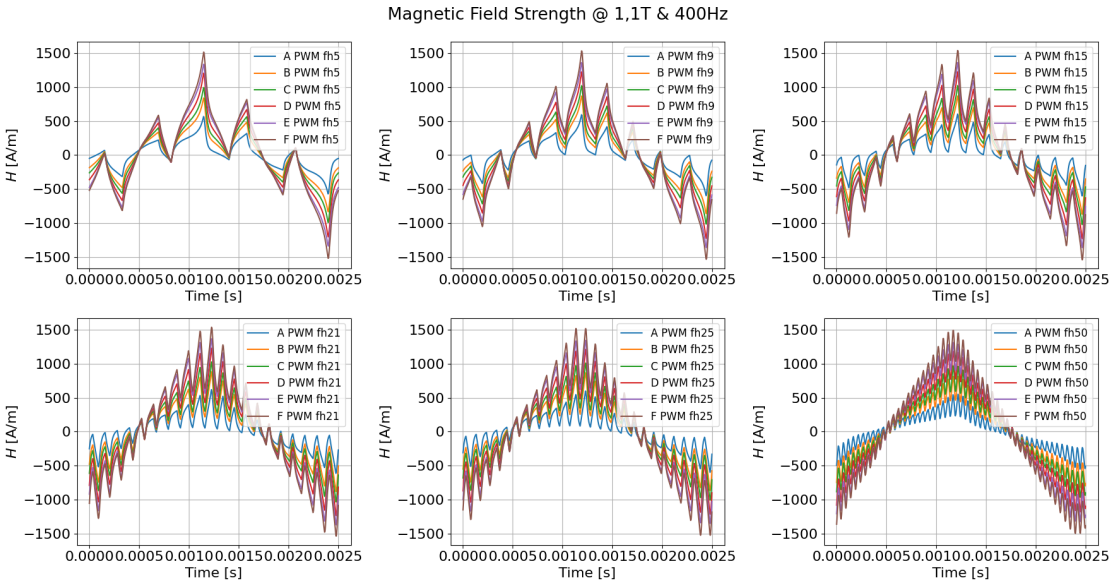

Figure 6.26: Time domain of $H = 1.1$ T, for different Fha, where the legend in each figure shows the Fha number.

This can be analyzed looking at the FFT of the H for this point. The FFT can be seen for the different Fha in Figure 6.27. Focusing on the fundamental content, which is the largest peak, and the switching harmonic content which is the Fha multiplied with the fundamental frequency, in this case 400 Hz.

First, the switching harmonic content can be seen moving higher in frequency as Fha is increasing. Second, as the Fha is increasing, the amount of harmonic content is lowered at f_s and increased at f_1. For Fha 5 the fundamental content is around 700 A/m, while for Fha 50 the content is around 1100 A/m.

Zooming in on the fundamental frequency content, in Figure 6.28, to analyze the degradation, it can be seen that the degradation is changing as Fha is changing. This seems to align with as for the sinusoidal degradation, the degradation is dependent on how much B and at what frequency content.

Same for the switching frequency harmonic content, in Figure 6.29 it is zoomed around this harmonic content. What can be noticed in this figure is that Fha 5 has the highest amount of degradation, and degradation is decreasing as Fha is increasing.

This is summarized in Table 6.14, where a few different observations have been noted. First, B_1, which is the fundamental flux density content, second H_{1x}/H_{1A}

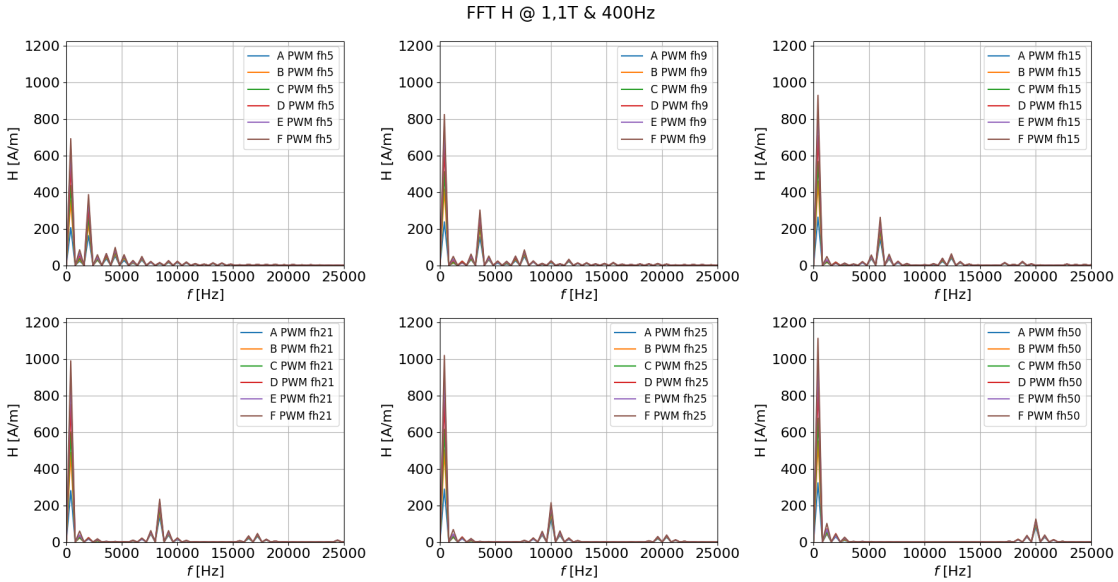

Figure 6.27: FFT of $H = 1.1$ T, for different Fha, where the legend in each figure shows the Fha number.

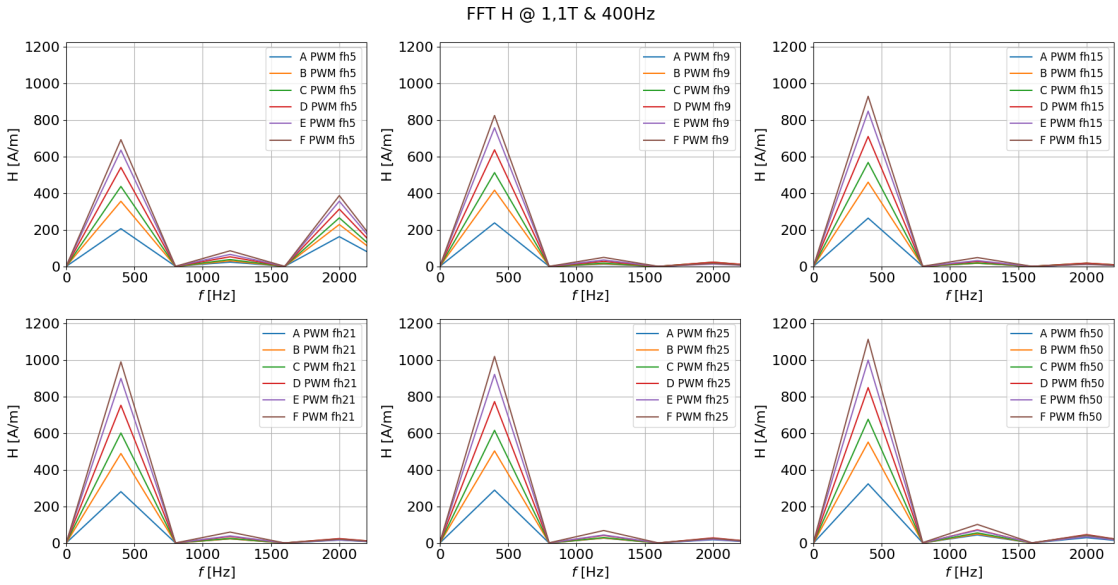

Figure 6.28: FFT of $H = 1.1$ T, for different Fha, zoomed around fundamental, where the legend in each figure shows the Fha number.

which is the H degradation at the fundamental frequency. Third, B_s, which is the switching frequency flux density content. Fourth, H_{sx}/H_{sA}, which is the H degradation at the switching frequency, and fifth, H_{sx}/H_{1x}, which is the amount of harmonic content at the switching frequency compared to its own sample fundamental content.

Table 6.14, show that for a peak value of 1.1 T, the fundamental B_1 is increasing as Fha is increasing. If applying same logic as for the sinusoidal excitation, then depending on B the degradation should increase as well. This is true until Fha 25,

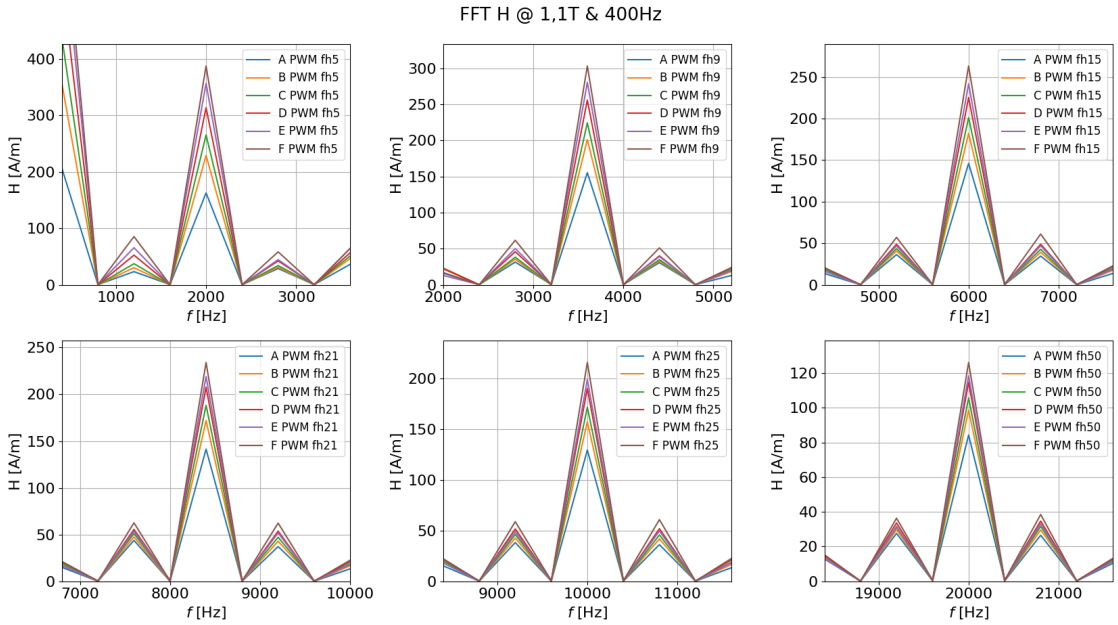

Figure 6.29: FFT of $H = 1.1$ T, for different Fha, zoomed around switching frequency.

then at Fha 50, the degradation is actually decreasing again. Probably this is due to that it is not only fundamental flux in the material but there is the harmonic flux as well which is effecting the degradation.

For the degradation at f_s, it can be noted that it is decreasing as the Fha is increasing, with the highest at Fha 5. It can also be noted that the B_s is decreasing as Fha is increasing, so this correlation can be seen that the degradation is dependent on the B level.

Another interesting observation is that the harmonic content compared to its own fundamental, H_{sx}/H_{1x}, is always highest for sample A. Since the degradation at the f_1 is larger than degradation at f_s, the content at f_s is actually decreasing compared to its own fundamental as sample width is decreasing.

Instead, looking at the power loss effect for different Fha, in Figure 6.30 the hysteresis loop can be seen for the different Fha at 1.1 T. This is also compared to the sinusoidal same measurement, and the power loss is written in the figure.

The figure shows that power loss is almost double the loss compared to the sinusoidal measurement in most Fha. But an interesting observation is that the PWM losses is actually increasing from Fha 5 until 15, and then decreasing again. This means that as number of loops are increasing by the increase of Fha, the losses are increasing, but then at some point, as the number of loops increase they also decrease in size. This happens after Fha 15, and then losses are decreasing.

Table 6.14: Flux density at switching frequency, fundamental degradation component, switching harmonic degradation component, and how large switching harmonic is compared to fundamental. At 1.1T and different Fha.

	A	B	C	D	E	F
FHA5, B_1[T]	0.74	0.74	0.74	0.75	0.74	0.75
FHA5, H_{1x}/H_{1A}	1.0	1.73	2.12	2.62	3.08	3.36
FHA5, B_s[T]	0.3	0.3	0.3	0.3	0.29	0.3
FHA5, H_{sx}/H_{sA}	1.0	1.41	1.63	1.93	2.19	2.38
FHA5, H_{sx}/H_{1x}	0.79	0.64	0.61	0.58	0.56	0.56
FHA9, B_1[T]	0.88	0.88	0.88	0.88	0.88	0.89
FHA9, H_{1x}/H_{1A}	1.0	1.75	2.15	2.68	3.18	3.47
FHA9, B_s[T]	0.19	0.19	0.19	0.19	0.19	0.19
FHA9, H_{sx}/H_{sA}	1.0	1.3	1.44	1.65	1.81	1.95
FHA9, H_{sx}/H_{1x}	0.65	0.48	0.44	0.4	0.37	0.37
FHA15, B_1[T]	0.97	0.97	0.97	0.98	0.97	0.98
FHA15, H_{1x}/H_{1A}	1.0	1.74	2.15	2.69	3.21	3.52
FHA15, B_s[T]	0.12	0.12	0.12	0.12	0.12	0.12
FHA15, H_{sx}/H_{sA}	1.0	1.25	1.38	1.54	1.66	1.8
FHA15, H_{sx}/H_{1x}	0.55	0.4	0.35	0.32	0.28	0.28
FHA21, B_1[T]	1.02	1.02	1.02	1.03	1.02	1.03
FHA21, H_{1x}/H_{1A}	1.0	1.74	2.14	2.68	3.2	3.53
FHA21, B_s[T]	0.08	0.08	0.08	0.08	0.08	0.08
FHA21, H_{sx}/H_{sA}	1.0	1.22	1.33	1.47	1.55	1.66
FHA21, H_{sx}/H_{1x}	0.5	0.35	0.31	0.28	0.24	0.24
FHA25, B_1[T]	1.03	1.04	1.04	1.05	1.04	1.05
FHA25, H_{1x}/H_{1A}	1.0	1.74	2.13	2.67	3.19	3.53
FHA25, B_s[T]	0.07	0.07	0.07	0.07	0.07	0.07
FHA25, H_{sx}/H_{sA}	1.0	1.22	1.33	1.47	1.54	1.67
FHA25, H_{sx}/H_{1x}	0.45	0.31	0.28	0.25	0.22	0.21
FHA50, B_1[T]	1.09	1.09	1.09	1.1	1.09	1.1
FHA50, H_{1x}/H_{1A}	1.0	1.71	2.09	2.63	3.09	3.44
FHA50, B_s[T]	0.03	0.03	0.03	0.03	0.03	0.03
FHA50, H_{sx}/H_{sA}	1.0	1.17	1.25	1.36	1.4	1.5
FHA50, H_{sx}/H_{1x}	0.26	0.18	0.16	0.13	0.12	0.11

This same thing can be viewed in Figure 6.31, where both the loss for sample A as Fha is changing can be seen, as well as the loss for all samples for 1.1 T. Here the

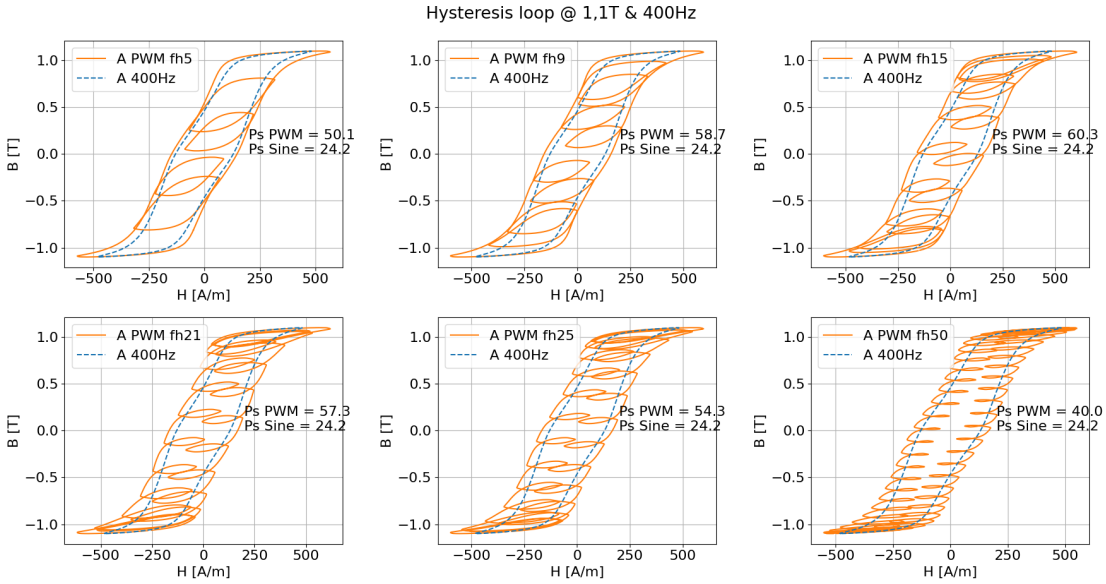

Figure 6.30: Hysteresis loop for different Fha at 1.1 T. This compared to sinusoidal hysteresis loop at 1.1 T. Solid: PWM, dashed: Sinusoidal.

peak loss is easily seen at Fha 15. Another interesting observation is that the power loss degradation stays very similar over all Fha, its linear but with different peak degradation. This will be seen in the next section, where more points of Fha has been measured to get a better resolution.

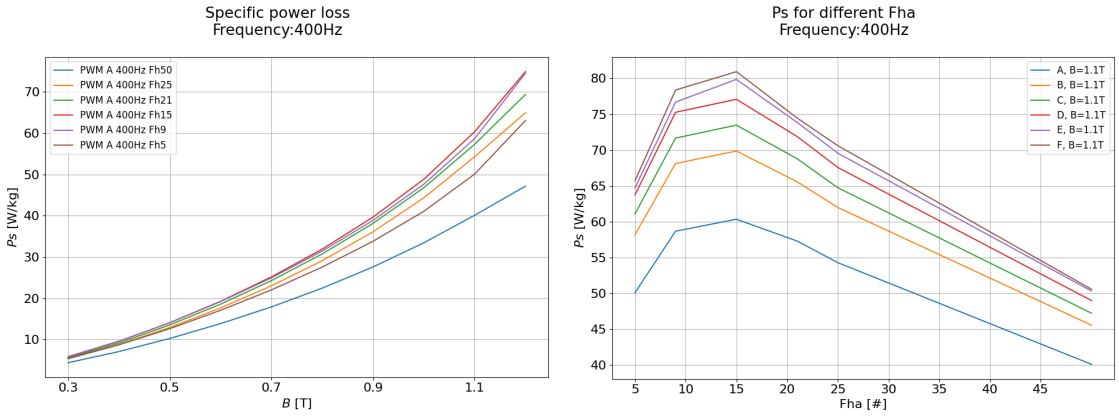

(a) Specific power loss for different Fha and sample A, measured at 400 Hz.

(b) Specific power loss vs Fha, at B 1.1 T. The peak is at 15 Fha.

Figure 6.31: The impact of different Fha on specific power loss.

6.2.2 Effects of Fha at 50 Hz

The second measurement to analyze the effect from changing Fha was measured at 50 Hz and 0.7 T as described earlier. The number of Fha measured was all odd values between 1 and 49. The measured data was analyzed in frequency domain, time domain, and the time averaged values. Notice that when Fha is equal to 1, the amplifier signal is a square wave.

Starting by looking at the hysteresis loop for the different Fha levels, which can be seen in Figure 6.32. In the figure the calculated power loss can also be seen, this was calculated by (2.4), taking the surface integral over the hysteresis loop. Since its hard to analyze the degradation here in the hysteresis loop, the time averaged values were investigated as well.

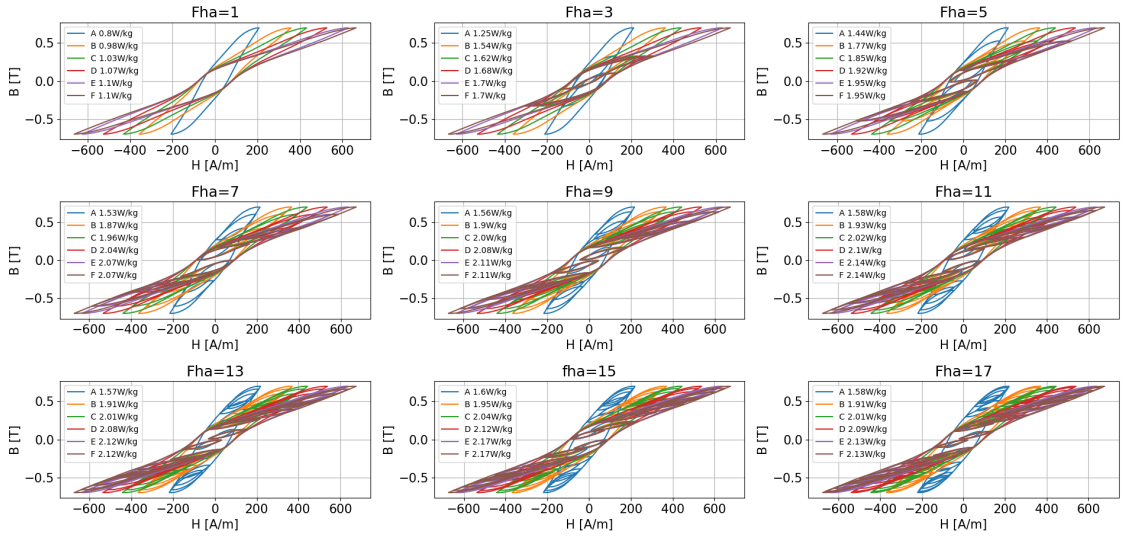

Figure 6.32: Hysteresis loop for different Fha at 0.7 T. For different samples A to F.

The measured H value for each of the Fha as well as the calculated H degradation can be seen in Figure 6.33. Looking at the measured H first, it can be seen that to reach the same B value, the square wave, or Fha 1, needs the lowest amount of H. It also seems like as Fha is increasing, the H value looks very similar.

Looking at the H degradation instead then, using the peak values, it can be noticed that for all the Fha values, the degradation looks very similar, an exponential function. It can also be seen that the degradation is very similar to each other. By only looking at the maximum degradation for all Fha, the largest maximum degradation is for Fha 1 and its around 3.2. The smallest maximum degradation happens at Fha 31 and is about 3.07. So the spread fairly close to one another.

The impact of the Fha seems to have lower impact compared to changing the fundamental. What should be remembered here is that the degradation here is only

compared to itself and not to sinusoidal, and also its using the peaks values. The lowest H value is actually for Fha 1, but this is where the degradation is at its max as well due to this larger fundamental signal.

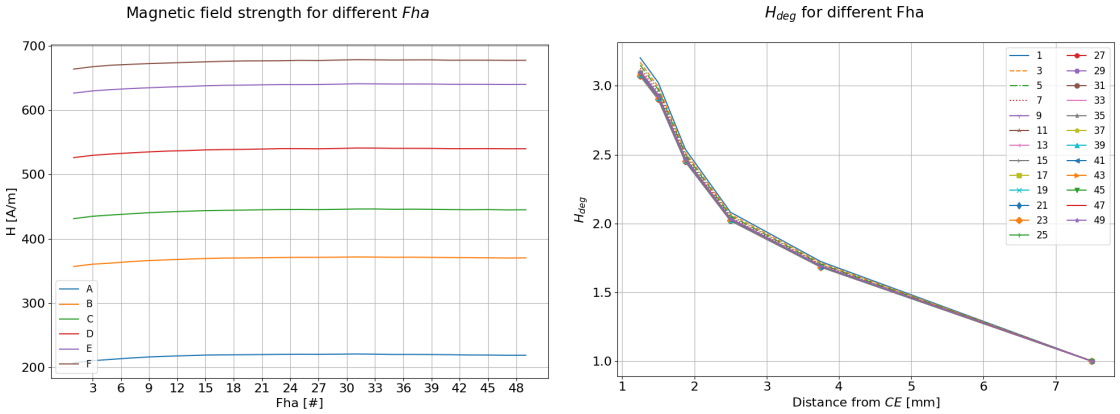

(a) H vs Fha for different samples A to F. Measured at 50 Hz.

(b) H degradation vs distance from CE for different Fha. Measured at 50 Hz.

Figure 6.33: Impact of different Fha on magnetic field strength.

The same comparison was done for measuring the specific power losses, which can be seen in Figure 6.34. Here loss for different Fha can be seen to the left, and loss degradation for different Fha to the right. Compared to the H, the Ps changes quite drastically over the Fha. Seeing the lowest losses at Fha 1, since its a square wave and no minor loops are introduced. Then increasing and having some sort of knee point around Fha 9. After this point the peak losses actually happens around Fha 15 and then decreasing losses as Fha increases.

Looking at the degradation instead, same as the H degradation, its very similar for all Fha. Looking again at the maximum degradation points, the largest maximum degradation happens at Fha 1, which is the square wave and the degradation is 1.377. The smallest maximum degradation happens at Fha 49 and is 1.322. From largest to smallest maximum its 0.055 which is quite small difference. The degradation doesn't seem to change its shape, and looks quite linear.

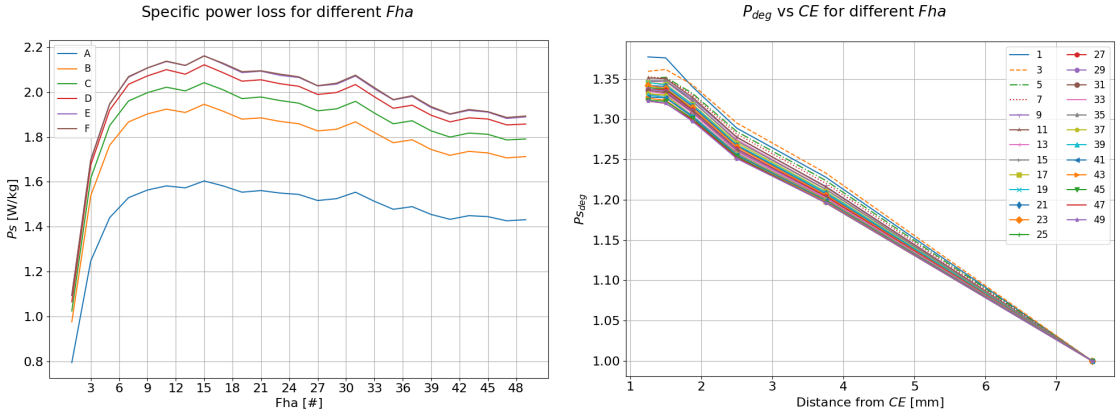

(a) Ps vs Fha for different samples A to F. Measured at 50 Hz.

(b) Ps degradation vs distance from CE for different Fha. Measured at 50 Hz.

Figure 6.34: Impact of different Fha on specific power loss.

6.3 Effects of Changing Vr

The last measurement that was done was to compare the effects of a changing Vr. As mentioned earlier, controlling EM's with the PWM signal the Vr will change depending on the speed and load of the machine. Therefore, there is an interest to see what the impact of changing Vr has on the degradation of its magnetic properties.

The measurement was completed at Vr from 1 to 2.25 with steps of 0.05. The Fha is kept at a constant 49. All measured at 50 Hz and 0.7 T. At Vr equal to 1 means that the PWM is in full modulation, and as Vr is increasing, it is going toward normal modulation. The effect of over modulation was skipped due to time limit.

Starting with looking at the hysteresis loop of the measurement, where some of the different cases with various Vr values can be seen in Figure 6.34. Since Fha is kept constant, the number of loops is always the same. What is changing as Vr is increasing is the depth of the minor loops, so thereby larger Vr means more losses due to more area under the hysteresis loop.

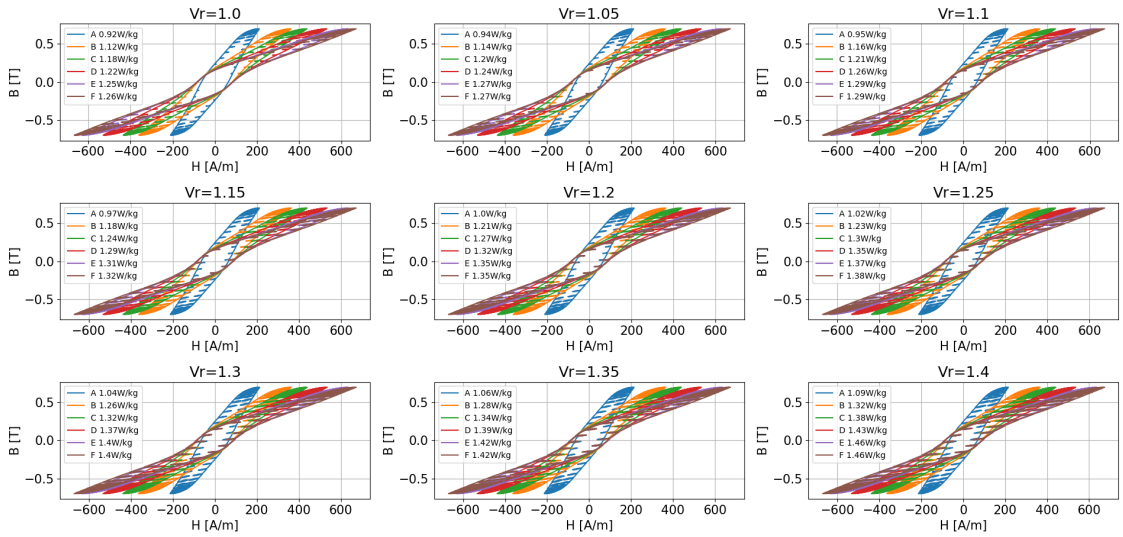

Figure 6.35: Hysteresis loop for different Vr at 0.7 T. For different samples A to F.

Looking at the peak values instead, starting with H in Figure 6.36, where the H can be seen for different Vr to the left, and to the right the H degradation for the different Vr can be seen. Noticing once again that the H degradation looks very similar for each Vr. With the largest maximum degradation at Vr equal to 1, with 3.17 degradation, and the smallest maximum degradation of 3.06 at Vr equal to 2.15. So here the degradation is actually lowering as the Vr is increasing.

The values of degradation is very similar though and not as drastic as changing fundamental frequency. Looking at the H values, it can be seen that the highest H is at max Vr, and lowest H at lowest Vr. It also looks as a quite linear increase of

H depending on Vr.

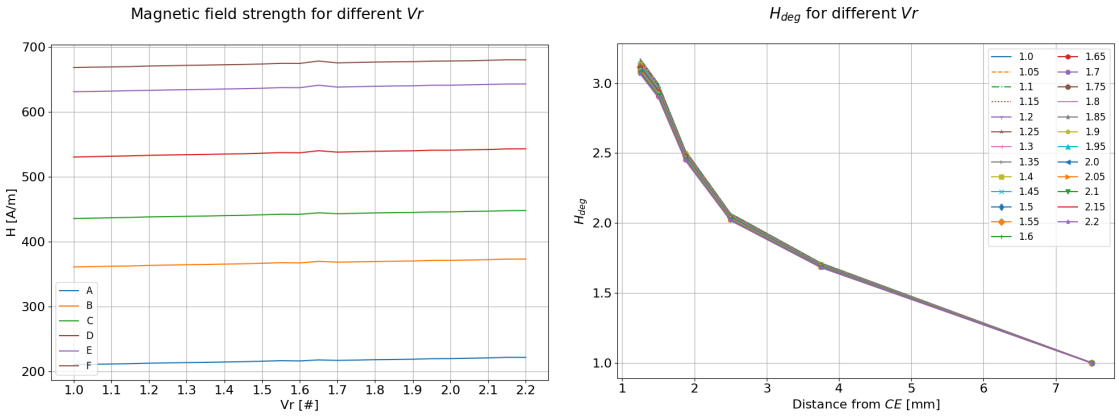

(a) H vs Vr for different samples A to F. Measured at 50 Hz.

(b) H degradation vs distance from CE for different Vr. Measured at 50 Hz.

Figure 6.36: Impact of different Vr on magnetic field strength.

The measurement of specific power loss, and degradation, which can be seen in Figure 6.37. This has very similar trend to the H, the power loss is increasing as Vr is increasing, this due to the increase of size of the minor loops. And the degradation is largest at Vr equal to 1 with P_{deg} of 1.35, while lowest maximum degradation of 1.317 at Vr equal to 2.15. Once again the degradation looks very similar and has a linear increase.

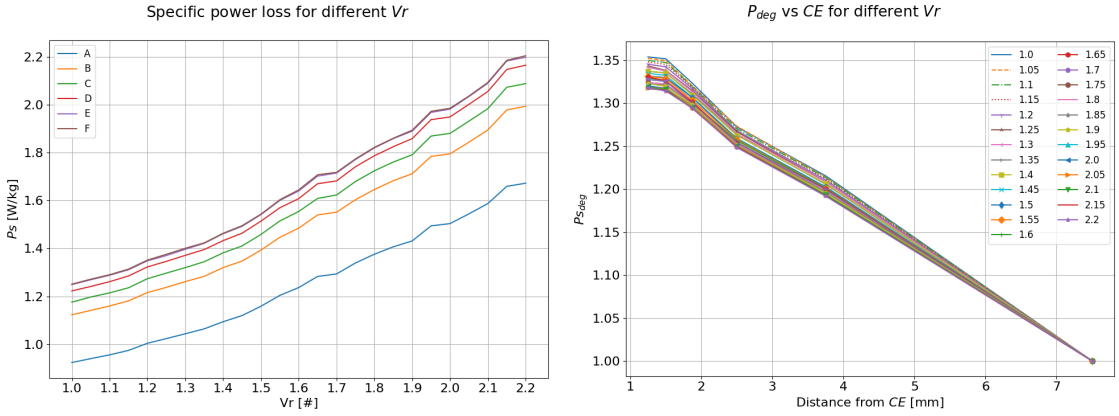

(a) Ps vs Vr for different samples A to F. Measured at 50 Hz.

(b) Ps degradation vs distance from CE for different Vr. Measured at 50 Hz.

Figure 6.37: Impact of different Vr on specific power loss.

The changing of Vr and Fha does effect the degradation, but not as severe as the fundamental changing of B and f. The more fundamental part the higher degradation, which can be seen both for the Vr and Fha, since it had the most degradation when it was a square wave and normal modulation which is closer to a square wave.

The discussions and conclusions from all the measurements will be presented even further in the coming chapters.

7

Comparing losses in FEM based simulations

7.1 Model of PMSM

To get an idea of the total impact from the laser cut degradation in an electrical machine a FEM based simulation was performed. The designed machine parameters can be seen in Table 7.1.

Table 7.1: PMSM Machine parameters.

Variable	Value	Unit
Number of pole pairs	4	n
Number of slots	48	n
Number of parallel branches	4	n
Number of conductor per winding	9	n
Yoke outer diameter	213.15	mm
Yoke inner diameter	52.5	mm
Stator inner diameter	141.75	mm
Rotor outer diameter	140.175	mm
Air gap length	0.79	mm
Active length	138	mm
Iron material	NO25-1350H	N/A
DC voltage	400.0	V
Peak phase current	400.0	A
Base speed	3000.0	RPM
Peak torque	321.6	Nm

To implement some sort of cut degradation model, the EM was designed with layers from the cut edge in the machine, where different material properties could be assigned. There was 6 layers created from the cut edge, each layer having different width, all the way up to a total of 2 mm distance from the edge. The 7th layer, was the main part of the core with non degraded material. This can be seen in Figure 7.1.

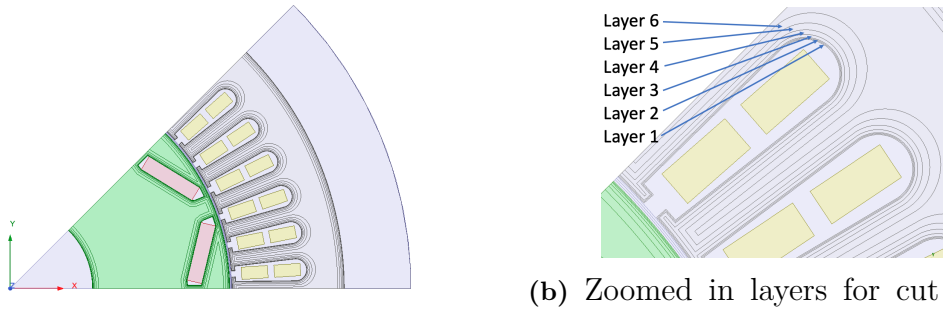

(a) PMSM Model in Ansys Maxwell.

(b) Zoomed in layers for cut edge model.

Figure 7.1: The PMSM model in Ansys Maxwell.

Since the highest degradation is happening closest to the cut edge, the width is designed to be most narrow there and then increasing for each layer. The different layer widths can be seen in Table 7.2.

Table 7.2: Layer width for cut degradation model.

Layer No.	1	2	3	4	5	6
Layer Width [mm]	0.1	0.1	0.2	0.3	0.5	0.8

The material in the EM is based on the non-degraded material, meaning the measured sample of sinusoidal excitation in Epstein Frame sample A. From the measured BH and Ps curves, the materials properties was calculated.

The degradation model is only implemented in the stator, to be able to only focus on the impact of the losses in the stator. Further development could be performed to see the whole impact of cut effect on stator and rotor in future studies.

Due to time limitations and complexity, the PWM degradation was performed with sinusoidal current excitation but with the PWM degradation model. The complexity of PWM excitation in FEM would take more time than allowed in this thesis work. The measured PWM degradation model is however implemented to see the impact from the PWM measurements.

7.2 Implementation of Degradation Models

To implement the degradation in the FEM simulation, some sort of model of degradation at specific CE distance was desired. This was implemented both for the sinusoidal degradation as well as for the non-sinusoidal degradation.

From the layers created in Table 7.2, the degraded material was implemented at the center of each layer. These layers could then be translated to the distance from CE

as in Table 7.3.

Table 7.3: FEM layers as distance from CE.

Layer No.	1	2	3	4	5	6
Distance from CE [mm]	0.05	0.15	0.3	0.55	0.95	1.6

These distances in Table 7.3 are the distances that the degradation model would be implemented at.

7.2.1 Implementation of Sinusoidal Degradation

To implement the degradation in the FEM simulation, the degradation calculated as distance from CE as in Figure 5.4 for H_{deg} and Figure 5.13 for P_{deg}. From these figures, the degradation models can be curve fitted to each B level to calculate the increase at that specific distance from CE. The two degradation models used here is

$$H_{degmod}^{Sine}(B) = 1 + b \cdot e^{-x \cdot c} \tag{7.1}$$

where H_{degmod}^{Sine} is the degradation model for H, x is distance from CE in mm, b and c are fitting coefficients. For the P model,

$$P_{degmod}^{Sine}(B) = m \cdot x + (1 - 7.5 \cdot m) \tag{7.2}$$

is used, where P_{degmod}^{Sine} is the degradation model, x is distance from CE in mm, m is fitting coefficient, 7.5 is from the reference sample A to set no degradation at 7.5mm. The two degradation models for sinusoidal degradation can be seen for a specific B level in Figure 7.2. The model is a simplification to test the degradation in the FEM simulations.

Applying these models as the same distances from the CE as the samples B to E, to test the accuracy of the model, can be seen in Figure 7.3. The distances closer to the CE has better accuracy compared to the ones further away, this can also be seen in Figure 7.2, where there is larger deviation at higher distances.

Looking at the difference between the measured and modelled degradation can be seen in Figure 7.4, here the max difference is around 7% for sample B and about 4% for sample E.

Applying the layer distances from Table 7.3 in (7.1) and (7.2), resulted in the degradation models in the left side of Figure 7.5 and Figure 7.6.

From the degradation at the different distances, by multiplying the degradation with the non degraded materials power losses and virgin BH curves, one would achieve

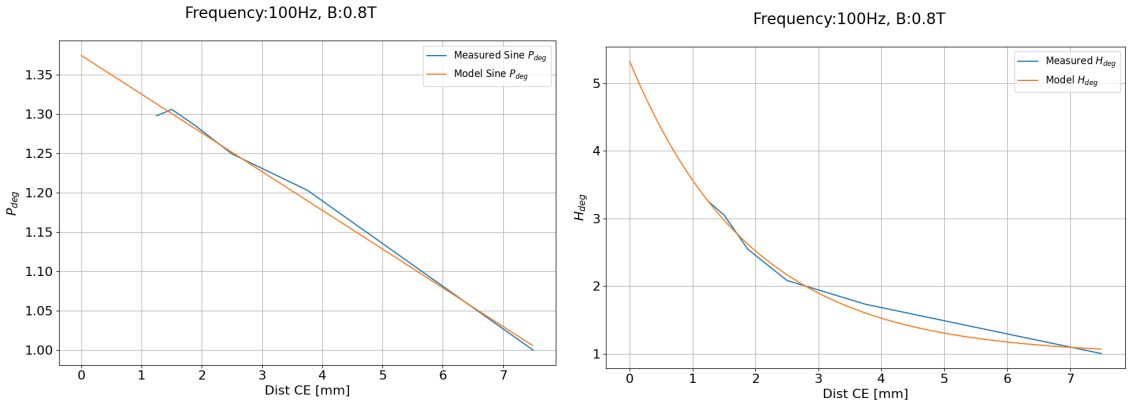

(a) Power loss degradation and model. **(b)** H degradation and model.

Figure 7.2: Degradation models for 0.8 T and 100 Hz, same implementation used for all B and frequencies.

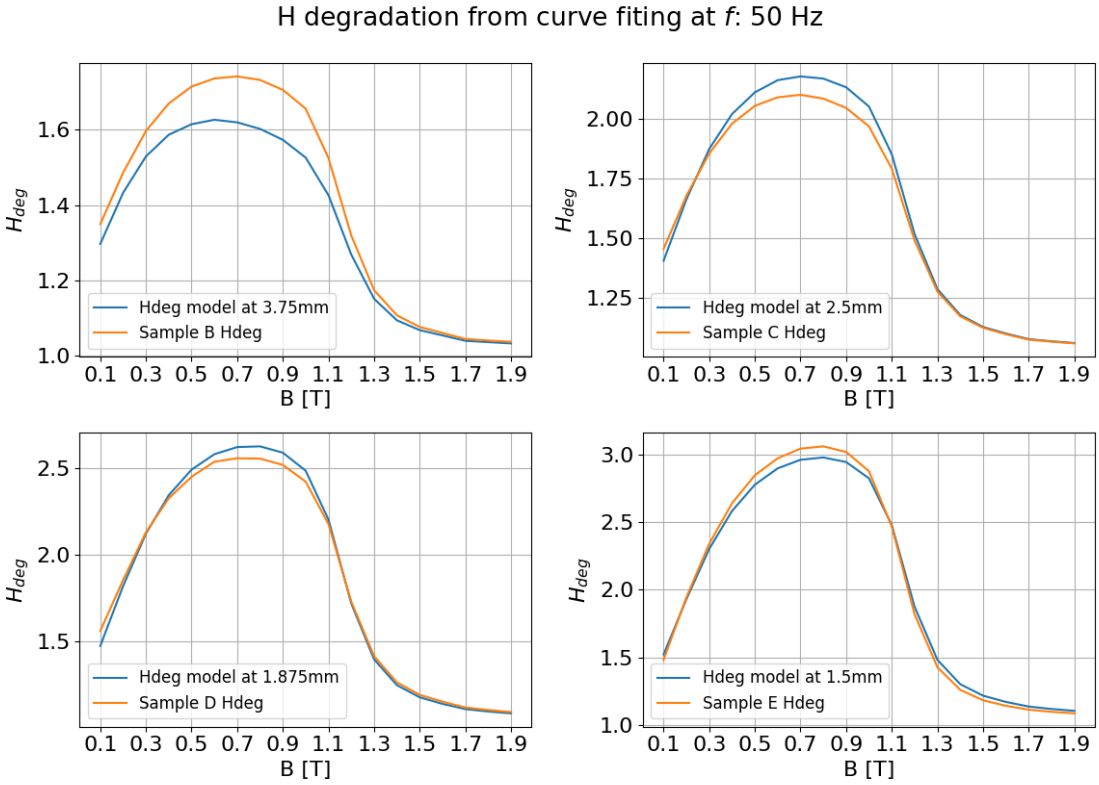

Figure 7.3: H_{deg} for different distances from CE, Upper left: Sample B, Upper right: Sample C, Lower left: Sample D, Lower right: Sample E

the parameters that would be implemented in the FEM simulation. The Specific power losses that will be implemented at the different layers can be seen in the right side of Figure 7.5. The magnetic field strength for different flux densities that will be implemented in the layers can be seen in the right side of Figure 7.6.

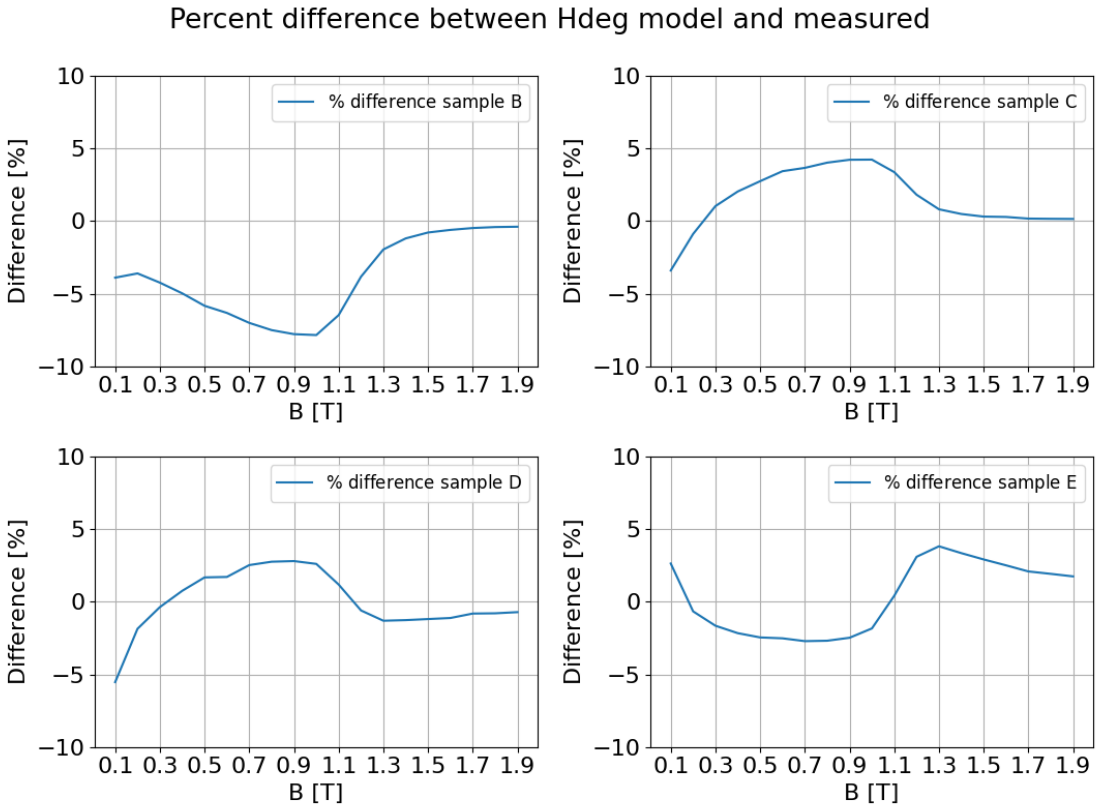

Figure 7.4: Difference from measured and model for different distances from CE, Upper left: Sample B, Upper right: Sample C, Lower left: Sample D, Lower right: Sample E

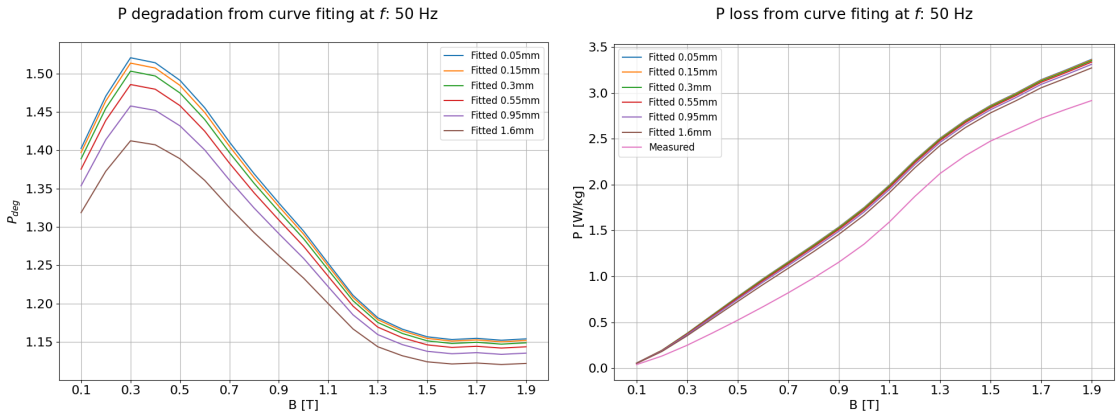

(a) Ps degradation model at different distances for 50 Hz.

(b) Power losses at different distances for 50 Hz.

Figure 7.5: Power loss degradation and Power losses from the applied loss model.

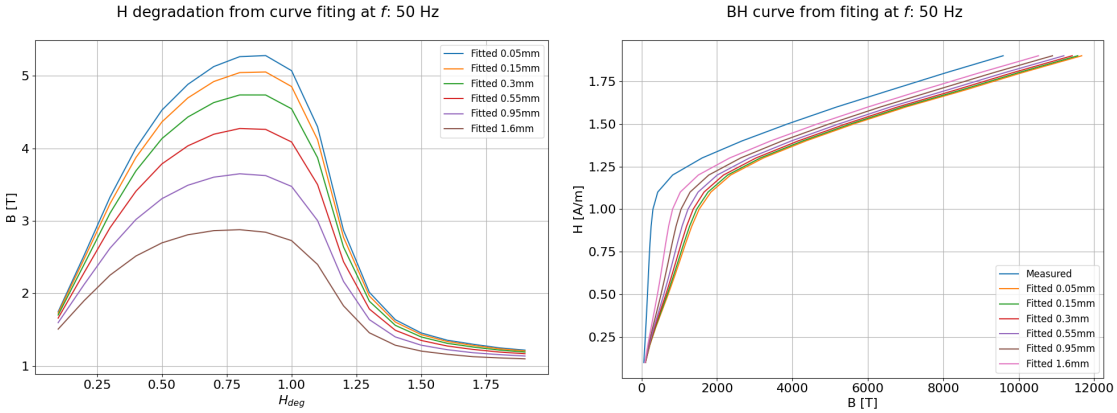

(a) H degradation model at different distances for 50 Hz.

(b) BH curves at different distances for 50 Hz.

Figure 7.6: Magnetic field strength degradation and Power losses from the applied loss model.

7.2.2 Implementation of PWM Degradation

As mentioned earlier in this chapter, the PWM simulation was performed with sinusoidal current excitation. The PWM degradation however was based on the PWM measurements and compared to the sinusoidal reference sample A to include the degradation both from the laser cut, as well as the PWM excitation during measurements.

Starting with the magnetic field strength degradation, which was curve fitted using

$$H_{degmod}^{PWM}(B) = a + b \cdot e^{-x \cdot c} \tag{7.3}$$

where $H_{degmod}^{PWM}(B)$ is the degradation model for different B levels, x is the distance from cut edge, and a, b, c are fitting coefficients. The difference from the sinusoidal degradation is the extra fitting coefficient a which is the offset due to the PWM measurement.

The degradation for the iron losses was curve fitted using

$$P_{degmod}^{PWM}(B) = m \cdot x + (s - 7.5 \cdot m) \tag{7.4}$$

where $P_{degmod}^{PWM}(B)$ is the model for degradation for different B, m is the slope of the degradation, and s is the new coefficient regarding the offset at the non degraded material.

The H_{degmod}^{PWM} was implemented on the different fundamental frequencies that was desired to be tested in the FEM simulation, and one of the resulting fittings can be seen in Figure 7.7. In this figure the different BH curves for the distances that was implemented in the FEM simulation can be seen.

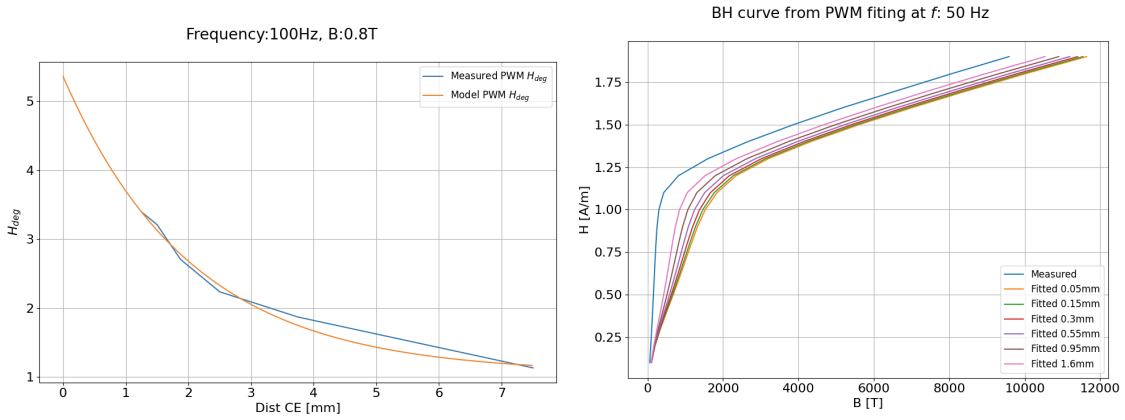

(a) H degradation and model. **(b)** Fitted BH curves at desired distances.

Figure 7.7: Degradation model for H, and resulting BH curves at 50 Hz.

The same can be seen in Figure 7.8, where the different fitted power loss curves can be seen for the desired distances. From these BH and Ps curves, the coefficients for

the loss models was calculated and implemented. In the discussions chapter, the complexity of the degradation model is discussed some, and some thoughts on how to improve the simulations.

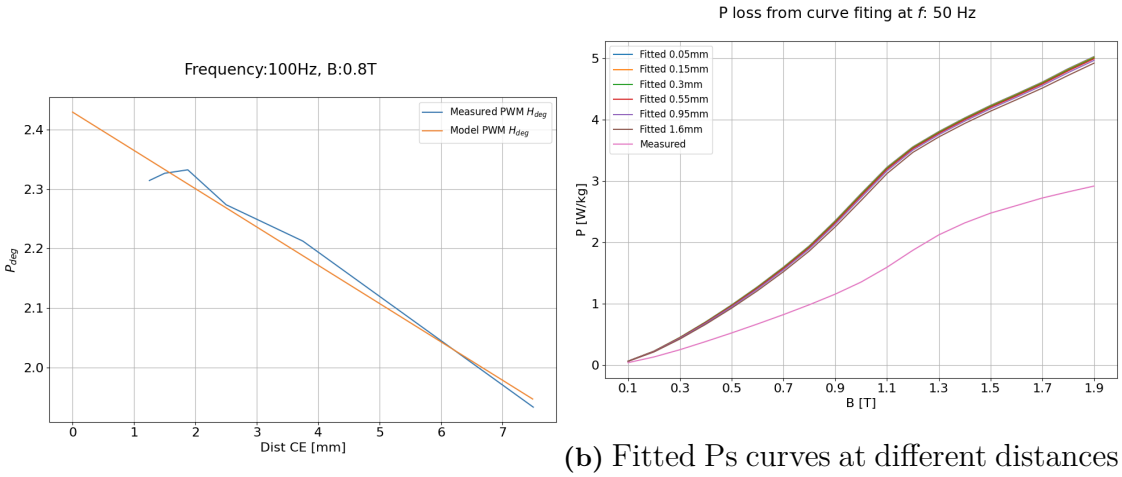

(a) Power loss degradation and model.

(b) Fitted Ps curves at different distances for PWM degradation model at 50 Hz.

Figure 7.8: Degradation model for Ps, and resulting Ps curves at 50 Hz.

7.3 FEM Simulations of PMSM

The FEM simulations was performed for six different fundamental frequencies, and these six fundamental frequencies was performed on four different types of models. The fundamental frequencies ranged from 50 Hz up to 1000 Hz.

First model was the non degraded PMSM with sinusoidal current excitation, second was with degradation model implemented and sinusoidal current excitation. The third simulation was for sinusoidal current excitation and PWM non degradation model, and fourth and final model was sinusoidal current excitation with the PWM degradation model implemented.

Each of the models and fundamental frequencies were simulated at half rated peak current, 200 A.

7.3.1 Non-Degraded Material Simulation with Sinusoidal Flux

The non degraded magnetic properties that was implemented in the FEM simulation can be seen in Table 7.4 where the BH values are the measured values from sample A with sinusoidal excitation.

The FEM simulation use the Bertotti's loss model for calculating the k coefficients. This is the same as in (2.15). The three different coefficients was first calculated so that each would have some physical meaning, as in Chapter 2, but the model did not fit using the same method.

So instead, first the k_{ec} is calculated as in (2.14), and then the two other was curve fitted using the Bertotti loss model, as best could fit. This meant that in this case does not have any physical meaning, but is only for curve fitting the measured loss curves. The iron losses was then only looked at as the total iron losses and not each specific sub category of losses, due to these coefficients. The calculated k coefficients in W/m^3 can be seen in Table 7.5.

Running the simulation for all the fundamental frequency points led to the summarized result Table 7.6. Here f_e is the electrical fundamental frequency, $P_{transmitted}$ is the power calculated from the Torque and mechanical angular velocity, P_{core} is the iron losses in the machine, P_{copper} is the copper losses from the winding's, T_{em} is the electro-mechanical torque, and η is the efficiency of the machine calculated from losses and transmitted power.

In the table, the P_{copper} can be seen as constant over all the frequencies, since its only depending on the resistivity of the winding and the RMS current running through it, since all tests are ran at half rated current this will stay constant.

Table 7.4: BH values for reference sample A, measured under sinusoidal excitation.

B[T]	$H(50Hz)$	$H(100Hz)$	$H(200Hz)$	$H(400Hz)$	$H(700Hz)$	$H(1000Hz)$
0.1	58.5	59.4	63.2	65.7	70.9	75.1
0.2	85.3	87.1	91.1	97.0	105.1	112.6
0.3	109.8	111.4	115.5	121.8	132.0	141.9
0.4	133.4	134.3	138.4	145.4	156.3	167.4
0.5	155.6	156.1	160.3	167.1	178.3	190.6
0.6	177.1	177.5	181.3	187.9	199.5	212.6
0.7	198.5	198.8	202.8	209.2	221.1	234.6
0.8	221.9	222.2	226.7	233.1	245.0	258.6
0.9	251.8	252.2	258.1	263.9	275.6	288.8
1	300.9	301.6	312.7	318.1	328.4	340.6
1.1	427.3	428.0	477.4	482.0	492.1	502.8
1.2	821.5	822.0	1190.4	1197.3	1205.4	1214.4
1.3	1601.9	1611.1	3095.9	3120.6	3114.7	3142.8
1.4	2660.3	2669.6	6343.8	6321.7	6294.4	
1.5	3871.1	3876.6				
1.6	5181.0	5193.8				
1.7	6618.2	6585.0				
1.8	8067.1	8043.2				
1.9	9585.8	9584.6				

Table 7.5: Bertotti loss coefficients for non degraded material.

Frequency [Hz]	k_h $[W/m^3]$	k_{ec} $[W/m^3]$	k_{ex} $[W/m^3]$
50	3.352e-08	0.174	26.51
100	2.109e-15	0.174	21.05
200	74.23	0.174	14.20
400	66.82	0.174	12.94
700	72.15	0.174	11.62
1000	134.62	0.174	9.14

The results from this machine is to have something to compare to as a reference case. The difference and increase/decrease will be compared to these results.

Table 7.6: Summarized results from non degraded sinusoidal excitation.

f_e [Hz]	$P_{transmitted}$ [kW]	P_{core} [kW]	P_{copper} [kW]	T_{em} [Nm]	η [%]
50	12.54	0.08	1.38	159.61	88.31
100	25.05	0.19	1.38	159.5	93.72
200	48.18	0.41	1.38	153.35	96.27
400	96.12	1.07	1.38	152.97	97.44
700	167.6	2.34	1.38	152.43	97.78
1000	242.65	3.94	1.38	154.47	97.81

7.3.2 Degraded Material Simulation With Sinusoidal Flux

The degraded simulation was implemented as described in the earlier section, with the values for BH from Figure 7.6 and the values for Ps from Figure 7.5. The same fundamental frequencies were tested and at the same operating point. The values for B, H, and Ps for the different layers can be seen in Appendix B.

One observation from the flux distribution is that for some stator teeth the flux distribution can be seen pushed to the middle of the tooth due to the degradation closer to the edge. Another observation is that for the stator teeth that is under higher flux densities, such as 1.4-1.7 T, the flux actually still runs in the degraded material, and this would cause an increase of iron losses.

In Table 7.7, the summarized results from all the different simulations can be seen. Here, same as for the non degraded, the copper losses stay the same due to the current point and resistivity of the winding's. For the non degraded the efficiency was increasing as fundamental frequency was increasing. Here the efficiency is increasing until 700 Hz, then its reducing, due to an increase of iron losses and that torque is reducing.

Table 7.7: Summarized results from degraded sinusoidal excitation.

f_e [Hz]	$P_{transmitted}$ [kW]	P_{core} [kW]	P_{copper} [kW]	T_{em} [Nm]	η [%]
50	12.24	0.07	1.38	155.87	88.09
100	24.46	0.17	1.38	155.74	93.63
200	45.92	0.42	1.38	146.18	96.06
400	91.04	1.1	1.38	144.9	97.27
700	158.77	2.46	1.38	144.4	97.58
1000	225.05	4.2	1.38	143.27	97.52

Comparing the two results instead, can be seen in Table 7.8, here the difference has been calculated as

$$difference = \frac{x_{deg} - x_{nondeg}}{x_{nondeg}} \tag{7.5}$$

where the x represents the different measurements, power, torque and losses. In the table the copper losses are removed since they stayed the same for both simulations.

In the table, starting with losses, the losses are actually lower at 50 and 100 Hz, with about 7-9 % decrease. But after 100 Hz, the losses start to increase compared to the non degraded and has a maximum of 6.7 % increase at 1000 Hz. This is a questionable result, since the degradation model is implemented it would be assumed that the should be an increase of iron losses for all frequencies. This will be discussed further in the discussion chapter.

Looking at the torque, the torque is lowered for all frequencies, with a maximum decrease at 1000 Hz of 7 %. Since the transmitted power is calculated from the torque the power has the same trend as the torque. With the degraded model, the decrease of relative permeability, would push the flux more to the center, to avoid using the lower permeability parts. Since simulation was performed with current excitation and the current is kept at a constant setting, with the degradation, a different magnetic flux distribution would happen in the EM due to this degradation. This change in B would result in a lower torque in this case. There is also a feedback of the iron loss calculations in the FEM program which then calculates the torque in each time step, since the iron losses increase the torque will then decrease due to this feedback. To get an even better understanding, more points should be investigated in the EM's FEM simulation.

Table 7.8: Difference between non degraded and degraded results.

f_e [Hz]	$P_{transmitted}$ diff [%]	P_{core} diff [%]	T_{em} diff [%]	η diff [%]
50	-2.349	-9.513	-2.349	-0.218
100	-2.355	-7.798	-2.355	-0.091
200	-4.679	2.684	-4.679	-0.207
400	-5.279	2.682	-5.279	-0.174
700	-5.269	5.307	-5.269	-0.202
1000	-7.25	6.765	-7.25	-0.29

Looking at the efficiency, it has the highest difference at 1000 Hz, with a decrease of 0.29%. This due to the lower torque and higher losses at 1000 Hz.

7.3.3 Non-Degraded PWM Model Simulation

Same as for the sinusoidal current excitation, the k coefficients was calculated using Bertotti's model on the iron losses, here again the loss separation does not have any physical meaning, but is mainly used to curve fit the loss model.

The BH curves from the measured PWM excitation was implemented as the non-degraded material in the FEM simulation. The BH curves can be seen in Table 7.9, where 4 different fundamental frequencies were implemented.

Table 7.9: BH values for reference sample A, measured under PWM excitation.

B[T]	$H(50Hz)$	$H(100Hz)$	$H(400Hz)$	$H(700Hz)$
0.1	60	64	80	87
0.2	88	94	117	133
0.3	115	121	150	172
0.4	140	147	181	207
0.5	163	172	211	242
0.6	187	197	241	277
0.7	211	223	274	314
0.8	237	252	311	357
0.9	270	288	359	412
1.0	322	344	433	494
1.1	452	476	598	662
1.2	840	851	1219	1239
1.3	1616	1623	3025	2952
1.4	2674	2670	6105	5981
1.5	3883	3881		
1.6	5201	5191		
1.7	6596	6592		
1.8	8059	8056		
1.9	9588			

Since the PWM degradation model is performed with sinusoidal current excitation, the main interesting parameter to investigate is the core losses. The torque is not really applicable here since it will be different when running with PWM voltage excitation. So here the main parameter that was analyzed was the core losses. In Table 7.10 the result is summarized from the simulation, with the core losses for the different fundamental frequencies.

Some of the simulation results here will be continued to be discussed in the discussion chapter.

Table 7.10: Summarized results from non-degraded sinusoidal excitation with PWM degradation model.

f_e [Hz]	P_{core} [kW]
50	0.21
100	1.03
400	1.93
700	4.25

7.3.4 Degraded PWM Model Simulation

The PWM degradation model was implemented as in Section 7.2.2, resulting in the following BH curves which can be found in Appendix E.

The flux density levels has risen even further and have a larger part of the rotor at 2 T. The degradation model can be seen implemented in the stator teeth as the flux gets pushed to the center of the tooth due to the degraded magnetic properties closer to the edge. Once again if the flux runs in the degraded material that would also lead to an increase of core losses.

In Table 7.11 the summarized result for the different fundamental frequencies can be seen. The result here is similar to the sinusoidal simulation, where there is an decrease of core losses at the lower frequencies, and an increase for the higher. The main idea here was to try implement the degradation model from the measurements. But the execution could have been performed better if there was more time allotted.

Table 7.11: Summarized results from degraded sinusoidal excitation with PWM degradation model

f_e [Hz]	P_{core} [kW]
50	0.13
100	0.53
400	2.14
700	4.86

In Table 7.12, the difference of iron losses between the degraded and non degraded is summarized. Here that increase is easy to see for the lower frequencies and the increase at higher. This will be discussed further in the discussion chapter.

Table 7.12: Difference between non degraded and degraded results with PWM degradation model.

f_e [Hz]	P_{core} diff [%]
50	-36.579
100	-48.429
400	10.423
700	14.36

8

Discussion

8.1 Measurement Uncertainty and Complexity

The laser cutting degradation analysis with non sinusoidal flux density is a newer field and a very complex one. As mentioned several times in this report the measurement of the magnetic properties is determined by peak values, and properties such as relative permeability is calculated from this.

With PWM harmonics are introduced both in H as well as B, thereby its hard to compare the same degradation with pure sinusoidal measurements. The amount of degrees of freedom to look at, the PWM degradation is also a complex problem. Since in our machines the modulation index, modulation frequency index, fundamental frequency, flux density, and more is constantly changing. To create a perfect model that represents all the changes is a difficult task.

Another problem with the PWM measurement was the uncertainty at low B levels, such as 0.1 T to 0.3 T, for certain fundamental frequencies. Same for higher B levels above 1.2 T, it is very important to verify each measured point in the raw data, and this leads to a lot of data handling when handling multiple points, samples, and frequencies.

For all the measurements in this thesis its important to take this measurement uncertainty into consideration. The degradation pattern seems to be similar for all fundamental frequencies, but the actual peak values could be different from reality.

Another interesting measurement observation was the changing of Fha, the controller seemed to have problems regulating even numbers of Fha, so the result for 2500 Hz and 1000 Hz, where the Fha is 4 and 10, might have some uncertainty as well. As Fha was increasing above 20, the controller seemed to have less issues.

The measurement equipment and amplifier does however have limitations. For electrical machines, inverters are typically switched with frequencies of around 10 kHz. The controller in the MPG software tries to always keep a perfect square PWM shape, but higher switching frequency means that there is very high harmonic during the switch between negative and positive polarity, this leads to over voltage across the inductor due to its characteristic. The controller cannot control a perfect voltage at the secondary side. So here its important to always analyze the time

domain signals, and ensure that the measurement is still as desired.

8.2 Degradation Models

To create a degradation model is also a complex task. Several different methods was tested to find some sort of degradation model. A method of using lumped parameters with reluctance was tested but not succeeded. This was also due to time limitations in this thesis project, and maybe with more time a better degradation model could have been achieved. As mentioned the degradation model in this thesis was a simplified version to be able to implement in a FEM simulation to see the effect on the total machine, and not just the steel.

Here the complexity of the harmonics was also an issue, since the relative permeability degradation was calculated with the peak values, the degradation at the fundamental and switching frequency was lumped together. Here some improvements could be implemented and dive deeper into the degradation at the different harmonic levels.

The power loss degradation and loss models is another complex problem. Starting with the loss models, using the Bertotti's model worked great for sinusoidal excitation without any degradation. One issue with this was that a k coefficient was calculated for each B level instead for each fundamental frequency. This could unfortunately not be implemented in the FEM program that was used, Ansys, and the loss model was not as accurate. Here, with more time maybe this could be implemented which could have resulted in better loss coefficients.

Another issue was the PWM losses, and specifically the effects of minor loops. To get a good working loss model here would take quite some time so this was not in the scope for the thesis. This would be an interesting investigation for future studies to see which loss model would fit best here, and probably working in the time domain.

For the loss degradation model, this comes back to the uncertainty of the measurements around certain B levels measured. Here more investigation is needed in future studies.

As mentioned earlier, there is so many different degrees of freedom here, the problem becomes very complex. There is impact of steel samples, fundamental frequencies, Fha, Vr, H degradation, Ps degradation, comparing between samples, comparing between PWM and PWM, comparing between PWM and sinusoidal, and the list goes on. Here the possibilities are endless to improve and find more degradation models than what has been found in this thesis.

8.3 FEM Simulations

The FEM simulations was performed to be able to have some sort of impact of the degradation in the electrical steel in the complete EM. Since only one operating point was completed at different fundamental frequencies, there is more work to be done here. Just noticing how the degradation has different impact at different frequencies and B levels, it would be interesting to get a full mapping of the EM to get better understanding of what the full impact is. The degradation model could also be an continuous model as in [41], instead of discrete model of layers with different magnetic properties. This could be done for better total overview of the magnetic flux distribution.

Due to time limitations, it was better to get some result compared to none in the FEM simulations so a decision was made to only do one operating point at different fundamental frequencies. The study could be extended to include a whole torque speed map, to see the full impact of the degradation due to cutting.

The FEM simulation did have some issues regarding the result for some of the fundamental frequencies. The main focus in this thesis was to measure and analyze the degradation so there was some time limitations regarding the FEM simulations. If some more debugging would have been completed for the FEM simulation maybe some better results would have come out of the simulation. Here it is important to just the that it is possible to implement the degradation model in the FEM simulation. But the actual result from the FEM simulation could vary for if the simulations were analyzed further.

To implement the degradation from the measured PWM experiment into the FEM simulation some caution had to be considered as well. Since when measuring with PWM excitation and then creating some model that can be used in the FEM program, and then using PWM excitation in the FEM program, double effect for losses and magnetic properties, from the higher harmonics might be applied. So here its important to understand what the FEM simulation takes into consideration, and what is the difference between running PWM with sinusoidal degradation model, versus PWM with PWM degradation model.

The FEM simulations with the PWM degradation did have some questionable result for some of the fundamental frequencies. This once again could be due to simulation problems and could have been fixed if more time was allowed. The main key point here is that with the help measurements a degradation model could be implemented in a FEM based program.

8.4 Ethics and Sustainability

As the automotive business is moving over to more electric vehicles (EV), the discussion regarding ethics and sustainability becomes an interesting topic. One interesting topic regarding the design of more efficient electrical machines, is to have better simulations during the design phase. Without taking the cutting effects into consideration, the iron losses could vary quite drastically, and thereby even if the design had high efficiency at simulation stage it could be different when building the actual motor.

By building more efficient EM's, electric vehicles could either have longer range with same battery and power electronic specifications. Or with better efficiency, less batteries could be used in the electric vehicles and thereby less impact extracting material for this. Same for the EM, by creating simulations that are more realistic, there would be less unnecessary reproducing of EM's if they do not match the expectations.

Therefore, its very important to understand all the different manufacturing effects on the EM, so that those are taken into consideration and the design could be changed ahead, to optimize the use of the electrical steel sheets.

Another question, as discussed earlier in this thesis, what is a valid measurement? Just comparing the SST measurement with the Epstein Frame, the results vary quite a bit at different flux density levels, and the question is, which of the measurements are correct ? This is a very important observation, to always analyze measurements and simulation with caution. For example, the degradation models in this thesis has had some simplifications, but there is still some conclusions that can be drawn from it. But regarding the amplitude of degradation, one should always validate with own measurements and conclusions.

9
Conclusion

The primary objective of this thesis was to quantitatively measure, analyze, and develop a model for the degradation of cutting effects on iron losses and magnetic properties. Through conducting over 1500 individual measurements, an extensive analysis and multiple comparison methods were employed to ensure increased confidence and accuracy in the results.

First, the measurement equipment underwent testing to ensure measurement repeatability and to gain a better understanding of the equipment's sensitivity to control parameters. To enhance comprehension of loss separation, a method was devised to determine which loss model, Jordan's or Bertotti's, best aligned with the measured losses. The addition of the excess loss coefficient in Bertotti's model yielded a more accurate fit for the measured iron losses. However, the developed loss separation model generated fitting coefficients based on specific magnetic flux densities rather than frequencies, which may restrict its implementation in certain finite element method (FEM) simulations.

While the measurement of sinusoidal flux distribution has received significant attention in recent years, research on non-sinusoidal flux distribution and its impact on cut degradation remains relatively unexplored. To deepen understanding of pulse width modulation (PWM) and the minor loops it induces in the material, a comprehensive test was conducted across different frequencies, flux densities, amplitude modulation ratios, and frequency modulation ratios. The results indicated that iron losses and magnetic field strength were influenced by both the amplitude and frequency modulation indices, with bipolar, normal modulation, and low-frequency modulation exhibiting the most significant degradation in iron losses.

To establish a reference case for comparison, measurements and analysis were first performed for sinusoidal flux distribution across different fundamental frequencies and magnetic flux densities. Two types of degradation were examined: the impact on magnetic properties, specifically the additional magnetic field strength required to reach the same magnetic flux point in the material, and the increase in iron losses resulting from cut effect degradation. It was observed that the degradation varied in magnitude depending on the frequency and magnetic flux distribution in the material. The peak magnetic field strength degradation occurred at approximately 0.8 T to 1.0 T for all fundamental frequencies, with the degradation amplitude decreasing as the fundamental frequency increased. This phenomenon was attributed to the skin effect, which caused the flux to be pushed into the degraded material despite

its lower permeability. At 200 Hz and a distance of 1.25 mm from the cut edge, the degradation reached a peak of around 3.3 times increased magnetic field strength. As the material approached saturation, the degradation of magnetic field strength also reached a saturation point, exhibiting similar degradation across all distances from the cut edge. When considering a simplified degradation analysis from the cut edge, magnetic field strength degradation displayed an exponential trend, increasing as the flux approached the cut edge. In contrast, iron loss degradation exhibited a peak around lower magnetic flux densities, approximately 0.3 T to 0.4 T, and displayed a more consistent degradation pattern across different fundamental frequencies. The degradation in iron losses demonstrated a linear relationship with the distance from the cut edge, with a peak degradation of 1.48 times increased losses at 1.25 mm and 10 kHz.

Investigating the cut effect degradation under non-sinusoidal flux distribution and PWM excitation presented a complex task. Non-sinusoidal excitation involves harmonics, and the measurement equipment is designed to control peak signals, making direct comparison with pure sinusoidal degradation challenging. Various comparison methods were developed, including comparing PWM measurements to sinusoidal measurements using Sample A as a reference, comparing PWM measurements to PWM measurements using Sample A as a reference, and comparing different steel samples, i.e., comparing PWM to sinusoidal measurements using the same samples. In terms of magnetic field strength peak degradation, PWM exhibited lower degradation when compared to itself, but when compared to sinusoidal excitation, it displayed higher degradation, reaching a peak of 3.76 at 700 Hz. This indicates that transitioning from sinusoidal to PWM excitation inherently results in a decrease in magnetic properties. The lower degradation observed when comparing PWM measurements to itself can be attributed to the material already being subject to other stresses due to higher harmonics, causing the degradation to approach saturation.

Another notable finding was the difference in degradation between the fundamental component and the harmonic components. This discrepancy was related to the amount of flux density at each harmonic, which correlated with the sinusoidal measurements. Therefore, as the fundamental component increased relative to the ripple amplitude, i.e., higher frequency modulation index (Fha), the degradation at the fundamental frequency also increased. Conversely, as Fha decreased, the harmonic content shifted more towards the switching frequency component, resulting in higher degradation. Comparing different samples, the most significant degradation occurred when transitioning from sinusoidal to PWM excitation, indicating that the largest impact stems from the shift in excitation type. Similar to the degradation observed in sinusoidal flux distribution, the non-sinusoidal degradation also displayed an exponential degradation pattern when considering the distance from the cut edge. The shape of the loss degradation with non-sinusoidal flux density closely resembled that of the sinusoidal degradation. Comparing the loss degradation to the sinusoidal reference sample, the peak shifted from 0.3 T to 1.0 T, resulting in a peak degradation of approximately 3. This substantial increase in losses near the cut edge highlights the significant impact of the degradation.

Furthermore, an analysis was conducted to investigate the impact of changing the modulation ratio index (Vr) and frequency modulation index (Fha). As Fha increased from 1 to 49, iron losses exhibited a peak around Fha 15 due to the increased ripple magnitude, which remained significant. However, as Fha increased further, losses decreased. In contrast, magnetic field strength increased consistently with higher Fha values. As mentioned earlier, different degradation occurred at various harmonics, so altering Fha revealed that a higher content at the fundamental frequency (i.e., higher Fha) resulted in greater degradation at the fundamental component. Conversely, decreasing Fha shifted the harmonic content towards the switching frequency component, leading to increased degradation. The degradation in both losses and magnetic field strength maintained a consistent pattern, with losses degrading linearly and magnetic field strength exhibiting an exponential degradation trend for all Fha values. When adjusting Vr from full modulation to normal modulation, both magnetic field strength and iron losses increased. However, the overall degradation pattern remained similar, yielding comparable results to those obtained by varying Fha. Consequently, changing the fundamental frequency had the most significant impact on degradation.

For electrical machines, typical magnetic flux densities in stator teeth range from 1.5 T at no load to 2 T or higher under load conditions. Consequently, the degradation of H is expected to reach saturation more quickly, potentially exerting less influence. The most common frequencies used in electrical machines range from 50 to 500 Hz, which unfortunately align with the peak degradation observed. Consequently, an assumption can be made that higher losses occur at these higher flux density levels, and the degradation further exacerbates these losses. As the magnetic properties degrade, the flux is pushed further into the material's central region, reducing the need for increased losses. However, if the flux is forced to utilize the degraded portion of the material, losses will increase.

Additionally, a finite element method (FEM) simulation was conducted to evaluate the overall impact of the degradation model on electrical machines. Initially, a simulation comparing the degradation under sinusoidal current excitation was performed, followed by a simulation incorporating PWM degradation model. Under sinusoidal excitation, a torque decrease of approximately 5% and an efficiency decrease of around 0.3% were observed. It should be noted that this simulation was conducted at a few different fundamental frequencies and at half-rated current, and thus, the decrease may not be uniform across the entire torque-speed map. Since the simulation used current excitation and half-rated current, the material could not achieve the same flux density for the same current level due to degradation. Consequently, as the magnetic flux decreases, so does the torque. Moreover, torque is back-calculated from the iron losses, so increasing the losses leads to a corresponding decrease in torque. The simulation was time limited and therefore there was some issues regarding the result of the simulation. The main idea is that there is a possibility to implement the degradation in FEM program, using the degradation measured.

Due to time constraints, sinusoidal current excitation was employed for the PWM degradation model and to exclude the double loss effect from PWM excitation. Since the PWM model was derived from PWM measurements, the harmonic effects were already incorporated into the model. Running PWM excitation in FEM, which would re-introduce the harmonic effects, could result in double loss effects. The FEM simulation incorporating PWM excitation showed an increase in iron losses ranging from 60% to 500%, depending on the fundamental frequency. Similar to the sinusoidal degradation simulation, the PWM degradation model should be tested across the entire torque-speed map to gain a more comprehensive understanding of the laser cut effect with non-sinusoidal flux distribution. The simulation results here had some doubts, due to some decrease in the iron losses for certain fundamental frequencies. The main focus of this thesis report was the measurement and analysis of the degradation, so the main idea with the PWM degradation model was to show that it was possible to implement in a FEM program.

References

[1] S. Zheng, X. Zhu, Z. Xiang, L. Xu, L. Zhang, and C. H. Lee, "Technology trends, challenges, and opportunities of reduced-rare-earth PM motor for modern electric vehicles," *Green Energy and Intelligent Transportation*, vol. 1, no. 1, p. 100012, 6 2022.

[2] P. Waide and C. U. Brunner, "Energy-Efficiency Policy Opportunities for Electric Motor-Driven Systems InternatIonal energy agency Energy Efficiency Series," Tech. Rep., 2011.

[3] The International Electrotechnical Commission, "IEC 60404-2," Tech. Rep., 2008.

[4] TATA Steel, "NO25-1350H Data sheet thin non-oriented electrical steel," Tech. Rep. [Online]. Available: www.tatasteeleurope.com

[5] The International Electrotechnical Commission, "IEC 60404-3," Tech. Rep., 2010.

[6] M. Bali and A. Muetze, "Modeling the Effect of Cutting on the Magnetic Properties of Electrical Steel Sheets," *IEEE Transactions on Industrial Electronics*, vol. 64, no. 3, pp. 2547–2556, 3 2017.

[7] M. Bali, H. De Gersem, and A. Muetze, "Finite-element modeling of magnetic material degradation due to punching," *IEEE Transactions on Magnetics*, vol. 50, no. 2, pp. 745–748, 2014.

[8] T. Nakata, M. Nakano, and K. Kawahara, "Effects of Stress Due to Cutting on Magnetic Characteristics of Silicon Steel," *IEEE Translation Journal on Magnetics in Japan*, vol. 7, no. 6, pp. 453–457, 1992.

[9] M. Bali, H. De Gersem, and A. Muetze, "Determination of Original Nondegraded and Fully Degraded Magnetic Characteristics of Material Subjected to Laser Cutting," *IEEE Transactions on Industry Applications*, vol. 53, no. 5, pp. 4242–4251, 9 2017.

[10] A. A. Mohammadi, S. Zhang, A. C. Pop, and J. J. Gyselinck, "Effect of Electrical Steel Punching on the Performance of Fractional-kW Electrical Machines," *IEEE Transactions on Energy Conversion*, vol. 37, no. 3, pp. 1854–1863, 9 2022.

[11] P. Lazari, J. Wang, and K. Atallah, "Effects of laser cut on the performance of permanent magnet assisted synchronous reluctance machines," in *2015 IEEE International Magnetics Conference, INTERMAG 2015*. Institute of Electrical and Electronics Engineers Inc., 7 2015.

[12] E. G. Araujo, J. Schneider, K. Verbeken, G. Pasquarella, and Y. Houbaert, "Dimensional effects on magnetic properties of fesi steels due to laser and mechanical cutting," *IEEE Transactions on Magnetics*, vol. 46, no. 2, pp. 213–216, 2010.

[13] R. Sundaria, A. Lehikoinen, A. Arkkio, and A. Belahcen, "Effects of Manufacturing Processes on Core Losses of Electrical Machines," *IEEE Transactions on Energy Conversion*, vol. 36, no. 1, pp. 197–206, 3 2021.

[14] M. Bali and A. Muetze, "The degradation depth of non-grain oriented electrical steel sheets of electric machines due to mechanical and laser cutting: A state-of-the-art review," in *IEEE Transactions on Industry Applications*, vol. 55, no. 1. Institute of Electrical and Electronics Engineers Inc., 1 2019, pp. 366–375.

[15] C. Tong, *Introduction to Materials for Advanced Energy Systems*. Cham: Springer, 2019.

[16] F. Ossart, E. Hug, O. Hubert, C. Buvat, and R. Billardon, "Effect of punching on electrical steels: Experimental and numerical coupled analysis," *IEEE Transactions on Magnetics*, vol. 36, no. 5 I, pp. 3137–3140, 2000.

[17] A. Pulnikov, P. Baudouin, and J. Melkebeek, "Induced stresses due to the mechanical cutting of non-oriented electrical steels," Tech. Rep., 2003.

[18] F. Martin, U. Aydin, R. Sundaria, P. Rasilo, A. Belahcen, and A. Arkkio, "Effect of Punching the Electrical Sheets on Optimal Design of a Permanent Magnet Synchronous Motor," *IEEE Transactions on Magnetics*, vol. 54, no. 3, 3 2018.

[19] R. Sundaria, D. G. Nair, A. Lehikoinen, A. Arkkio, and A. Belahcen, "Effect of Laser Cutting on Core Losses in Electrical Machines - Measurements and Modeling," *IEEE Transactions on Industrial Electronics*, vol. 67, no. 9, pp. 7354–7363, 9 2020.

[20] R. Sundaria, A. Lehikoinen, A. Hannukainen, A. Arkkio, and A. Belahcen, "Mixed-Order Finite-Element Modeling of Magnetic Material Degradation Due to Cutting," *IEEE Transactions on Magnetics*, vol. 54, no. 6, 6 2018.

[21] M. Bali and A. Muetze, "Influences of CO2 Laser, FKL Laser, and Mechanical Cutting on the Magnetic Properties of Electrical Steel Sheets," *IEEE Transactions on Industry Applications*, vol. 51, no. 6, pp. 4446–4454, 11 2015.

[22] A. Schoppa, H. Louis, F. Pude, and C. Von Rad, "Influence of abrasive waterjet cutting on the magnetic properties of non-oriented electrical steels," Tech. Rep., 2003.

[23] E. C. Jameson, *Electrical discharge machining*. Society of Manufacturing Engineers, Machining Technology Association, 2001.

[24] A. Krings, S. Nategh, O. Wallmark, and J. Soulard, "Influence of the welding process on the performance of slotless pm motors with sife and nife stator laminations," in *IEEE Transactions on Industry Applications*, vol. 50, no. 1. Institute of Electrical and Electronics Engineers Inc., 2014, pp. 296–306.

[25] H. Wang, Y. Zhang, and S. Li, "Laser welding of laminated electrical steels," *Journal of Materials Processing Technology*, vol. 230, pp. 99–108, 4 2016.

[26] W. M. Arshad, T. Ryckebusch, F. Magnussen, H. Lendenmann, J. Soulard, B. Eriksson, and B. Malmros, "Incorporating lamination processing and component manufacturing in electrical machine design tools," Tech. Rep., 2007.

[27] A. Schoppa, J. Schneider, C.-D. Wuppermann, and T. Bakon, "Influence of welding and sticking of laminations on the magnetic properties of non-oriented electrical steels," Tech. Rep., 2003.

[28] Brockhaus measurements, "MPG-Expert 3 - Manual," Ludenscheid, 2018.

[29] A. Krings, "Iron losses in electrical machines : influence of material properties, manufacturing processes and inverter operation," Ph.D. dissertation, Electrical Engineering, Stockholm, 4 2014.
[30] C. D. Graham, "Physical origin of losses in conducting ferromagnetic materials (invited)," *Journal of Applied Physics*, vol. 53, no. 11, pp. 8276–8280, 11 1982.
[31] D. Ribbenfjard, "Electromagnetic transformer modelling including the ferromagnetic core," Ph.D. dissertation, 2010.
[32] W. Chen, J. Ma, X. Huang, and Y. Fang, "Predicting iron losses in laminated steel with given non-sinusoidalwaveforms of flux density," *Energies*, vol. 8, no. 12, pp. 13 726–13 740, 2015.
[33] A. Boglietti, A. Cavagnino, M. Lazzari, and M. Pastorelli, "Predicting iron losses in soft magnetic materials with arbitrary voltage supply: An engineering approach," *IEEE Transactions on Magnetics*, vol. 39, no. 2 II, pp. 981–989, 3 2003.
[34] C. P. Steinmetz, "On the law of hysteresis," *Proceedings of the IEEE*, vol. 72, no. 2, pp. 197–221, 1984.
[35] A. Krings and J. Soulard, "Overview and Comparison of Iron Loss Models for Electrical Machines," Tech. Rep., 2010.
[36] A. Krings, S. Nategh, A. Stening, H. Grop, O. Wallmark, and J. Soulard, "Measurement and Modeling of Iron Losses in Electrical Machines," Tech. Rep.
[37] Oskar Wallmark, *AC Machine Analysis, Fundamental Theory.* Stockholm: Division of Electric Power and Energy Systems, KTH Royal Institute of Technology, 2020.
[38] G. Bertotti, "General Properties of Power Losses in Soft Ferromagnetic Materials," Tech. Rep., 1988.
[39] N. Mohan, T. M. Undeland, and W. P. Robbins, *Power Electronics: Converters, Applications, and Design*, 3rd ed., B. Zobrist, Ed. Wiley, 2003.
[40] TRUMPF, "TruLaser Cell 7040 TRUMPF," 2023.
[41] S. Elfgen, S. Böhmer, S. Steentjes, D. Franck, and K. Hameyer, "Continuous model of magnetic material degradation due to cutting effects in the numerical simulation of electro laminations," *ETG-Fachbericht 146: IKMT*, 9 2015.

A

Repeatability Test SST and Epstein

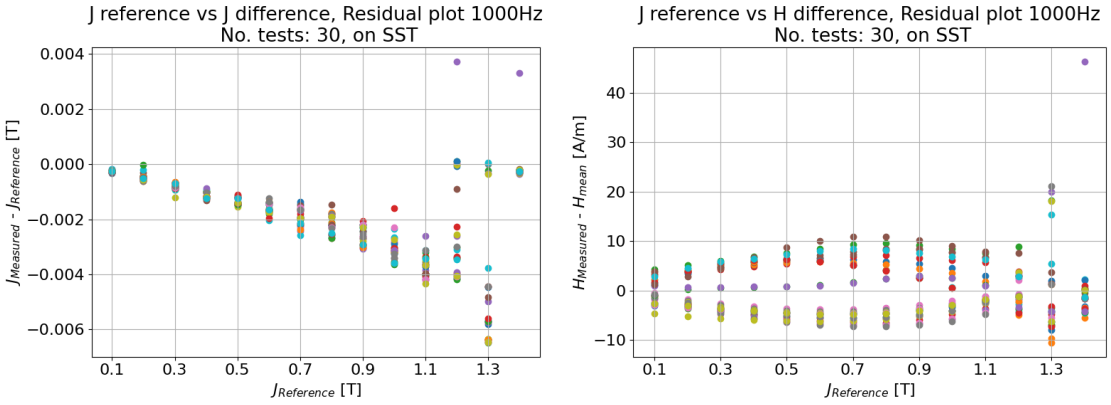

(a) J_{ref} vs J_{diff} scatter plot. **(b)** J_{ref} vs H_{diff} scatter plot.

Figure A.1: Residual plots for SST measurements of 1000 Hz

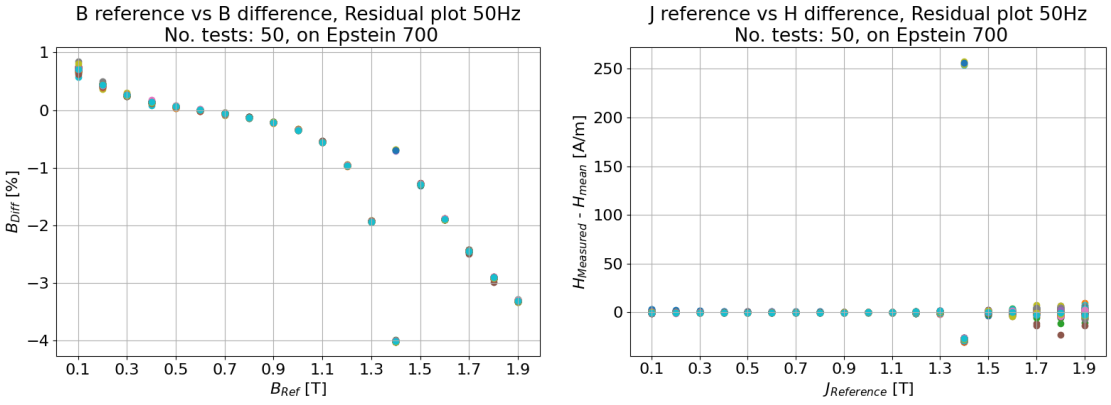

(a) J_{ref} vs J_{diff} scatter plot. **(b)** J_{ref} vs H_{diff} scatter plot.

Figure A.2: Residual plots for EP700 measurements of 50 Hz

Table A.1: SST repeatability test, RSD result.

SST Frequency: 50 Hz			
J [T]	J_{RSD} [%]	H_{RSD} [%]	Ps_{RSD} [%]
0.1	0.19	3.36	2.88
0.2	0.16	2.38	2.13
0.3	0.11	2.43	1.84
0.4	0.19	2.61	1.78
0.5	0.1	2.74	1.65
0.6	0.13	2.87	1.56
0.7	0.08	2.98	1.44
0.8	0.13	3.06	1.34
0.9	0.19	3.08	1.11
1.0	0.04	3.12	1.09
1.1	0.03	2.86	0.95
1.2	0.03	2.06	0.8
1.3	0.02	0.96	0.67
1.4	0.02	0.39	0.55
1.5	0.03	0.27	0.67
1.6	0.03	0.23	1.41
1.7	0.02	0.13	2.01
1.8	0.02	0.16	2.26

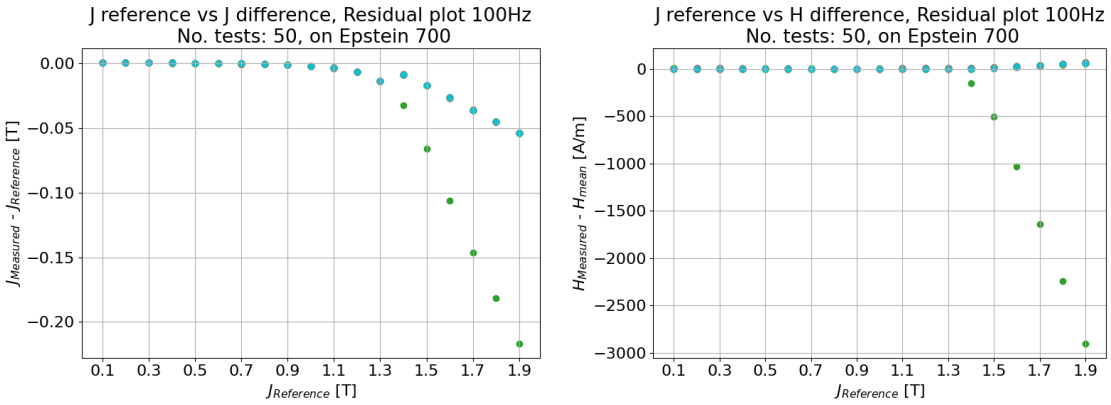

(a) J_{ref} vs J_{diff} scatter plot.

(b) J_{ref} vs H_{diff} scatter plot.

Figure A.3: Residual plots for EP700 measurements of 100 Hz

Table A.2: Epstein repeatability test, RSD result.

EP700 Frequency: 50 Hz			
J [T]	J_{RSD} [%]	H_{RSD} [%]	Ps_{RSD} [%]
0.1	0.04	2.88	2.29
0.2	0.02	1.23	0.78
0.3	0.01	0.75	0.5
0.4	0.01	0.62	0.41
0.5	0.01	0.54	0.35
0.6	0.01	0.46	0.31
0.7	0.01	0.36	0.27
0.8	0.01	0.26	0.23
0.9	0.01	0.15	0.19
1.0	0.01	0.09	0.16
1.1	0.01	0.2	0.12
1.2	0.01	0.34	0.11
1.3	0.01	0.36	0.11
1.4	0.99	14.03	1.69
1.5	0.01	0.07	0.1
1.6	0.01	0.06	0.1
1.7	0.01	0.09	0.11
1.8	0.01	0.09	0.15
1.9	0.01	0.06	0.18

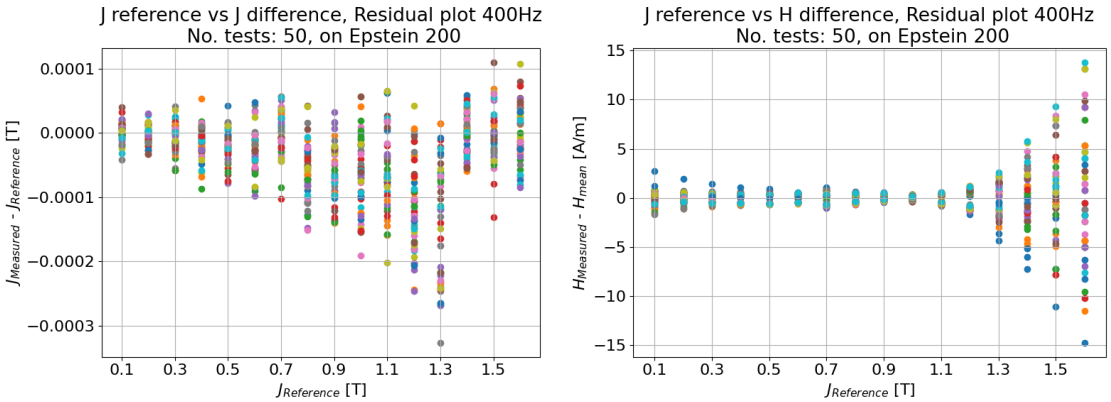

(a) J_{ref} vs J_{diff} scatter plot.

(b) J_{ref} vs H_{diff} scatter plot.

Figure A.4: Residual plots for EP200 measurements of 400 Hz

Table A.3: Epstein repeatability test, RSD result Fixed regulator settings.

EP700 Frequency: 50 Hz			
J [T]	J_{RSD} [%]	H_{RSD} [%]	Ps_{RSD} [%]
0.1	0.02	1.75	1.65
0.2	0.01	0.56	0.43
0.3	0.01	0.29	0.14
0.4	0.01	0.15	0.06
0.5	0.0	0.06	0.05
0.6	0.01	0.05	0.06
0.7	0.0	0.04	0.05
0.8	0.0	0.04	0.03
0.9	0.0	0.03	0.02
1.0	0.0	0.02	0.02
1.1	0.0	0.02	0.01
1.2	0.0	0.01	0.01
1.3	0.0	0.06	0.02
1.4	0.0	0.05	0.04
1.5	0.0	0.03	0.03
1.6	0.0	0.02	0.04
1.7	0.0	0.02	0.08
1.8	0.0	0.02	0.08
1.9	0.0	0.01	0.07

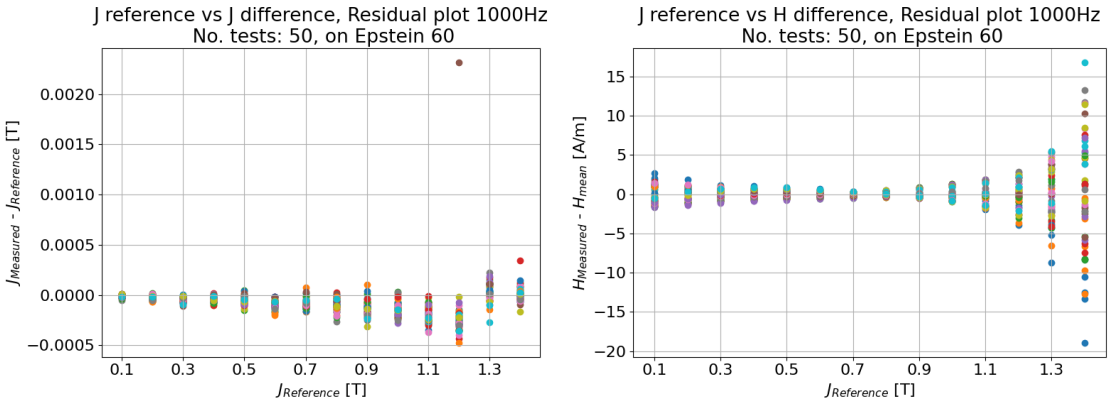

(a) J_{ref} vs J_{diff} scatter plot.

(b) J_{ref} vs H_{diff} scatter plot.

Figure A.5: Residual plots for EP60 measurements of 1000 Hz

Table A.4: Epstein repeatability test, RSD result.

EP700 Frequency: 100 Hz			
J [T]	J_{RSD} [%]	H_{RSD} [%]	Ps_{RSD} [%]
0.1	0.01	3.01	2.31
0.2	0.01	1.27	0.78
0.3	0.0	0.66	0.41
0.4	0.0	0.45	0.29
0.5	0.0	0.35	0.24
0.6	0.0	0.26	0.21
0.7	0.0	0.19	0.17
0.8	0.0	0.12	0.16
0.9	0.0	0.1	0.14
1.0	0.0	0.16	0.12
1.1	0.0	0.28	0.1
1.2	0.0	0.44	0.08
1.3	0.0	0.45	0.08
1.4	0.24	2.57	0.34
1.5	0.46	4.16	0.39
1.6	0.69	5.04	0.26
1.7	0.91	5.43	0.12
1.8	1.06	5.47	0.48
1.9	1.2	5.47	0.83

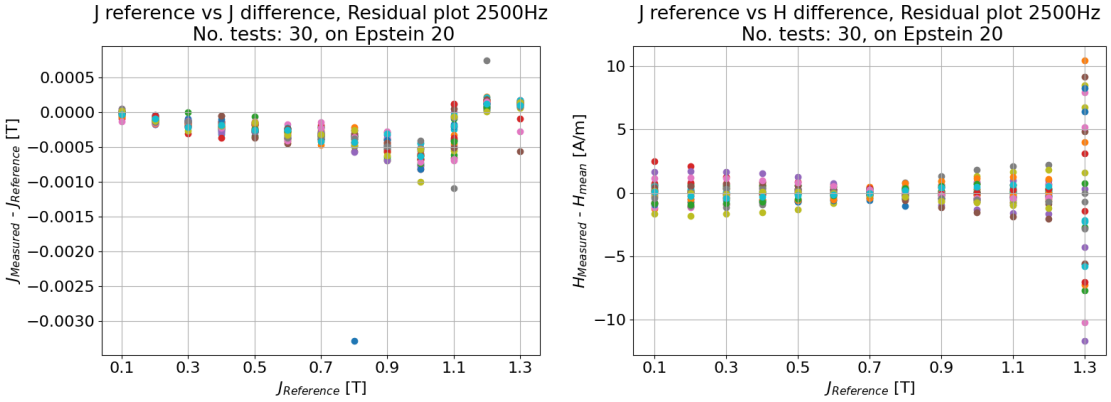

(a) J_{ref} vs J_{diff} scatter plot.

(b) J_{ref} vs H_{diff} scatter plot.

Figure A.6: Residual plots for EP20 measurements of 2500 Hz

Table A.5: Epstein repeatability test, RSD result.

EP200 Frequency: 400 Hz			
J [T]	J_{RSD} [%]	H_{RSD} [%]	Ps_{RSD} [%]
0.1	0.02	1.67	1.24
0.2	0.01	0.79	0.47
0.3	0.01	0.57	0.34
0.4	0.01	0.5	0.28
0.5	0.0	0.45	0.24
0.6	0.01	0.35	0.18
0.7	0.0	0.48	0.23
0.8	0.01	0.29	0.17
0.9	0.0	0.16	0.13
1.0	0.01	0.12	0.1
1.1	0.01	0.23	0.09
1.2	0.01	0.35	0.08
1.3	0.01	0.38	0.07
1.4	0.0	0.24	0.08
1.5	0.0	0.15	0.09
1.6	0.0	0.12	0.16

Table A.6: Epstein repeatability test, RSD result.

EP60 Frequency: 1000 Hz			
J [T]	J_{RSD} [%]	H_{RSD} [%]	Ps_{RSD} [%]
0.1	0.01	2.31	0.98
0.2	0.01	1.04	0.47
0.3	0.01	0.56	0.26
0.4	0.01	0.42	0.19
0.5	0.01	0.31	0.15
0.6	0.01	0.21	0.13
0.7	0.01	0.14	0.12
0.8	0.01	0.15	0.11
0.9	0.01	0.22	0.12
1.0	0.01	0.32	0.13
1.1	0.01	0.45	0.14
1.2	0.03	0.58	0.14
1.3	0.01	0.71	0.12
1.4	0.01	0.63	0.13

Table A.7: Epstein repeatability test, RSD result.

EP20 Frequency: 2500 Hz			
J [T]	J_{RSD} [%]	H_{RSD} [%]	Ps_{RSD} [%]
0.1	0.04	1.35	0.81
0.2	0.02	0.8	0.47
0.3	0.02	0.54	0.29
0.4	0.02	0.41	0.24
0.5	0.01	0.3	0.24
0.6	0.01	0.18	0.23
0.7	0.01	0.12	0.25
0.8	0.07	0.16	0.32
0.9	0.01	0.2	0.3
1.0	0.01	0.24	0.31
1.1	0.03	0.25	0.32
1.2	0.01	0.23	0.28
1.3	0.01	1.1	0.27

B

Cut Effects with Sinusoidal Flux Density

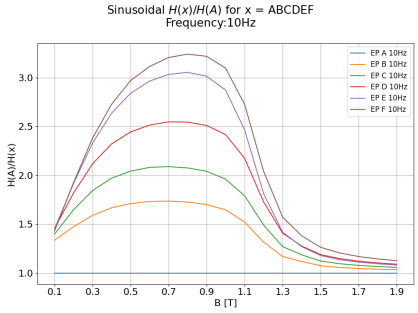

(a) H deg 10 Hz.

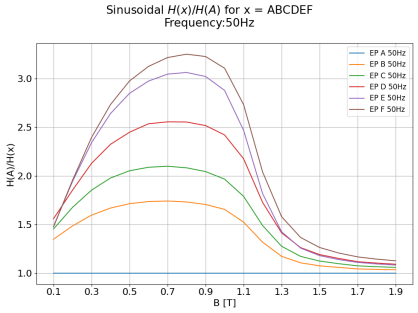

(b) H deg 50 Hz.

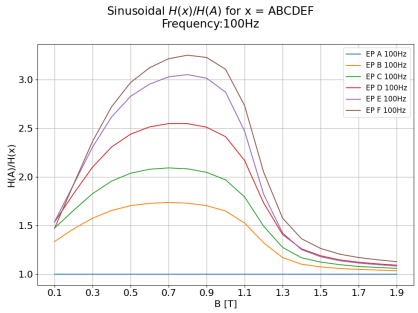

(c) H deg 100 Hz.

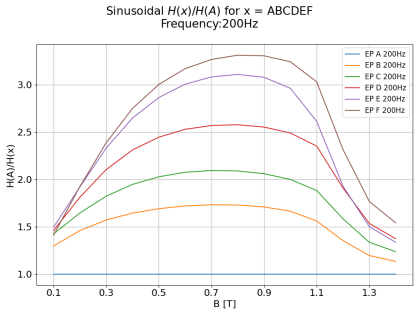

(d) H deg 200 Hz.

Figure B.1: H deg for sinusoidal excitation.

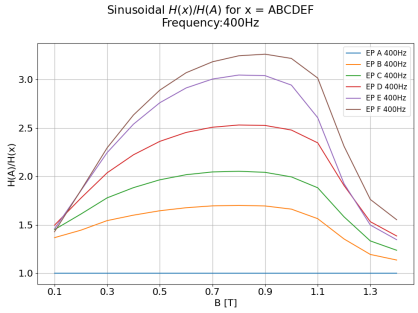

(a) H deg 400 Hz.

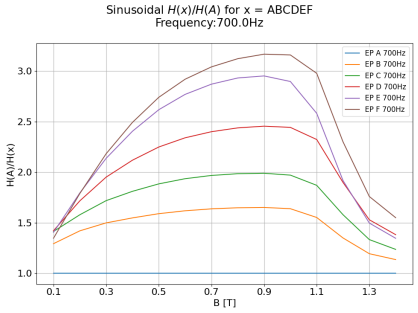

(b) H deg 700 Hz.

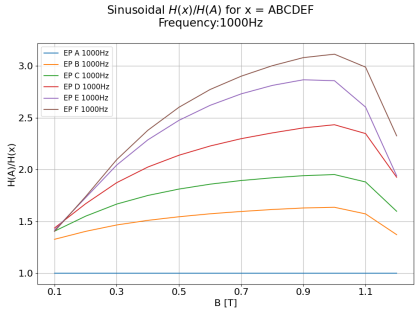

(c) H deg 1000 Hz.

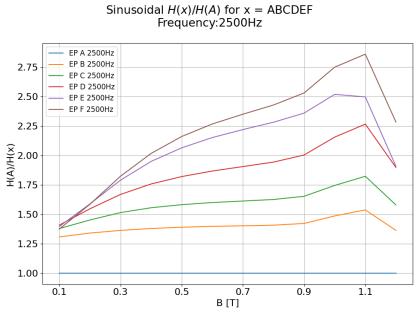

(d) H deg 2500 Hz.

Figure B.2: H deg for sinusoidal excitation.

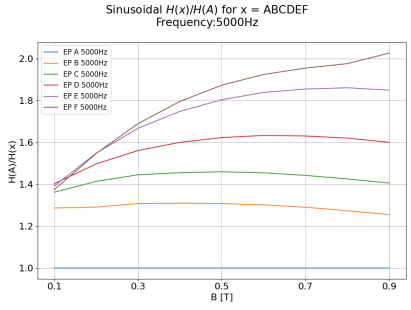

(a) H deg 5000 Hz.

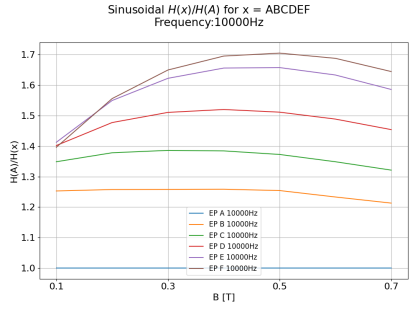

(b) H deg 10000 Hz.

Figure B.3: H deg for sinusoidal excitation.

C

Cut Effects with Non-Sinusoidal Flux Density

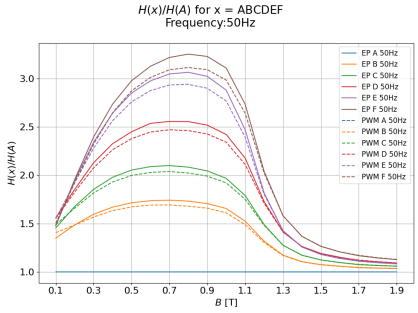

(a) H deg PWM 50 Hz.

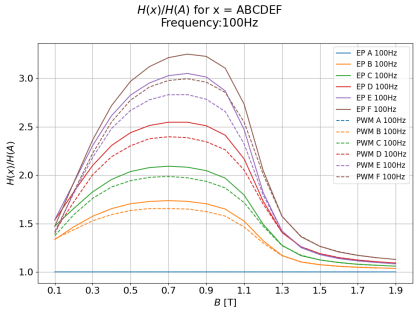

(b) H deg PWM 100 Hz.

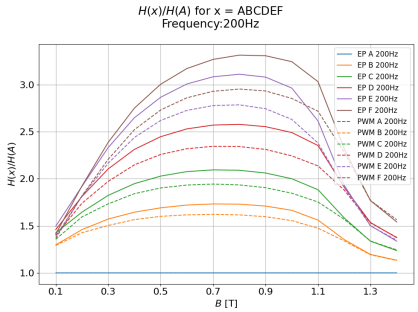

(c) H deg PWM 200 Hz.

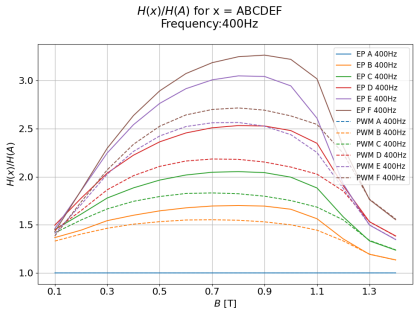

(d) H deg PWM 400 Hz.

Figure C.1: H deg for PWM excitation.

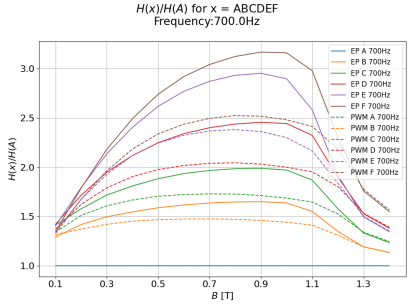

(a) H deg PWM 700 Hz.

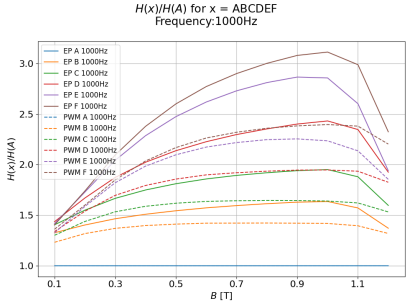

(b) H deg PWM 1000 Hz.

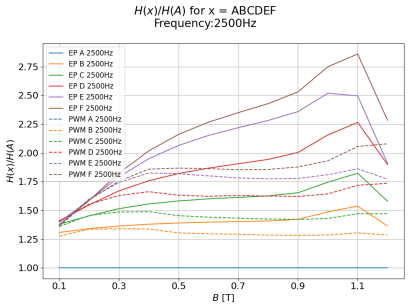

(c) H deg PWM 2500 Hz.

Figure C.2: H deg for PWM excitation.

D

FEM Simulation with Sinusoidal Excitation

Table D.1: Material properties for 50 Hz, B in [T], and H in [A/m], for different layers.

B	$H(0.05)$	$H(0.15)$	$H(0.3)$	$H(0.55)$	$H(0.95)$	$H(1.6)$
0.1	102.24	101.17	99.60	97.11	93.44	88.21
0.2	215.53	211.17	204.91	195.15	181.16	162.13
0.3	365.57	355.53	341.21	319.17	288.18	247.30
0.4	534.24	516.93	492.35	454.84	402.81	335.60
0.5	704.74	679.42	643.61	589.27	514.64	419.76
0.6	864.68	831.60	784.95	714.47	618.31	497.34
0.7	1018.15	977.20	919.58	832.86	715.28	568.86
0.8	1168.81	1120.02	1051.51	948.75	810.14	639.00
0.9	1329.55	1272.56	1192.67	1073.17	912.73	716.08
1	1526.20	1460.28	1367.98	1230.19	1045.76	820.83
1.1	1837.19	1761.32	1655.10	1496.53	1284.30	1025.48
1.2	2359.34	2280.67	2170.15	2004.23	1780.16	1502.94
1.3	3227.27	3145.62	3030.76	2858.01	2623.99	2333.02
1.4	4355.03	4269.41	4149.01	3968.03	3723.11	3419.05
1.5	5628.90	5540.63	5416.46	5229.69	4976.66	4662.03
1.6	7017.89	6926.25	6797.29	6603.18	6339.92	6011.98
1.7	8595.73	8489.88	8341.65	8120.21	7823.55	7461.21
1.8	10079.45	9976.34	9831.50	9614.11	9320.59	8957.63
1.9	11669.61	11564.81	11417.40	11195.72	10895.46	10522.25

Table D.2: Material properties for 100 Hz, B in [T], and H in [A/m], for different layers.

B	$H(0.05)$	$H(0.15)$	$H(0.3)$	$H(0.55)$	$H(0.95)$	$H(1.6)$
0.1	105.42	104.24	102.53	99.82	95.83	90.18
0.2	216.42	212.06	205.80	196.05	182.09	163.12
0.3	365.88	355.79	341.41	319.29	288.24	247.37
0.4	536.24	518.66	493.71	455.67	403.01	335.20
0.5	706.41	680.80	644.61	589.74	514.49	419.03
0.6	865.52	832.15	785.11	714.11	617.35	495.90
0.7	1018.32	977.21	919.37	832.37	714.48	567.85
0.8	1168.59	1119.77	1051.22	948.40	809.76	638.63
0.9	1330.07	1273.07	1193.17	1073.66	913.20	716.53
1.0	1529.78	1463.50	1370.73	1232.27	1047.06	821.37
1.1	1838.54	1762.70	1656.51	1497.97	1285.76	1026.90
1.2	2371.07	2291.93	2180.72	2013.76	1788.23	1509.12
1.3	3235.11	3153.27	3038.18	2865.13	2630.84	2339.77
1.4	4371.51	4283.82	4160.69	3975.99	3726.86	3419.25
1.5	5642.22	5552.79	5427.08	5238.15	4982.57	4665.49
1.6	7015.32	6924.14	6795.86	6602.83	6341.18	6015.55
1.7	8521.21	8423.10	8285.18	8077.92	7797.56	7449.79
1.8	10054.26	9954.08	9813.09	9600.84	9312.89	8954.06
1.9	11686.45	11580.38	11431.22	11206.98	10903.45	10526.52

Table D.3: Material properties for 200 Hz, B in [T], and H in [A/m], for different layers.

B	$H(0.05)$	$H(0.15)$	$H(0.3)$	$H(0.55)$	$H(0.95)$	$H(1.6)$
0.1	106.82	105.71	104.09	101.52	97.74	92.38
0.2	226.63	221.99	215.33	204.97	190.17	170.11
0.3	386.84	375.81	360.11	336.02	302.32	258.17
0.4	567.93	548.52	521.04	479.27	421.71	348.17
0.5	748.16	719.85	679.93	619.62	537.34	433.89
0.6	916.82	879.98	828.16	750.19	644.52	513.01
0.7	1076.28	1031.23	967.97	873.10	745.15	587.22
0.8	1236.55	1183.16	1108.33	996.39	846.08	661.84
0.9	1419.31	1356.42	1268.40	1137.11	961.59	747.95
1.0	1695.89	1618.78	1511.11	1351.01	1138.14	881.24
1.1	2360.75	2253.88	2104.84	1883.70	1590.67	1238.94
1.2	4055.11	3898.94	3680.50	3354.87	2920.09	2391.90
1.3	7379.75	7144.92	6816.59	6327.46	5675.04	4883.73
1.4	12477.66	12139.89	11667.79	10964.84	10028.01	8893.27

Table D.4: Material properties for 400 Hz, B in [T], and H in [A/m], for different layers.

B	$H(0.05)$	$H(0.15)$	$H(0.3)$	$H(0.55)$	$H(0.95)$	$H(1.6)$
0.1	109.72	108.74	107.31	105.02	101.63	96.73
0.2	229.62	225.23	218.92	209.08	194.97	175.72
0.3	387.71	377.06	361.88	338.56	305.87	262.93
0.4	567.83	548.67	521.55	480.34	423.58	351.14
0.5	748.97	720.68	680.81	620.65	538.69	435.88
0.6	921.84	884.59	832.22	753.55	647.15	515.24
0.7	1084.08	1038.45	974.42	878.50	749.41	590.56
0.8	1247.47	1193.39	1117.64	1004.42	852.64	667.03
0.9	1429.89	1366.70	1278.28	1146.38	970.08	755.53
1.0	1704.29	1627.49	1520.19	1360.54	1148.01	891.06
1.1	2360.08	2254.32	2106.76	1887.60	1596.76	1246.85
1.2	4067.84	3911.41	3692.60	3366.41	2930.85	2401.64
1.3	7422.22	7185.26	6854.06	6360.94	5703.79	4907.92
1.4	12651.23	12296.96	11802.39	11067.39	10090.84	8913.78

Table D.5: Material properties for 700 Hz, B in [T], and H in [A/m], for different layers.

B	$H(0.05)$	$H(0.15)$	$H(0.3)$	$H(0.55)$	$H(0.95)$	$H(1.6)$
0.1	111.61	110.70	109.38	107.27	104.12	99.59
0.2	237.17	232.89	226.73	217.11	203.28	184.36
0.3	394.07	383.65	368.80	345.97	313.93	271.77
0.4	570.23	551.50	524.98	484.67	429.14	358.21
0.5	751.25	723.22	683.73	624.16	543.11	441.61
0.6	926.75	889.39	836.92	758.18	651.93	520.63
0.7	1094.25	1047.97	983.12	886.14	755.98	596.54
0.8	1264.35	1209.10	1131.79	1016.47	862.33	674.75
0.9	1454.91	1390.00	1299.28	1164.19	984.13	766.00
1.0	1726.05	1648.38	1539.91	1378.56	1163.89	904.57
1.1	2373.98	2268.12	2120.39	1900.97	1609.72	1259.21
1.2	4070.34	3914.09	3695.54	3369.77	2934.83	2406.51
1.3	7389.99	7154.41	6825.15	6334.94	5681.70	4890.63
1.4	12581.65	12228.60	11735.84	11003.81	10031.81	8861.41

Table D.6: Material properties for 1000 Hz, B in [T], and H in [A/m], for different layers.

B	$H(0.05)$	$H(0.15)$	$H(0.3)$	$H(0.55)$	$H(0.95)$	$H(1.6)$
0.1	109.72	108.74	107.31	105.02	101.63	96.73
0.2	229.62	225.23	218.92	209.08	194.97	175.72
0.3	387.71	377.06	361.88	338.56	305.87	262.93
0.4	567.83	548.67	521.55	480.34	423.58	351.14
0.5	748.97	720.68	680.81	620.65	538.69	435.88
0.6	921.84	884.59	832.22	753.55	647.15	515.24
0.7	1084.08	1038.45	974.42	878.50	749.41	590.56
0.8	1247.47	1193.39	1117.64	1004.42	852.64	667.03
0.9	1429.89	1366.70	1278.28	1146.38	970.08	755.53
1.0	1704.29	1627.49	1520.19	1360.54	1148.01	891.06
1.1	2360.08	2254.32	2106.76	1887.60	1596.76	1246.85
1.2	4067.84	3911.41	3692.60	3366.41	2930.85	2401.64
1.3	7422.22	7185.26	6854.06	6360.94	5703.79	4907.92
1.4	12651.23	12296.96	11802.39	11067.39	10090.84	8913.78

E

FEM Simulation with PWM Excitation

Table E.1: Material properties for 50 Hz, B in [T], and H in [A/m], for different layers PWM model.

B	$H(0.05)$	$H(0.15)$	$H(0.3)$	$H(0.55)$	$H(0.95)$	$H(1.6)$
0.1	101	101	100	99	97	93
0.2	199	196	193	188	179	166
0.3	342	335	325	309	286	252
0.4	509	496	476	445	401	342
0.5	682	660	629	582	516	428
0.6	845	816	774	710	622	508
0.7	1003	966	913	833	723	583
0.8	1160	1115	1051	954	822	657
0.9	1324	1271	1196	1083	929	738
1	1530	1467	1379	1246	1068	848
1.1	1842	1769	1666	1513	1306	1052
1.2	2349	2275	2170	2012	1796	1525
1.3	3205	3129	3022	2860	2637	2355
1.4	4329	4249	4137	3967	3733	3439
1.5	5610	5527	5409	5231	4988	4680
1.6	7012	6924	6800	6613	6356	6032
1.7	8495	8402	8272	8075	7806	7467
1.8	10029	9935	9801	9599	9322	8971
1.9	11640	11542	11403	11192	10903	10538

Table E.2: Material properties for 100 Hz, B in [T], and H in [A/m], for different layers PWM model.

B	$H(0.05)$	$H(0.15)$	$H(0.3)$	$H(0.55)$	$H(0.95)$	$H(1.6)$
0.1	99	98	97	96	95	92
0.2	198	196	193	188	180	168
0.3	343	336	327	311	288	256
0.4	516	502	482	451	407	348
0.5	692	670	639	591	524	437
0.6	857	827	785	721	633	519
0.7	1015	978	926	846	736	597
0.8	1169	1124	1062	967	837	674
0.9	1337	1284	1211	1099	948	759
1	1542	1481	1394	1265	1089	872
1.1	1849	1778	1677	1527	1325	1074
1.2	2368	2293	2187	2027	1809	1536
1.3	3201	3126	3019	2857	2636	2355
1.4	4329	4249	4136	3965	3731	3435
1.5	5603	5520	5403	5225	4983	4676
1.6	7000	6913	6790	6604	6350	6028
1.7	8495	8402	8272	8074	7803	7463
1.8	10014	9920	9788	9588	9313	8965

Table E.3: Material properties for 200 Hz, B in [T], and H in [A/m], for different layers PWM model.

B	$H(0.05)$	$H(0.15)$	$H(0.3)$	$H(0.55)$	$H(0.95)$	$H(1.6)$
0.1	105	104	104	102	101	98
0.2	215	213	209	204	195	182
0.3	375	367	356	338	312	276
0.4	557	542	519	485	436	371
0.5	743	718	684	631	558	462
0.6	921	888	841	770	672	548
0.7	1089	1048	990	902	782	630
0.8	1260	1210	1141	1036	893	714
0.9	1455	1396	1313	1189	1021	813
1	1735	1663	1562	1410	1207	958
1.1	2370	2268	2126	1915	1633	1294
1.2	4003	3854	3646	3335	2916	2403
1.3	7284	7059	6743	6270	5637	4862
1.4	12648	12289	11788	11042	10052	8858

Table E.4: Material properties for 400 Hz, B in [T], and H in [A/m], for different layers PWM model.

B	$H(0.05)$	$H(0.15)$	$H(0.3)$	$H(0.55)$	$H(0.95)$	$H(1.6)$
0.1	123	123	122	120	118	115
0.2	226	224	222	217	209	198
0.3	389	381	371	354	330	296
0.4	574	559	538	504	457	393
0.5	766	742	707	655	582	487
0.6	946	913	867	797	700	577
0.7	1121	1080	1022	935	816	665
0.8	1297	1248	1179	1075	934	756
0.9	1496	1438	1356	1234	1068	862
1	1770	1700	1602	1455	1257	1012
1.1	2351	2255	2121	1922	1655	1331
1.2	3945	3799	3595	3291	2881	2380
1.3	7103	6887	6583	6129	5519	4769
1.4	12261	11918	11439	10726	9777	8629

Table E.5: Material properties for 700 Hz, B in [T], and H in [A/m], for different layers PWM model.

B	$H(0.05)$	$H(0.15)$	$H(0.3)$	$H(0.55)$	$H(0.95)$	$H(1.6)$
0.1	127	127	126	125	123	120
0.2	249	247	244	239	231	219
0.3	416	409	398	381	357	322
0.4	603	588	567	534	487	423
0.5	796	772	738	687	615	520
0.6	988	955	908	837	739	614
0.7	1176	1134	1075	985	862	708
0.8	1374	1322	1250	1141	993	809
0.9	1593	1532	1446	1317	1143	928
1	1883	1810	1708	1554	1348	1093
1.1	2406	2314	2185	1991	1731	1412
1.2	3905	3761	3559	3258	2854	2362
1.3	7021	6802	6494	6035	5419	4667
1.4	11977	11651	11194	10513	9601	8490

DEPARTMENT OF ELECTRICAL ENGINEERING
CHALMERS UNIVERSITY OF TECHNOLOGY
Gothenburg, Sweden
www.chalmers.se

CHALMERS
UNIVERSITY OF TECHNOLOGY